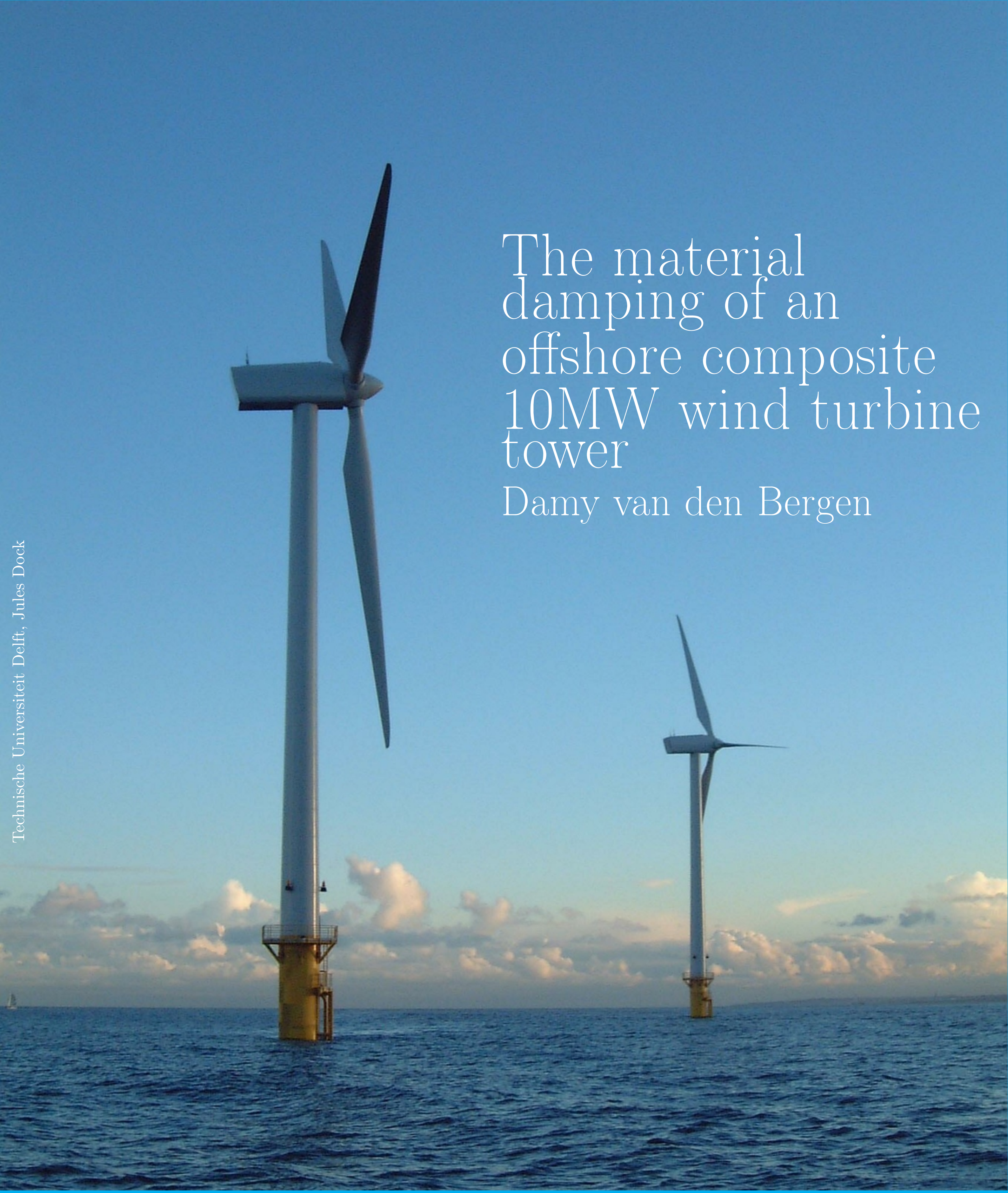

The material damping of an offshore composite 10MW wind turbine tower

Damy van den Bergen

Technische Universiteit Delft, Jules Dock

Cover image from [1]

The material damping of an offshore composite 10MW wind turbine tower

by

Damy van den Bergen

to obtain the degree of Master of Science
at the Delft University of Technology,
to be defended publicly on Friday December 15, 2017 at 13:00 AM.

Student number:	4078047	
Project duration:	November 24, 2016 – December 15, 2017	
Thesis committee:	Prof. dr. ir. R. Benedictus,	TU Delft, ASM Structural Integrity & Composites, Chair
	Dr. ir. O. K. Bergsma,	TU Delft, ASM Structural Integrity & Composites, Thesis supervisor
	Dr. B. Chen,	TU Delft, ASM Aerospace Structures & Computational Mechanics
	Ir. I.W. Wieling,	Supervisor at Jules Dock

This thesis is confidential and cannot be made public until January 1, 2023.

Delft University of Technology
Faculty of Aerospace Engineering
Department of Aerospace Structures and Materials

GRADUATION COMMITTEE

Dated: December 15th, 2017

Chair holder:

Prof.dr.ir. R. (Rinze) Benedictus

Committee members:

Dr.ir O.K. (Otto) Bergsma

Dr. B. (Boyang) Chen

Ir. I.W. (Ivo) Wieling

Preface

During my search to an interesting thesis project, I stumbled upon the company Jules Dock. Currently Jules Dock is developing, in collaboration with Knowledge Centre WMC, a 10MW composite wind turbine tower. This composite tower could be the next giant step for the wind turbine industry. The master's thesis project that Jules Dock offered, was part of the project comprising the composite wind turbine tower (the C-Tower project). Due to the innovative nature of the entire C-Tower project, my choice was easily made and I accepted the assignment. After accepting this thesis project, Dr. Ir. Otto Bergsma became my supervisor on the university and Ir. Ivo Wieling became my supervisor at Jules Dock.

I would like to thank Dr. Ir. Otto Bergsma and Ir. Ivo Wieling for all their support during my graduation project. Our conversations certainly helped me out a lot. Also I would like to thank the CEO of Jules Dock, Felix Moonen, for making my thesis project possible and for providing the required facilities and materials. Also I would like to thank two of Jules Dock's employees, Damien Zamboni and Remco Petersen. Without their assistance, my samples probably did not look as good as they did. I would like to thank Tjeerd, Marten Jan and Gerben of WMC for answering all my questions regarding the dynamic behavior of the composite wind turbine tower. Also I would like to thank Peter Heins of Euroresins and Jelte Vonk for answering my questions regarding foams and providing me with a large amount of foam samples.
Of all the employees working at the 'vliegtuighal', I would like to thank Lijing Xue for testing my first couple of samples and Frans Oostrum for teaching me how to use the DMA machine and for all of his assistance during the DMA measurements. Also I want to thank Gertjan Mulder and the other employees with helping me out with the all the other measurements. Last but not least, I would like to thank my girlfriend, family, friends and fellow students for supporting me through this entire project.

Damy van den Bergen
Delft, November 2017

Summary

In the coming years the dutch government plans to build a large amount of offshore wind turbines, which should cover approximately 3% of all energy produced in the Netherlands. Therefore, it will be necessary to decrease the costs of the transportation, installation and maintenance of these wind turbines.
Jules Dock tries to achieve this by replacing the steel design of the next generation 10MW wind turbine tower by a flexible composite design. The current tower design consists of a sandwich structured glass fiber reinforced vinylester with mainly 90° and ±45° oriented plies. Damping is an important parameter of flexible structures, since it dissipates the energy of the vibrations and therefore increases the fatigue life of the structure. Due to a lack of knowledge, the current damping ratio of the composite structure has been assumed to be equal to the damping ratio of a regular steel wind turbine tower. The damping capability of large vibrating composite structures is still a subject that requires a tremendous amount of research. Therefore a research thesis has been set-up, in cooperation with the companies Jules Dock and WMC, to determine the damping properties of the large composite tower.

The main focus of this thesis is to estimate the modal damping loss factors of the composite tower and the influence of the loading frequency and temperature on the tower's damping behavior. This goal is achieved by performing measurements and by translating the results of these measurements to the tower's damping behavior by means of a numerical model.
All the measurements are conducted by a Dynamic Mechanical Analyzer. Another measurement method has been considered, however this method appeared to be inadequate. According to the results of these measurements, the damping loss factors of the viscoelastic materials like resins, composites and foams are both depending on the loading frequency and the temperature. Of these materials, the 0° oriented composite laminates can be considered to be the least affected by these factors and are in terms of damping behavior comparable with steel.
The measured damping loss factors will serve as an input for the damping model. This damping model is based on Chortis' model for the viscoelastic material damping of wind turbine blades. In order to simplify this model several assumptions have been made. For example only linear (amplitude independent) viscoelastic damping has been considered, while other material damping mechanisms are neglected and the damping due to structural connections is considered outside the scope of this project.

The resulting damping behavior of the tower can be considered quite frequency and temperature independent for its intended frequency and temperature ranges. Also the difference in modal damping between the first and second bending mode can be neglected, which means that the modal damping loss factor can be considered equal for the most important low frequency motions. The modal damping loss factors of the first two bending modes are approximately 71% higher than the damping loss factors of a steel tower with the same dimensions. Since the damping loss factor is approximately twice the damping ratio, the damping ratio will show a 71% increase as well. This 71% increase of the damping ratio, results in an approximately 71% reduction of the time that a certain excitation requires to return to its steady-state. This means that the amplitude will return faster to zero and that the system is subjected to less loading cycles. The fatigue life of the material will therefore be increased as well.

Contents

Summary v

List of Figures viii

List of Tables x

1 Introduction 1

2 Project plan 3
- 2.1 Research question, aims and objectives 3
- 2.2 Theoretical Content/Methodology 4
- 2.3 Experimental Set-up 4
  - 2.3.1 DMA test 4
  - 2.3.2 Other experimental tests 4
- 2.4 Results, Outcome and Relevance 4
- 2.5 Project Planning 5

3 Background information 7
- 3.1 The dynamic loading on a wind turbine tower 7
- 3.2 Damping mechanisms of wind turbines 10
- 3.3 Material damping 11
  - 3.3.1 Viscous damping 11
  - 3.3.2 Hysteretic 11
  - 3.3.3 Coulomb 11
  - 3.3.4 Radiational damping 11
- 3.4 Damping of composite materials 12
  - 3.4.1 Viscoelastic damping 12
  - 3.4.2 Damping due to the fiber-matrix interphase 14
  - 3.4.3 Damping due to damage 14
  - 3.4.4 Viscoplastic damping 14
  - 3.4.5 Thermoelastic damping 14
- 3.5 Factors influencing damping 15
  - 3.5.1 Laminate parameters 15
  - 3.5.2 Other factors 15
- 3.6 Theories on damping 16
  - 3.6.1 Quantities of damping 17
  - 3.6.2 Damping models 20

4 DMA measurements 21
  - 4.0.3 Resin tests 24
  - 4.0.4 Results Vinylester 24
  - 4.0.5 Results Epoxy 24
- 4.1 Composite material 25
  - 4.1.1 Composite laminates 26
  - 4.1.2 Composite plies 27
  - 4.1.3 Composite materials versus steel 28
- 4.2 Foam material 30
  - 4.2.1 PVC foam 30
  - 4.2.2 PET foam 31
- 4.3 Sandwich structured composites 34
- 4.4 Validation of the DMA measurements 35
- 4.5 Conclusion 36

5 Damping Model **37**
- 5.1 Ply damping . . . 38
- 5.2 Laminate and cross-sectional damping . . . 39
- 5.3 Tower Damping . . . 40
- 5.4 Model sensitivity . . . 43
  - 5.4.1 The influence of the composite laminate's architecture . . . 44
  - 5.4.2 The influence of the tower's architecture . . . 45
  - 5.4.3 The influence of a core . . . 46
  - 5.4.4 Mode dependency . . . 46
- 5.5 Model implementation and results . . . 48
  - 5.5.1 Implementation of the current design . . . 48
  - 5.5.2 Comparison with a steel design . . . 49
  - 5.5.3 Optimization of the current design for damping . . . 50

6 Conclusion and Recommendations **51**
- 6.1 Conclusion . . . 51
- 6.2 Recommendations . . . 52

APPENDICES **53**

A Measuring Damping **55**
  - A.0.1 First measurement tests using the 10N load cell . . . 56
  - A.0.2 Tests using the 1kN load cell . . . 58

B Production of samples **61**
- B.1 Resin Samples . . . 61
- B.2 Foam and steel samples . . . 61
  - B.2.1 Foam samples . . . 61
  - B.2.2 Steel samples . . . 61
- B.3 Composite samples . . . 62
  - B.3.1 Composite laminates and plies . . . 62
  - B.3.2 Sandwich structured composite . . . 64

C Used material properties **67**

D Shear energy distribution **69**
  - D.0.3 Three-point-bending configuration . . . 69
  - D.0.4 cantilever beam configuration . . . 70

E Classical laminate theory **73**

F Saravanos-Chamis Micromechanical model **75**

G ABD-matrices of a tubular cross-section **77**

H Validation of the FEM model **81**

I Influence tower architecture **83**

J The influence of the core on the tower's damping behavior **85**

Bibliography **89**

List of Figures

1.1 The development of wind turbines in time [31]. 1

2.1 The flow chart of the Master's Thesis Project. 5

3.1 Examples of several types of support structures [65]. 7
3.2 Example of the several loading frequency bands [74]. 8
3.3 Basic mathematical model of an Offshore Wind Turbine [6]. 8
3.4 The first four eigenmodes of an offshore wind turbine tower. These eigenmodes are from left to right: first bending mode, second bending mode, torsion and axial displacement [11]. 9
3.5 An example of the hysteresis loop. Here σ is the stress and ϵ the strain [101]. 11
3.6 Modulus-loss factor map of some common materials at room temperature at 1 Hz [72]. 12
3.7 The stress-strain response of an elastic (a), viscous (b) and viscoelastic (c) material [66]. 13
3.8 Several viscoelastic models [100].. 13
3.9 A typical temperature-damping curve [19]. 16
3.10 The relation between the frequency and the damping loss factor for a 'stiff' composite laminate. Note that the relation depends on the fiber orientation [15]. 16
3.11 A simple representation of a decaying vibration [63]. 17
3.12 A typical power spectrum of decaying vibrations [98].The formulas described in the figure can be used to calculate the damping ratio. 18
3.13 A typical Dynamic Mechanical Analyzer and the corresponding input and output curves [69]. 19

4.1 The DMA instrument at the Aerospace Engineering faculty. 22
4.2 3-point-bending configuration of the Pyris Diamond DMA instrument [50]. 23
4.3 general bending configuration of the Pyris Diamond DMA instrument [50]. 23
4.4 Loss factor versus temperature and frequency for the VE370SC vinylester. 24
4.5 Loss factor versus temperature for both resin systems at a 1Hz loading frequency. 25
4.6 Loss factor versus temperature for the 90° GFRV laminates. 26
4.7 Loss factor versus temperature for a glass fiber reinforced vinylester and epoxy. In the left figure the composite materials have a 0° fiber orientation and in the right figure a 90° fiber orientation 28
4.8 Loss factor versus temperature for steel. 29
4.9 Loss factor versus temperature for several kinds of material. Note that GFRV stands for glass fiber reinforced vinylester. 29
4.10 Loss tangent versus frequency and temperature for the C70.75. 31
4.11 Extruded honeycomb structure of the PET foams. Note that direction z corresponds with the extrusion direction and the blue rectangles indicate the different kind of samples. 32
4.12 Lost factor versus temperature for several PET foams. 32
4.13 The influence of the frequency and temperature on the Airex T92.200 and the Airex T92.80. 33
4.14 The influence of the frequency and temperature on a sandwich structured GFRV. 34

5.1 Schematic overview of all translation steps that have to be taken. [31] 37
5.2 The effect of the rotation matrix on the composite ply's damping loss factors. 39
5.3 A simple representation of a typical tubular beam cross-section geometry and coordinate systems. [31] . . 40
5.4 The conversion from 3D tubular structure to 2D beam element. 41
5.5 A typical two-node beam element. a) the global coordinate system. b) the local coordinate system. [31] . . 42
5.6 The linear shape functions of a two-node beam finite element [31]. 43
5.7 The effect of the fiber orientation on the tower's damping loss factor for two different modes. 44
5.8 Ring shaped section of the composite tower with corresponding detailed views of several local laminates. Section I is the front view at the area indicated by the left red dashed rectangle and coincides with the cross-section of the laminate. Section II is the front view at the area indicated by the right red rectangle. Both sections show the local fiber orientation. 45
5.9 The influence of the fiber orientation and tower's radius on the modal damping loss factor of the first bending mode. Note that the tower's element length is $1m$ and the tower's wall thickness is $100mm$ 46

5.10 The influence of the fiber orientation and the core stiffness on the modal damping loss factor of the first bending mode. The symbol C represents the multiplication factor, which is multiplied by both the core's tensile//compressive modulus and the core's shear modulus. Both moduli are equal to the moduli of the Airex T92.80 foam material, which can be seen in Appendix C. Note that the tower's radius is $5m$, the tower's element length is $1m$ and the total thickness of the face sheets is $100mm$. The core has a thickness of $100mm$ as well and a loss factor of 0.1 for both axial and shear damping. 47
5.11 The influence of the fiber orientation and tower's wall thickness on the modal damping loss factor of the first two bending modes. Note that the circular tower's radius is $5m$, the wall thickness is $100mm$ and the element length is $1m$. 47
5.12 The influence of the temperature on the tower's modal damping loss factor. 49

A.1 Example of an experimental set-up [4]. 55
A.2 Test set-up of the simple bending test. 56
A.3 Stress-strain response of a certain material / structure [94]. 56
A.4 Thickness distribution of the thickened samples. 58

B.1 Extruded honeycomb structure of the PET foams. Note that direction z corresponds with the extrusion direction and the blue rectangles indicate the different kind of samples. 61
B.2 Simplified representation of the vacuum infusion set-up. 62
B.3 Picture of several vacuum infused plates. 63
B.4 A picture of several samples. From left to right: Epoxy sample, Vinylester sample, 0° GFRV laminate, 90° GFRV laminate, ±45° GFRV laminate and a steel sample. 64
B.5 The final appearance of the sandwich structured composite samples. 65

D.1 Free body diagram of the entire 3-point-bending configuration and of a small section. 69
D.2 Free body diagram of the entire cantilever beam configuration and of a small section. 70

G.1 A simple representation of the tower's circular cross-section. 78

I.1 The influence of the fiber orientation and tower's radius on the modal damping loss factor of the first bending mode. Note that the tower's element length is $1m$ and the tower's wall thickness is $100mm$ 83
I.2 The influence of the fiber orientation and tower's length on the modal damping loss factor of the first bending mode. Note that the tower's radius is $5m$ and the tower's wall thickness is $100mm$ 84
I.3 The influence of the fiber orientation and tower's wall thickness on the modal damping loss factor of the first bending mode. Note that the tower's radius is $5m$ and the tower's element length is $1m$ 84

J.1 The influence of the fiber orientation and the core stiffness on the modal damping loss factor of the first bending mode. The symbol C represents the multiplication factor, which is multiplied by both the core's tensile//compressive modulus and the core's shear modulus. Both moduli are equal to the moduli of the Airex T92.80 foam material, which can be seen in Appendix C. Note that the tower's radius is $5m$, the tower's element length is $1m$ and the total thickness of the face sheets is $100mm$. The core has a thickness of $100mm$ as well and a loss factor of 0.1 for both axial and shear damping. 85
J.2 The influence of the fiber orientation and the core's loss factor on the modal damping loss factor of the first bending mode. Note that the tower's radius is $5m$, the tower's element length is $1m$ and the total thickness of the face sheets is $100mm$. The core has a thickness of $100mm$ as well and the moduli are same as for the Airex T92.80 foam. 86
J.3 The influence of the fiber orientation and the core thickness on the modal damping loss factor of the first bending mode. Note that the tower's radius is $5m$, the tower's element length is $1m$ and the total thickness of the face sheets is $100mm$. The core has a damping loss factor of 0.1 and the moduli are same as for the Airex T92.80 foam. 86

List of Tables

3.1 Table with the eigenfrequencies and frequency bands . . . 10

4.1 Sample properties and the corresponding strain energy ratios. . . . 22
4.2 Average loss factor at room temperature of the vinylester samples. . . . 24
4.3 Average loss factor at room temperature of the epoxy samples. . . . 25
4.4 Damping loss factors of the two resin systems at 1Hz and at room temperature. . . . 25
4.5 Measured damping loss factors of 90° GFRV laminates. . . . 26
4.6 Measured damping loss factors of 0° GFRV laminates. . . . 27
4.7 Measured damping loss factors of symmetrical ±45° GFRV laminates. . . . 27
4.8 Average loss factor at room temperature for the reinforced vinylester samples. . . . 27
4.9 Damping loss factors of the two reinforced (0 degrees orientation) resin systems at 1Hz and at room temperature. . . . 28
4.10 Average loss factors of steel. . . . 28
4.11 Damping loss factors of the various foams at a frequency of 3Hz and at room temperature [51]. . . . 30
4.12 Average loss factors for the Airex C70.75. . . . 31
4.13 Damping loss factors of the various PET foams at a frequency of 1Hz and at room temperature. . . . 32
4.14 Average loss factors of the Airex T92.80 samples. . . . 33
4.15 Average loss factors of the Airex T92.80X samples. . . . 33
4.16 Average loss factors of the sandwich structured GFRV. . . . 34
4.17 Damping loss factors of the various PET foams at a frequency of 1Hz and at room temperature. . . . 35
4.18 Loss factors of several composite material and one resin . . . 35

5.1 The damping loss factors of the material constituents and the composite ply at $1Hz$. . . . 38
5.2 Reduced damping loss factors of the composite ply at $1Hz$. . . . 38
5.3 Table with design parameters . . . 48
5.4 Modal damping loss factors of the first bending mode for three different frequencies. . . . 48
5.5 Material properties of steel. . . . 49
5.6 Comparison of the modal damping loss factors of the current composite design and a steel design. . . . 49

A.1 Average phase lags measured at certain frequencies and amplitudes. Note that the $*$ sign indicates that the sample has been removed and subsequently reclamped prior to testing and a ! indicates that each cycle has a incomparable phase lag. . . . 57
A.2 Average phase lags measured at a 0.1Hz frequency and several amplitudes for the second 0 degrees laminate sample. . . . 57
A.3 Average loss factors for the Airex T92.80. . . . 57
A.4 Average loss factors for the Airex T92.80. . . . 57
A.5 Average loss factors for the Airex T92.80. . . . 58
A.6 Average loss factors for the Airex T92.80. . . . 58
A.7 Average loss factors for the Airex T92.80. . . . 59
A.8 Average loss factors for the Airex T92.80. . . . 59

B.1 Table with all types of manufactured samples . . . 63

C.1 Table with the material properties of E-glass fibers [41]. . . . 67
C.2 Table with the material properties of VE370SC vinylester resin [78]. . . . 67
C.3 Table with the material properties of a fiber reinforced vinylester ply . . . 68
C.4 Table with the material properties of the Airex T92.80 core. . . . 68

H.1 Displacements due an axial load of 100 kN at the top of the tower. . . . 81
H.2 Displacements due an out-of-plane (bending) load of 100 kN at the top of the tower. . . . 82
H.3 Displacements due a torsional load of 100 kN at the top of the tower. . . . 82

1

Introduction

The transportation, installation and maintenance of offshore wind turbines is a very costly process. At the moment there are 289 offshore wind turbines in the Netherlands, which have a combined capacity of 957 MW. In the Agreement on Energy for Sustainable Growth it is stated that the total capacity of wind turbines should be at least 4450 MW [83] in 2023. This means that a significant number of wind turbines have to be build in the coming years. Although the increase of the wind turbine size results in a decrease of the amount of wind turbines that have to be build. In Figure 1.1 the development of wind turbines in time can be seen. [31]

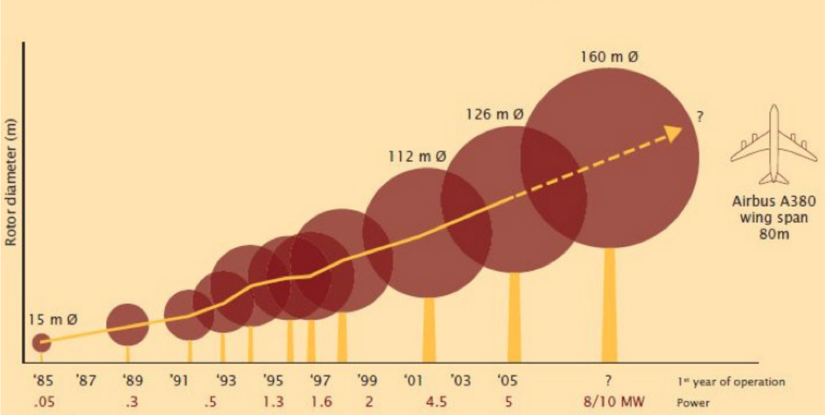

Figure 1.1: The development of wind turbines in time [31].

Still a large amount of wind turbines has to be placed in the coming years. Note that larger wind turbines require larger ships and/or updated cranes to transport and install the wind turbine parts, which obviously will increase the cost of placing [75]. The current guideline is to decrease these costs with 40% by 2020 [76].
Currently, Jules Dock is trying to achieve a cost saving by replacing the current steel tower design by a lighter composite design. This tower design can be up to 40% lighter than the steel tower design and therefore will result in a decrease of the installation and transportation costs. Also the tower is designed to carry a 10MW wind turbine, which will be the next generation of wind turbines [8].
In the last couple of years, only a limited amount of other public researches are performed to composite wind turbine towers. Most of these researches are limited to theoretical or small scale feasibility studies and do not consider the 1P and 3P loading [64], [79], [91]. A large scale feasibility project was the MegaWind project, which was funded by the European Commission. The resulting tower design of this project, was a heavy composite-concrete design[39].
Still no large scale and light weight design, considering all the dynamic loadings has been manufactured.

In order to decrease the weight as much as possible, the composite tower design will be a flexible design, which is possible due to the nature of the material and the fact that the frequency of the 10MW rotor's 1P frequency band coincides with the statistical wave frequency band of the North Sea [8]. This project is in cooperation with the company WMC, which is responsible for calculating the tower's mechanical and dynamical properties and the tower's fatigue life.

Since a flexible design has been chosen, the damping properties and the level of fatigue in the laminate will be important factors. The higher the damping properties of the tower, the longer the fatigue life [43]. According to WMC, an increase

in the structural damping does not result in a significant fatigue life increase in the fore-aft direction, since the most dominant damping mechanism in this direction is the aerodynamic damping. The aerodynamic damping can even be maximized for several wind velocities by altering the wind turbine blades' pitch angle.
However, in the side-to-side direction, the aerodynamic damping mechanism can be considered insignificant and therefore an increase in the material damping will result in a significant increase of the tower's fatigue life.
The current design applies a material damping ratio of 1%, which is approximately the maximum value for steel wind turbine towers. This value can be considered low. Composite materials on the other hand show better damping capabilities depending on the design of the composite material. [15].
Currently only a small amount of public knowledge is present about the damping of low frequency vibrations in large composite towers and therefore a research is required. Also aspects like the loading frequency and the temperature have to be included.

In Chapter 2 the project plan is discussed. In the project plan the research objective, the research questions, the used methodology, the experimental set-ups, the planning and the desired outcomes are discussed.
In Chapter 3 the literature study can be found, which will comprise of general background information about the dynamic behavior of wind turbines, of information about the damping capabilities of composite materials and of information about several damping definitions and models.
In Chapter 4 the DMA measurements, in Chapter 5 the wind turbine's damping model and in Chapter 6 the conclusions and recommendations will be discussed.

2

Project plan

In this chapter a description of the proposed research plan will be given. Among others the objective, research question, methodologies, experimental test set-ups, the desired outcomes and the project planning will be discussed.

2.1. Research question, aims and objectives

The research objective of this thesis is to determine the material damping ratio of the flexible tower, which is made of glass fiber reinforced sandwich-structured composite, and to gain knowledge about the influence of the laminate design and external factors on the damping ratio. This is done by applying both analytical and numerical models and by performing experimental tests. WMC or another party could use the resulting knowledge model to increase the fatigue life of the current flexible design, which uses the damping ratio of a steel wind turbine tower. The damping due to the structural connections will be considered outside the scope of this research and therefore only the material damping will be considered.
Note that the parameters of the composite wind turbine tower's current design (dimensions, used materials and corresponding material properties, etc.) will serve as an input for the damping model. The damping properties of the material constituents will be measured by performing experimental tests.

The subgoals of this project are:

- Determine the damping properties of the material constituents (in this case E-glass fibers, a vinylester matrix and an Airex T92.80 core).
- Determine the damping loss factors of a composite ply.
- Calculate the damping ratio of the current conical thin walled tower using the damping loss factor of the composite ply.
- Gain general knowledge about why and how certain material/structural properties improve the damping capability of the tower.
- Determine the relation between the loading frequency and the damping loss factor of the matrix and core.
- Determine the influence of environmental factors, like temperature , on the damping ratio of the matrix and core.

The research question of this project will be:

What is the material damping of a flexible composite tower, made of a glass fiber reinforced sandwich-structured composite, and in which way are the tower's damping capabilities affected by the loading frequency and temperature?

Subquestions of this research question are:

- What are the damping properties (loss factor and damping ratio) of the material constituents?
- What is the frequency, temperature and amplitude dependency of the damping properties of these material constituents (fibers, matrix and core)?
- In which way can the damping properties of the constituents (fibers, matrix and core) be converted to the damping properties of the laminate using one of the discussed methods?
- In which way can the current design (materials, fiber orientations, stacking sequence, core thickness, etc) be altered in order to improve the damping ratio?

The research questions and objectives are derived by applying the SMART principle. In order to achieve the main objective and to answer the research question, each of these subquestions have to be answered. Note that the answers to these research questions are unknown for large composite structures and therefore the answers will contribute to the general body of knowledge.

2.2. Theoretical Content/Methodology

According to the literature presented in Chapter 3, most of the research is done to the damping properties of simple composite beams. The analytical/numerical solutions proposed in the literature are therefore very limited. In order to calculate the damping properties of a hollow conical structure a discretization of the structure should be applied or a finite element method (FEM) should be used. There are several models capable of determining the damping loss factor of composite structures. However, Chortis' model [31] in combination with a simple micromechanical model, like the Saravanos-Chamis micromechanical model, seems to be the most suitable manner to determine the tower's damping loss factor.

Both methods can be implemented in MATLAB. Besides, a FEM based program, like Abaqus, can be used to validate certain parts of the model.

The theories that should be applied are listed below.

- **Classical Laminate Theory**: Estimation of the material properties of a composite laminate
- **Material viscoelasticity**: Theory on the viscoelastic behavior of the composite material, to understand the influence of the loading frequency and temperature on the tower's damping behavior.
- **Structural mechanics**: Required in order to estimate the effects of the composite wind turbine's structure.

2.3. Experimental Set-up

In order to determine the damping loss factors of the material constituents, to determine the influence of temperature and frequency, and to validate the analytical/numerical results. It is required to perform experimental tests. In the subsections below, the proposed tests and their purposes can be found.

2.3.1. DMA test

An easy manner to determine the damping loss factors, which are required for the proposed methods, is by performing tests like Dynamic Mechanical Analysis (DMA) or Laser Scanning Vibrometry. By applying these tests, the damping loss factor of the matrix and/or polymeric core can be determined. Also the frequency and amplitude dependency of the viscoelastic materials can be tested.

In order to validate the results of the applied methods, first of all small laminate specimen should be tested. This can be done by DMA or another 'To Be Determined (TBD)' method.

2.3.2. Other experimental tests

Probably other experimental tests have to be performed in order to determine other material properties or in order to validate the current model. Each of these material properties requires a different test set up, e.g. in case of the elastic modulus, a draw bench can be used. Which material properties are required to know and what the corresponding test set-ups will be, will be determined during the actual project.

2.4. Results, Outcome and Relevance

As stated before, the most important output is the modal damping ratio, which serves as a new input for Jules Dock's current design. According to WMC, a 10% increase of the structural damping ratio results in a significant increase of the structure's fatigue life. Note that the model will only incorporate material damping and therefore the final output might differ considerably from reality.

Other desired outcomes of this research are:

- To have knowledge of the temperature's influence on the tower's damping ratio.
- To have knowledge of the loading frequency's influence on the tower's damping ratio.
- To know how to optimize the tower for damping.

The first two outcomes of the list are quite relevant, since they tell something about the sensitivity to external factors of the current design. The last outcome is the least relevant, since the current design does not allow large changes in the laminate. The overall accuracy of the results and therefore the feasibility of this research depends on the applied models and whether or not the other damping mechanisms and other loads can be neglected.

The verification of the model will be done by checking whether the model does what it is supposed to do. This is done by quality control (e.g. testing and debugging of the Matlab code) and sensitivity analyses.

2.5. Project Planning

In general the planning consists of two parts. First of all, the damping properties of the fibers, matrix and core have to be determined. This is done by preparing and performing DMA tests. The other required and unknown material properties will be determined by performing 'TBD' experimental tests. The results of the DMA and the other tests serve as an input for the created model. In case these results are not reliable, the samples should be improved and/or another measurement method should be used. Subsequently, a model will be created in order to determine the damping properties of the current model. Finally, the model will be validated. In case the analytical results differ too much from reality, the model should be altered and validated again. In Figure 2.1 the project's flow chart can be seen.

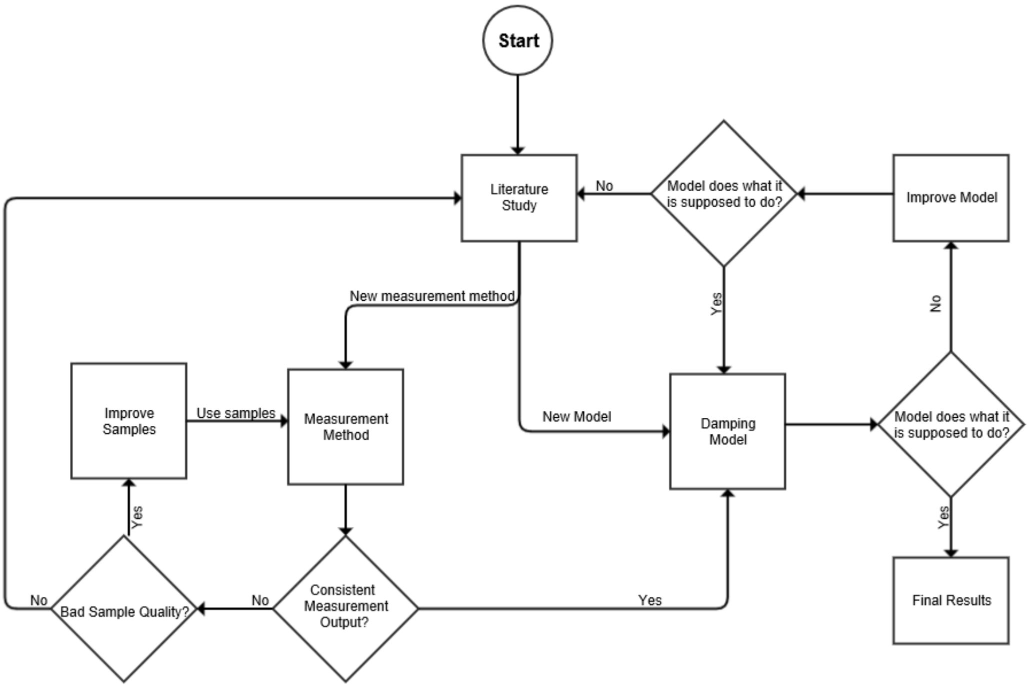
Start
Literature Study
No
Model does what it is supposed to do?
Improve Model
New measurement method
Yes
No
Improve Samples
Use samples
Measurement Method
New Model
Damping Model
Model does what it is supposed to do?
Yes
Yes
Final Results
No
Bad Sample Quality?
No
Consistent Measurement Output?
Yes

Figure 2.1: The flow chart of the Master's Thesis Project.

3

Background information

In this chapter background information is given regarding wind turbines and the dynamics of wind turbine towers. Besides, some insight will be given into the dynamic behavior of the current composite tower design.

3.1. The dynamic loading on a wind turbine tower

An offshore wind turbine tower is a unique tall structure with a slender geometry and a heavy mass at the top. A typical wind turbine consists of several components. [65]
These are:

- The nacelle, which houses the generator, the gearbox and several other systems. The wind turbine blades (typically three blades) are attached to the nacelle.
- The tower, which supports the nacelle.
- The support structure, which supports the whole tower-nacelle structure. The tower is mounted to a transition piece, which in turn is connected to the rest of the support structure. There are several types of support structures, e.g. monopiles, jacket structures, tripod structures, gravity based structures and floating structures.

  A variety of support structures can be seen in Figure 3.1 [65].

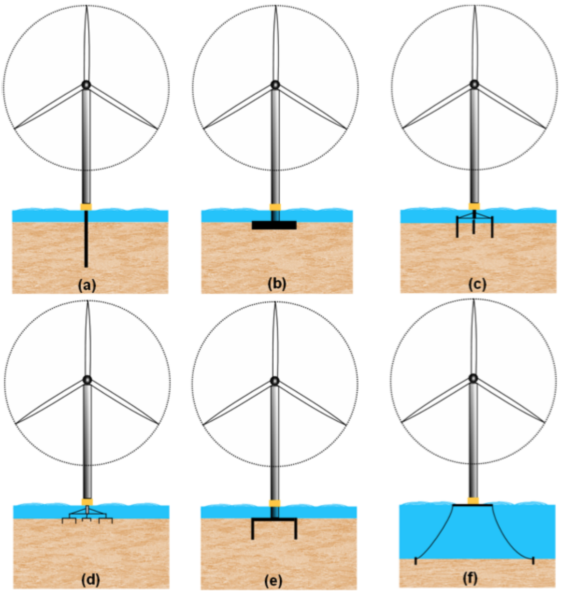

Figure 3.1: Examples of several types of support structures [65].

Typically a wind turbine structure is subjected to four different main loads: wind, wave, 1P and 3P [74]. The loads imposed by the wind and waves are variable in both space en time and therefore they are often described statistically. Also both loads can be considered independent of each other, since they may act in two different directions. The 1P loading is due to the constant rotations of the rotor and is caused by mass and aerodynamic imbalances. The 2P/3P loading (the 2 or 3 indicates the amount of wind turbine blades) is due to the blades passing the tower. Both the 1P and 3P loading are cyclic and can be described by a frequency. Also two types of rotors can be considered: a constant rotational speed rotor and a variable rotational speed rotor. The constant rational speed type typically has fixed 1P and 3P frequencies, while a variable rotational speed turbine has 1P and 3P frequency bands. Most wind turbines possess variable rotational speed rotors and therefore they have frequency bands. In Figure 3.2 several loading frequencies can be seen [74].

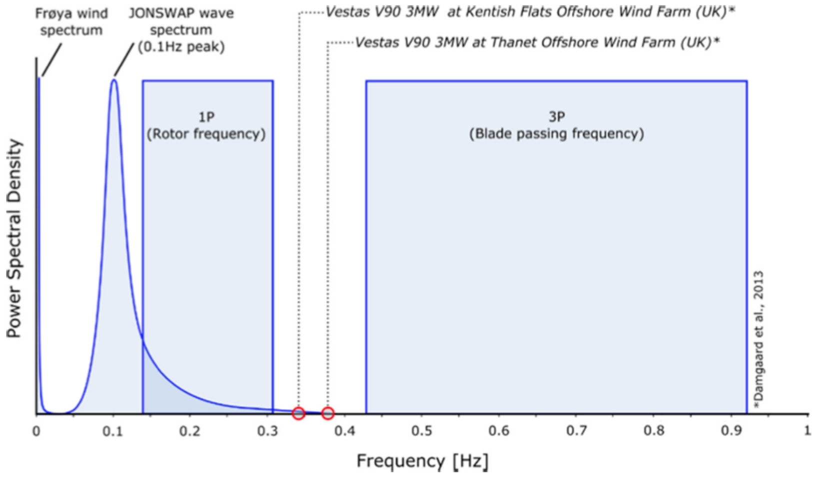

Figure 3.2: Example of the several loading frequency bands [74].

Note that larger rotors, like a 10MW rotor, will result in a lower 1P frequency band, which will coincide with the wave frequency band [8]. This means that the wave loading does not have to be considered.
A typical wind turbine design is a dynamic system subjected to low frequency vibrations. Just as every dynamic system, the system can be described by a set of spring stiffnesses and damping coefficients. This kind of system can be seen in Figure 3.3 [6].

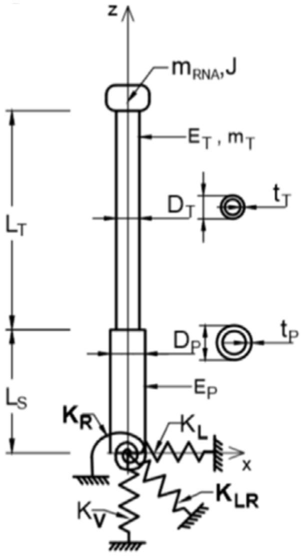

Figure 3.3: Basic mathematical model of an Offshore Wind Turbine [6].

In Figure 3.3 several components can be recognized: The top load or nacelle, the tower and the support structure. The spring stiffnesses k_v, k_L, k_r, k_{LR} describe the elasticity of the soil. The section with the diameter D_p is the monopile, while the section with the diameter D_t is the wind turbine tower. Note that this simple representation does not contain the system's damping mechanisms. In general the dynamic behavior of the tower can be described by Equation 3.1 [13].

$$[M]\ddot{u} + [C]\dot{u} + [K]u = F(t) \tag{3.1}$$

Here $\ddot{u}$, $\dot{u}$ and u are the acceleration, velocity and displacement matrices respectively. $[M]$ is the mass matrix, $[C]$ is the damping matrix, $[K]$ is the stiffness matrix and $F(t)$ is the time dependent force matrix.
The undamped eigen frequencies of the system can be computed by applying Equation 3.2 [30], [20].

$$\omega_n = \sqrt{\frac{[K]}{[M]}} \tag{3.2}$$

Note that complex systems like a wind turbine tower have a matrix of natural frequencies. Subsequently, the damped eigenfrequency of the system can easily be obtained by applying Equation 3.3 [13], [6].

$$\omega_d = (I - \zeta)\omega_n \tag{3.3}$$

Here I is the identity matrix and ζ is the matrix of the system's damping ratios, which can be described by Equation 3.4 [20].

$$\zeta = \frac{[C]}{[C_{crit}]} = \frac{[C]}{2[M]\omega_n} \tag{3.4}$$

Here $[C_{crit}]$ is the critical damping matrix.
Obviously, the damped natural or eigenfrequencies of the structure should not coincide with the frequencies of the occurring loads, since this will result in structural resonance. Note that each eigenfrequency corresponds to a certain eigenmode. In Figure 3.4 the first four eigenmodes can be observed [11].

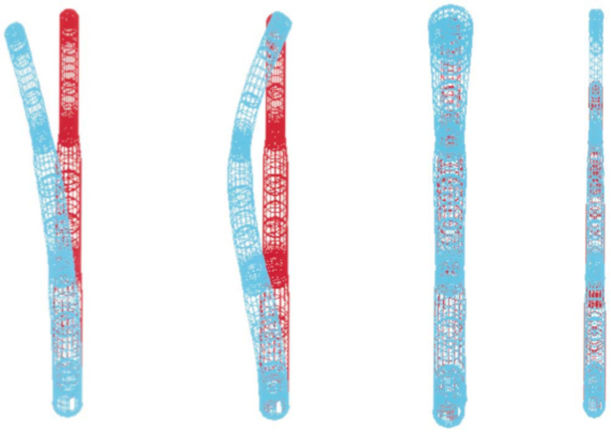

Figure 3.4: The first four eigenmodes of an offshore wind turbine tower. These eigenmodes are from left to right: first bending mode, second bending mode, torsion and axial displacement [11].

The first eigenmode corresponds to first bending mode, the second eigenmode to the second bending mode, the third to torsion and the fourth to the axial displacement. According to WMC, the first two eigenmodes are the most critical [102]. One should design the tower in such a manner that the eigenfrequencies will not coincide with the described loading frequencies. Three different design types are possible [6]:

- Soft-soft designs: The first eigenfrequency lies below the 1P frequency band. Typically these designs are very flexible and will result in the lightest possible designs. These designs are usable for floating support structures, however they are considered practically impossible for fixed steel wind turbine towers. This is due to the fact that steel lacks the required flexibility. A composite tower on the other hand might be possible. Also the wave frequency could result in high dynamic amplifications. This depends on the type of rotor, since larger rotors will result in a 1P frequency band with lower loading frequencies.
- Soft-stiff designs: The first eigenfrequency lies between the 1P and 3P frequency bands. These designs are the most common designs for fixed steel wind turbine towers.
- Stiff-stiff designs: The first eigenfrequency lies above the 3P frequency band. These designs result in extremely stiff, massive and heavy towers. Since these towers also require a large support structure, they are considered uneconomic.

In case of the current composite tower design, the first eigenfrequency lies below the 1P frequency band, while the second eigenfrequency lies above the 3P frequency band [102]. This means that the current design is a Soft-soft design, which is unique for offshore wind turbines.

Table 3.1: Table with the eigenfrequencies and frequency bands

Parameter	**Value**
1P range	$0.101 - 0.176 Hz$
3P range	$0.302 - 0.528 Hz$
First fore-aft eigenfrequency	$0.1 Hz$
Second fore-aft eigenfrequency	$0.83 Hz$
First side-to-side eigenfrequency	$0.1 Hz$
Second side-to-side eigenfrequency	$0.57 Hz$

3.2. Damping mechanisms of wind turbines

In general, wind turbine towers have two vibrational directions: the fore-aft and the side-to-side directions. The vibrations in these two directions are damped by several components of the system. The total damping of the entire system can be represented by Equation 3.5 [6], [30].

$$\zeta_{total} = \zeta_{aero} + \zeta_{struct} + \zeta_{soil} + \zeta_{hydro} + \zeta_{damper} \tag{3.5}$$

Here: [6], [30]

- ζ_{aero} is the aerodynamic damping ratio. Aerodynamic damping is a result of the relative velocity between the wind turbine and the surrounding air. A non-operational wind turbine has a similar aerodynamic damping in the fore-aft direction as in the side-to-side direction. An operating wind turbine on the other hand has more damping in the fore-aft direction than in the side-to-side direction due to the interaction between the rotating blades and the air flow.
- ζ_{struct} is the structural damping ratio. Structural damping consists of both material damping or hysteric damping, which dissipates energy in the form of heat and damping due to the overall structure and joints. Also the type of support structure influences the structural damping. Note that a difference can be made between the structural damping ratio of the flexible tower and the structural damping ratio of the stiff support structure.
- ζ_{soil} is the damping ratio due to the soil. Soil damping is due to the soil-structure interaction, which exists of soil material damping, wave radiation damping and pore fluid induced damping. The soil-structure interaction depends on the type of soil, the soil strain and the support structure. There are two types of soils: cohesionless soils like loose sand and cohesive soils like clay. In case the frequency of the support structure is below 1 Hz, the wave radiation damping and pore fluid induced damping will be negligible small.
- ζ_{hydro} is the hydrodynamic damping ratio. The hydrodynamic damping is due to the wave radiation damping and viscous damping. However, normally for low frequency structures viscous damping is low. The amount of hydrodynamic damping also depends on the depth of the sea.
- ζ_{damper} is the damping ratio due to additional dampers like slosh dampers.

The various damping mechanisms will be discussed in Section 3.3. Note that ζ_{soil} and ζ_{hydro} and therefore the total amount of damping of the tower depends on the kind of support structure. For example a floating support structure will not have any soil damping.

As mentioned before, the structural damping ζ_{struc} can be divided in the damping due to the structural connections and material damping. In case of the composite tower, T-bolt connections can be found both at the top and at the bottom of the tower [102]. Structural connections like bolted joints can contribute up to 90% of the structural damping [104]. The main damping source at the structural connections is friction due to the micro-slip and/or macro-slip at the contacting surfaces [104].
In general, the structural damping of bolted joints are affected by four major factors [104]:

- friction coefficients of the contacting surfaces
- bolt preload
- clamping boundary conditions
- micro-slip or macro-slip between the bolted surfaces.

Beside these four mechanisms, also the loading amplitude will have a significant effect on the structural damping of the bolted joints [61], [17]. This type of damping is therefore non-linear.

According to WMC, the structural damping ratio of a general steel wind turbine tower and monopile is approximately 1% [102] of which a significant part will be caused by the structural connections. In case of the composite wind turbine tower the structural damping of the bolted joints will probably be significant as well. Due to the viscoelastic nature of the composite material, a higher amount of material damping can also be expected. Since there are an endless amount of possibilities in connecting the several parts of the wind turbine, the damping due to the structural connections will almost be impossible to estimate. The material damping on the other hand depends solely on the type of material and therefore will be more practical to estimate. Hence, this research will mainly be focused on estimating the material damping of the composite tower design.

3.3. Material damping

Damping is a property, which is present in every structure and is the reason that the vibrational amplitude of every free vibrating structure will decay to zero [49]. Typically, it can be described as the amount of energy dissipated from a certain system to its environment [95]. Therefore it is a valuable property of every vibrating structure, since the higher the damping capabilities of a structure the faster the amplitude stress decays to zero. Obviously, this is beneficial for the fatigue life of the structure [43]. Several types of damping mechanisms can be distinguished.

3.3.1. Viscous damping

Viscous damping is the result of the system moving through a viscous fluid. The energy of the system will be dissipated from the system due to the resistance offered by the shearing fluid. Typically, viscous damping depends on the viscosity of the fluid, velocity and frequency of the moving system, and the amplitude of the vibrations. An example of a pure viscous damper is a dashpot. [20]

3.3.2. Hysteretic

Hysteretic or internal damping is a damping mechanism, which occurs inside the material. Due to the deforming of the material, internal planes, grains or molecules tend to slide along each other. This results in internal friction, which dissipates energy from the system and converts it to heat. This type of damping is in phase with the vibrations and proportional to the displacements of the system. Also its magnitude is independent of the frequency. [20]

Hysteretic damping can typically be depicted by a stress-strain curve. The stress-strain behavior during loading is different than during unloading. The difference between those curves can be seen as the amount of dissipated energy during one cycle. Another name for such a stress-strain curve is a hysteresis loop. In Figure 3.5 a typical hysteresis loop can be seen [101].

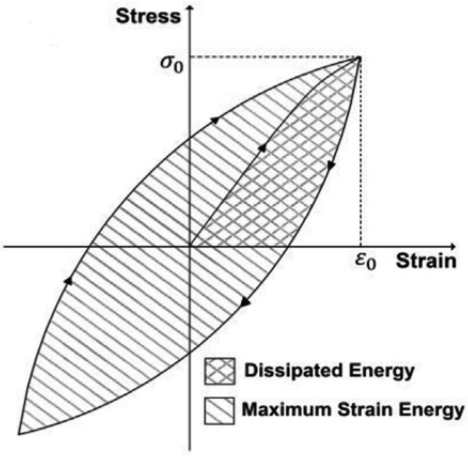

Figure 3.5: An example of the hysteresis loop. Here σ is the stress and ϵ the strain [101].

3.3.3. Coulomb

Coulomb damping is due to the friction induced by the sliding of two dry surfaces. This friction depends on the normal force and therefore the mass of the sliding objects. Just as hysteretic damping, Coulomb damping is frequency independent and converts the dissipated energy into heat [20].

3.3.4. Radiational damping

Radiational damping differs from the other damping mechanisms, since it dissipates the energy by passing on the vibrational energy to another medium. For example, a vibrating monopile will dissipate its energy by generating waves in the water. Subsequently these waves will spread in all directions and distribute their energy over a larger surface. The spreading results in a decreasing wave amplitude. The higher the density of the medium, the higher the amount of dissipated energy. Therefore the radiational damping of air is negligible small, while the radiational damping of water is significant [98].

3.4. Damping of composite materials

As mentioned in Section 3.1, steel towers lack the flexibility for a soft-soft design. Composites on the other hand are in general much more flexible and therefore more suited. In terms of damping, composites perform better as well, which can be seen in Figure 3.6 [72].

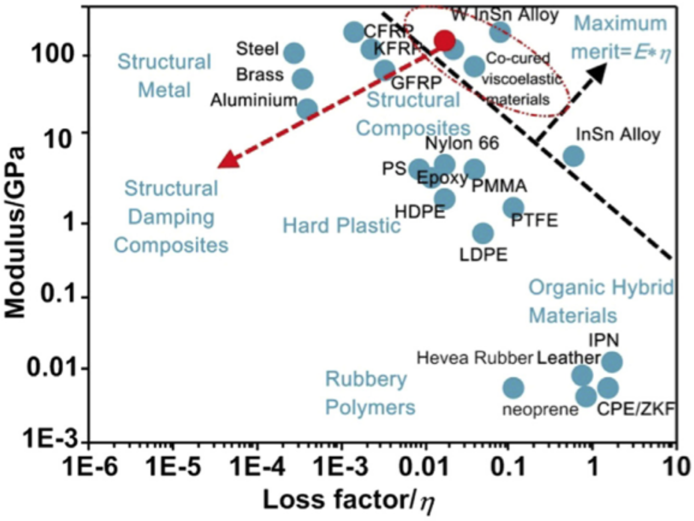

Figure 3.6: Modulus-loss factor map of some common materials at room temperature at 1 Hz [72].

Figure 3.6 shows that metals possess a high stiffness in general, but a low damping loss factor, while polymers like rubber possess a high damping loss factor but a low stiffness. Composites on the other hand can obtain both a high stiffness and a high damping loss factor depending on the design of the composite material. In order to design a structural damping composite (high stiffness and high damping), one should maximize Equation 3.6.

$$MaximumMerit = E\eta \tag{3.6}$$

Here E is the young's modulus and η is the damping loss factor.

In general five different damping principles can be distinguished for composites [24],[26], [95]. These damping principles are:

- Viscoelastic damping
- Damping due to the fiber-matrix interphase
- Damping due to damage
- Viscoplastic damping
- Thermoelastic damping

Each of these principles will be discussed briefly in the following subsections.

3.4.1. Viscoelastic damping

In general all polymer based materials can be considered viscoelastic. This means that the material possesses both elastic and viscous material properties. In Figure 3.7 the difference between the response of an elastic, a viscous and a viscoelastic material can be seen. [66]

In Figure 3.7(a) the stress-strain response of a purely elastic material can be seen. A purely elastic material stores all of its energy during loading and releases this energy again during unloading. Due to this, the stress and the strain will be in phase. Therefore, the elastic response can be described by Hooke's law [66].

The stress-strain response of a purely viscous material, which can be seen in Figure 3.7(b), is totally different. A purely viscous material will not release any of the stored energy when the load is removed. Therefore, a purely viscous material

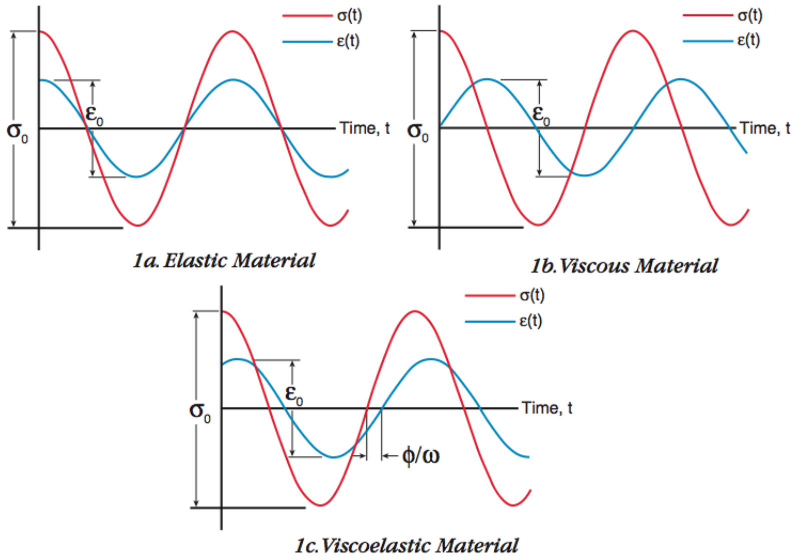

Figure 3.7: The stress-strain response of an elastic (a), viscous (b) and viscoelastic (c) material [66].

will not have a stiffness component but only a loss factor. The maximum stress in a viscous material occurs at the maximum strain rate [66].

In Figure 3.7(c) the stress-strain response of a viscoelastic material can be seen. Viscoelastic materials only release a part of the stored energy, while the other part is dissipated as heat. Therefore the frequency of the stress/load is out of phase with the strain frequency by a certain angle ϕ. This angle is called the phase lag angle. The higher the viscosity of the viscoelastic material, the higher this angle will be. A viscoelastic material can be described by a complex modulus, seen in Equation 3.7. [106]

$$E^* = E' + iE'' \tag{3.7}$$

Here E'' and E' are the loss and storage modulus respectively. Note that E' is a measure of the material's stiffness, while E'' is a measure of the material's energy dissipation. Beside a complex modulus there is a complex shear modulus as well (and therefore G' and G'').

In general there are several models capable of predicting viscoelastic behavior. These models estimate the viscoelastic behavior by combining an elastic spring and a viscous dashpot. How these are combined depends on the model. There are three common models, which can be seen in Figure 3.8. [100], [106]

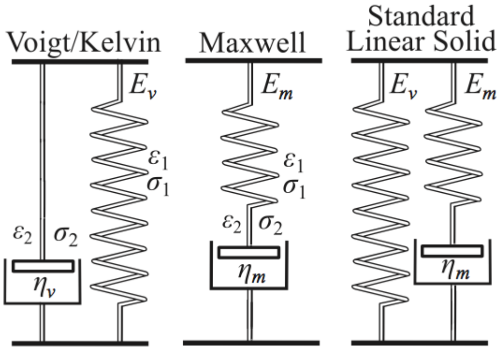

Figure 3.8: Several viscoelastic models [100].

The Maxwell model is a simple model which predicts the relaxation of viscoelastic materials quite accurate, while it results in a bad estimation of the creep behavior [100]. The Kelvin-Voigt model on the other hand predicts the creep behavior accurately, but results in a bad prediction of the relaxation [100]. The standard linear solid model predicts both the creep behavior and the relaxation pretty well, however it is more complicated and under certain loading conditions it returns inaccurate results for the strain [100].

Composites are a mix of different kind of materials and therefore the viscoelastic damping will be a combination of the fibers and the matrix as well. In general the damping capabilities of the fibers can be neglected except those of kevlar and polymeric fibers, since these fibers show good damping properties [24]. The matrix on the other hand has the best viscoelastic damping properties and therefore the viscoelastic damping of composites is mainly determined by the viscoelasticity of the matrix. Also this means that the damping properties are depending on the vibration mode or in other words on the direction of damping. According to Schultz and Tsai [88], in many cases the excitation amplitude strongly affects the damping ratio of the first eigenmode of a fiber reinforced beam. This is called non-linear viscoelastic damping. However, in case both the elastic stiffness and viscous damping are independent of vibration amplitude, which appears to be the case for undamaged and properly bonded composites vibrating at low strain amplitudes, linear viscoelastic damping can be assumed [48], [35], [47].

3.4.2. Damping due to the fiber-matrix interphase

The damping due to the fiber-matrix interphase can be considered a different principle of damping than viscoelastic damping. This is due to fact that the interphase region shows both viscoelastic damping as coulomb damping. The interphase is composed of polymeric particles, which are bonded to the fiber or the coating of the fiber [46].
The damping properties of the interphase region depend on both the bonding strength and the interphase stiffness [12]. A perfectly bonded interphase region can be assumed to have the same properties as the matrix and only shows viscoelastic damping. For a composite without an interphase (fibers are isolated from the matrix), the damping properties of the composite are slightly worse than a composite with a perfectly bonded interphase, however the amount of damping depends on the coulomb friction between the matrix and the fiber. A degraded interphase on the other hand shows a large increase in damping and shows both viscoelastic as coulomb damping. A degraded interphase means a loss in other properties as well.

In case of a perfectly bonded fiber-matrix interphase, the influence of the stiffness of the interphase is almost negligible small [82]. For a partly degraded interphase the damping capabilities of the composite can be altered drastically by using a different interphase stiffness (stiffness is as a percentage of the matrix stiffness) [12].
Note that the amount of damping due to the interphase also depends on the direction of damping [12]. For the model presented in Chapter 5, it is assumed that the matrix and the fibers are perfectly bonded and therefore the damping capabilities can be assumed to be equal to the damping capabilities of the matrix.

3.4.3. Damping due to damage

A remarkable treat of composites is that damage has a positive effect on the damping properties of the material. According to Zhang [109], damage results in a decrease of mechanical properties like the shear modulus, while it will result in an increase of the damping loss factor. Apparently, microcracks and other types of damage in the composite laminate are beneficial for the damping properties due to the extra friction they induce. The larger the cracks and debonding, the higher the damping loss factor. Zhuang [62] concluded the same effect for delamination. Apparently a larger amount of delamination results in more energy dissipation and therefore a higher loss factor. Note that the energy dissipation at cracks and delamination sites is not fully understood [48]. In general the influence of damage on the damping capabilities of the structure is complex and non-linear, i.e. it is amplitude dependent [35]. Also in the current design of the wind turbine tower, the damage initiation and propagations is not considered and therefore damping due to damage is beyond the scope of this research.

3.4.4. Viscoplastic damping

Viscoplastic damping is the damping induced by deforming a (thermoplastic) polymer, metal or a polymeric fiber, like an aramid fiber [22], plastically [53]. For high load cycles/high stress levels thermoplastic composites show a lot of plastic deformation. The plastic deformation results in a temporary higher energy dissipation and therefore will result in a higher damping loss factor. The plastic deformation also results in strain hardening and therefore the damping loss factor will decrease. The viscoplastic damping will therefore at its peak at the moment plastic deformation occurs.

3.4.5. Thermoelastic damping

The last of the five damping principles is thermoelastic damping. This type of damping has been researched by Lakes [57] and occurs at high temperature increases due to cyclic heating. Vibrations will result in fast elastic deformations in the composite material. Due to these deformations the compressive region becomes hotter while the extended region becomes colder (assuming a positive thermal expansion coefficient). Due to this thermal imbalance, a heat gradient starts to exist [108]. This heat gradient results in a heat flow, which dissipates energy from the vibrations. In general this damping mechanism is mainly present in metal based composites [16], although It has been proven that it occurs to some extent in thermoplastic composites as well. Especially if there is a high degree of cyclic heating [24]. Despite of this fact the thermoelastic damping will be neglected for the wind turbine's damping model.

3.5. Factors influencing damping

There are several factors influencing the damping properties of the composite material. Three main factors can be recognized, namely the laminate parameters (e.g. fiber volume, fiber orientation, etc), external factors (e.g. temperature) and (cyclic) loading. Note that for the current design only the damping capabilities of continuous fiber reinforced sandwich composites are relevant. Therefore other composite types like metal composites, sphere reinforced composites, chopped fiber reinforced composites, etc. will not be considered.

3.5.1. Laminate parameters

The damping of composite materials is obviously affected by their material properties and laminate parameters. In this subsection the effect of several laminate parameters will be discussed. The current wind turbine tower design exists of continuous composite laminates. Composite material properties like fiber length and fiber distribution will therefore not be discussed.

Fiber volume and related parameters

In Section 3.4 it was stated that the matrix is the main component determining the damping capabilities of a composite. This means that a lower fiber volume is beneficial for the damping loss factor, since this results in a larger influence of the matrix [40], [73]. This also means that the damping capabilities of composite materials depend on the direction of damping, since in certain directions the matrix will have a larger influence (i.e. in the direction perpendicular to the fiber). In the transverse directions this difference is mainly due to the difference in fiber spacing, fiber size and fiber shape [110], [77].

Fiber orientation

Obviously the fiber orientation will influence the damping capabilities of the composite as well. This effect also depends on the direction of damping, since each damping direction has an ideal fiber orientation. For example, in case a composite beam is subjected to a flexural vibration, the ideal fiber orientation will be approximately 35° [2]. This is due to the fact that both the damping coefficients in the x and xy directions are large, while the shear modulus is low. Besides the Q_{16} term of the transformed stiffness matrix is at its maximum at an fiber orientation of 30° [2]. This results in a large energy dissipation in shear [2], [15], [105], [40]. On the other hand, a fiber orientation of 0° results in the worst damping properties, due to the high stiffness moduli and low damping loss factors. In case of a torsional vibration, the ideal fiber orientation will be approximately 35° as well [2]. For angle ply composites, the ideal fiber orientation will be different. This is due to the fact that angle plies contain both the plus and minus orientation of a certain fiber angle and therefore certain terms of the ABD-matrix will be zero or small [2]. For example for an angle ply laminate with an even amount of plies, the D_{16} and D_{26} terms will be zero.

Fiber stacking sequence

Another parameter affecting the damping capabilities of a composite laminate is the fiber stacking. Naturally, this parameter is related to the fiber orientation, since the fiber orientation determines the influence of each layer in a composite. In general, the influence of a certain ply increases with an increasing distance to the neutral axis of the composite laminate [67], [33]. By applying the most beneficial fiber orientations to the outer laminate plies, the damping effect due to these plies will increase even more.

Core and viscoelastic layers

In case of a sandwich structured composite, the composite will exist of composite face sheets and a light weight core material. The damping capabilities of the core are influenced by several parameters like material, density, frequency, thickness and the damping mode [87], [7]. A viscoelastic core material with a high damping loss factor, could increase the damping properties of a sandwich structured composite significantly. However, this is only the case when the core's stiffness in a certain direction is sufficiently high compared to the overall stiffness of the sandwich in the same direction [58]. A more drastic increase of the damping loss factor can be achieved by using viscoelastic layers between the plies. Just as a core, these layers are depending on the frequency, thickness, material and damping mode [105], [72]. Also in order to have a significant effect on the overall damping, the stiffness of these layers should be sufficiently high compared to the composite material. In case of a low modulus viscoelastic layer, its influence on the overall damping can be increased by adding very stiff particles to the viscoelastic material. This increases the stiffness of the viscoelastic layer, while the original damping of the layer is barely affected [58]

3.5.2. Other factors

Beside laminate parameters, also a lot of other factors are influencing the damping capabilities of the composite laminate. These factors can be divided in environmental factors and other factors. The main environmental factors are temperature [19], water absorption [107], [5], [38] and UV radiation [90], [54]. Of these, the influence of UV radiation and water absorption can be countered by a protective coating.

The other factors that are influencing a composite laminate's damping loss factors are physical aging [92], [18], [68], the

loading frequency [15], fatigue [109] and cyclic heating [56], [55], [89]. As stated before, all damage related influences and therefore all influence due to fatigue will be neglected. Also it is assumed that the thermoset matrix has been fully and perfectly cured and that therefore the influence of the physical aging can be neglected [29]. The influence of the cyclic heating can be considered similar to the influence of the temperature and will therefore not be treated.
In short, the two influencing factors that must be considered are the temperature and the loading frequency.

Temperature

The matrix of a composite material is often a polymer in its glassy state and therefore the operational temperature will be below the matrix' glass transition temperature (T_g). Below the T_g, the internal polymer segments are 'frozen' [106] and therefore the damping properties of the matrix are low [19]. Above its T_g a part of these segments are defrosted and therefore the matrix will become rubbery [106]. Normally, this is undesirable since this results in a huge stiffness drop [19]. However, at the same time the damping loss factor increases drastically, which is beneficial for vibrational structures. The peak of the damping loss factor is located at the temperature at which the internal friction between the 'frozen' polymer segments and the 'defrosted' polymer segments is at its maximum. In general, this temperature is close to the T_g at low frequency vibrations [59], [19]. Normally the damping peak at a 1 Hz frequency is $15°C$ to $20°C$ above the material's T_g. In Figure 3.9, the relation between damping loss factor and the temperature can be seen [19].

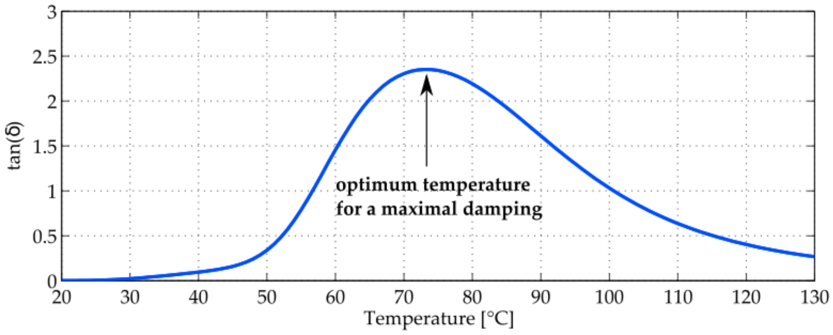

Figure 3.9: A typical temperature-damping curve [19].

Frequency

A unique feature of viscous and viscoelastic materials is that the damping loss factor depends on the frequency of the vibration. This is caused by the viscous damping of the material. Therefore the damping loss factor of a certain composite laminate is depending on the frequency as well. The frequency response of the stiff composite plies can be seen in Figure 3.10 [15].

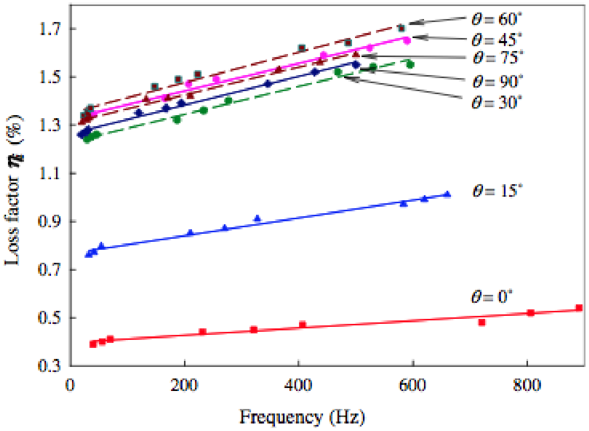

Figure 3.10: The relation between the frequency and the damping loss factor for a 'stiff' composite laminate. Note that the relation depends on the fiber orientation [15].

3.6. Theories on damping

In order to measure and estimate the damping behavior of a certain composite structure, some basic information has to be known about the different quantities of damping and about the several models that are capable of estimating these quantities.

3.6.1. Quantities of damping

There are several quantities of damping e.g. the damping ratio, the loss tangent, the damping loss factor, the logarithmic decrement, etc. Also identification methods can be done both in the time as in the frequency domain. [98] In the following subsections, several damping measurement and identification methods will be discussed.

Amplitude decrement method

An easy way to determine the damping capabilities of a vibrating system is by applying the amplitude decrement method. In Figure 3.11 a decaying vibration in the time domain can be seen [63].

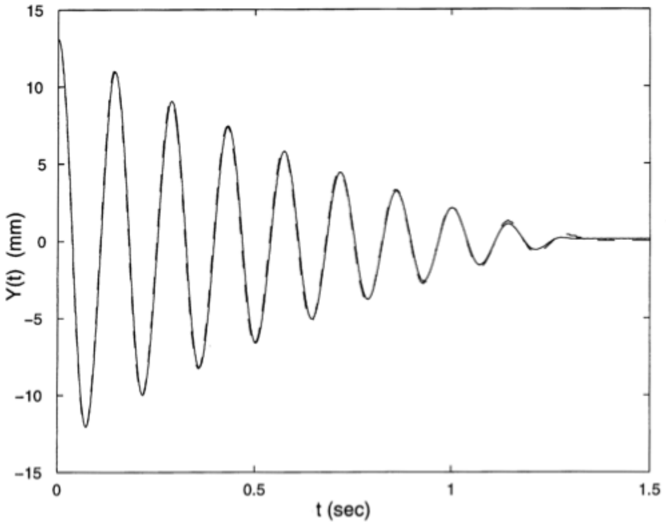

Figure 3.11: A simple representation of a decaying vibration [63].

This vibration is a typical response measured by a strain gauge or an accelerometer and can be expressed by Equation 3.8 [49].

$$x = Ae^{-\zeta\omega_n t} sin(\sqrt{1-\zeta^2}\omega_n t + \phi) \tag{3.8}$$

Here A is the amplitude of the vibration, ω_n the natural frequency, ϕ the phase of the vibration and ζ is the damping ratio. Note that ζ is a measure of the amount of damping relative to the critical damping of a system. In Equation 3.9 the definition of the damping ratio can be seen [49].

$$\zeta = \frac{c}{c_c} \tag{3.9}$$

Here c is the amount of damping of the system and c_c is the critical damping of the system. In general, a system could show three types of damped motions depending on the value of the damping ratio ζ: [49]

- Underdamped motion ($\zeta < 1$): The amplitude of the vibrating system will gradually decrease to its steady-state. The lower ζ, the more time the system requires to return to its steady-state. The typical definition of an underdamped vibration can be seen in Equation 3.8 [49].
- Critically damped ($\zeta = 1$): The system returns as quickly as possible to its steady-state without oscillating.
- Overdamped motion ($\zeta > 1$): The system returns to its steady-state without oscillating. The larger ζ, the more time the system requires to return to its steady-state.

Most wind turbine motions can be considered as underdamped [6].

The logarithmic decrement of the vibration can be expressed by the natural logarithm of the ratio of two successive amplitudes. This can be seen in Equation 3.10 [49].

$$\delta_i = \ln\frac{X_{n-1}}{X_n} = \frac{1}{n}\ln\frac{X_0}{X_n} \tag{3.10}$$

When using Equation 3.10 to calculate the logarithmic decrement of the decaying vibration described in Figure 3.11, Equation 3.11 is derived.

$$\delta_i = \ln \frac{X_1}{X_2} = \zeta \omega_n T_d \tag{3.11}$$

If $\zeta < 0.1$ the simple Equation 3.12 will be valid, while if $\zeta > 0.1$ Equation 3.13 will be valid [49].

$$\zeta = \frac{\delta_i}{2\pi} \tag{3.12}$$

$$\zeta = \frac{\frac{\delta_i}{2\pi}}{\sqrt{1 + (\frac{\delta_i}{2\pi})^2}} \tag{3.13}$$

The measurement can be performed in the frequency domain as well. In the frequency domain the response is represented as peaks with their corresponding energy and dissipation of the energy. Such a graphical representation is the power spectrum of the vibration and is obtained by taking the square of the absolute value of the Fourier-transformed vibration. An example of such a representation can be seen in Figure 3.12. [98]

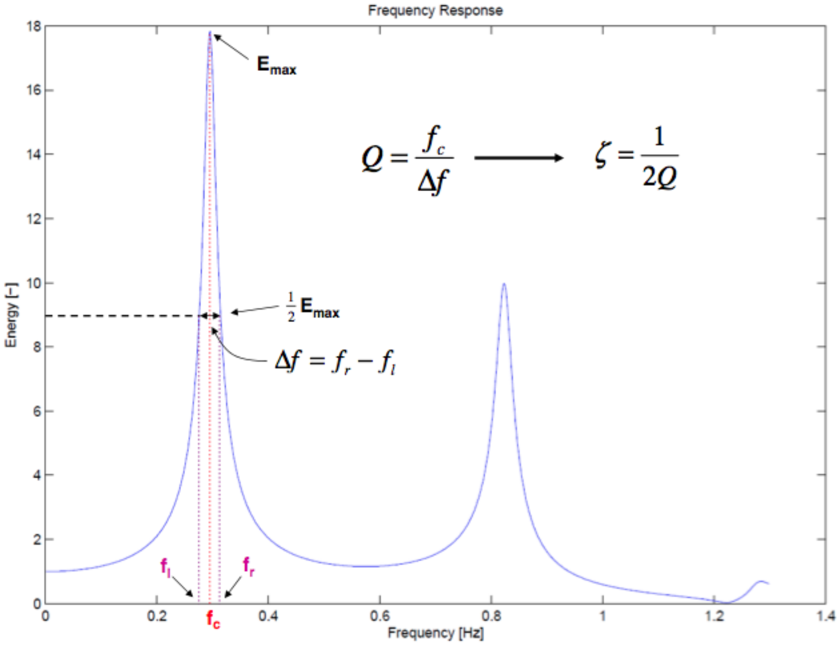

Figure 3.12: A typical power spectrum of decaying vibrations [98].The formulas described in the figure can be used to calculate the damping ratio.

The amount of damping can be derived from the slenderness of the frequency peaks (height/width ratio). The higher and narrower the peaks are, the lesser the amount of damping. Now by determining the Q factor of the peak, the amount of damping can be determined. Note that the definition for the Q factor is 2π times the ratio of the stored energy over the dissipated energy in one period. In Figure 3.12 the determination of the Q factor can be seen. First of all the power spectrum should be normalized, which means that at $f = 0Hz$ the energy should equal one, as is seen in Figure 3.12. Subsequently, the Q-factor is simply calculated by Equation 3.14.

$$Q = \frac{f_c}{\Delta f} \tag{3.14}$$

Here f_c is the center frequency of the peak and Δf is the width of the peak at the half of the maximum energy of the peak. Finally the viscous damping ratio is calculated by using Equation 3.15.

$$\zeta = \frac{1}{2Q} \tag{3.15}$$

The above described method is a very straightforward method, however the test set-ups vary with each article and depends on the size and shape of the test sample and on the desired direction of damping.

DMA

One of the most common methods to measure the damping properties of a certain material is Dynamic Mechanical Analysis (DMA). During a DMA measurement, the material is subjected to a sinusoidal load and subsequently the strain response of the material is measured. By comparing the strain response with the sinusoidal load, the phase lag angle ϕ can be determined. By using the tangent of ϕ (loss tangent), the storage modulus and the loss modulus of the material can be determined by using Equation 3.19. [69], [21]

$$\tan(\delta) = \frac{E''}{E'} \tag{3.16}$$

A representation of a typical Dynamic Mechanical Analyzer and the corresponding input and output curves can be seen in Figure 3.13. [69]

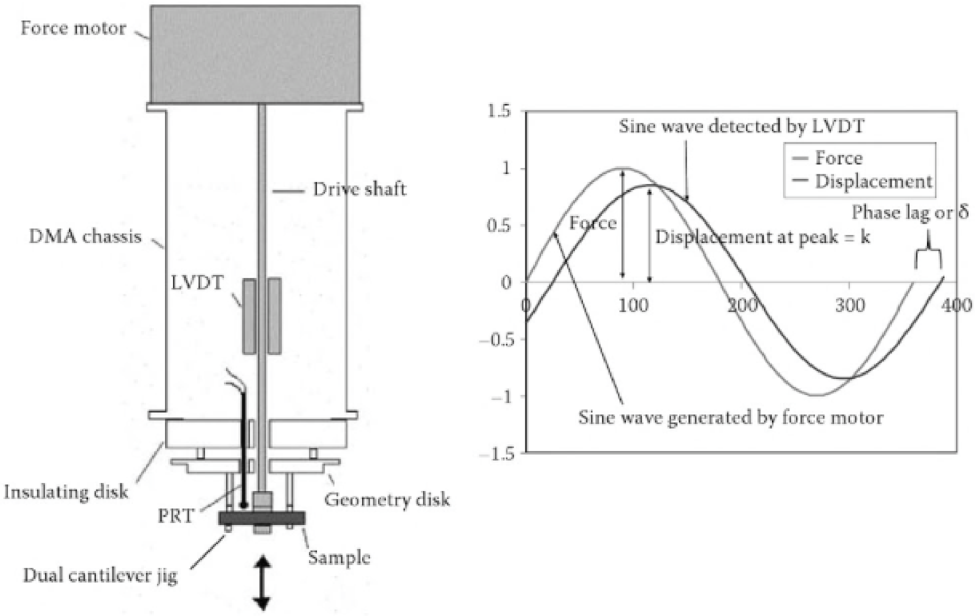

Figure 3.13: A typical Dynamic Mechanical Analyzer and the corresponding input and output curves [69].

The specimen can be subjected to a certain vibration of which the amplitude and the frequency can be altered.The Linear Variable Differential Transformer (LVDT) measures the response of the material and subsequently sends the results to a computer. For more complex Dynamic Mechanical Analyzers, the specimen can be placed inside an oven and therefore the influence of the temperature on the stress-strain response can be measured. The temperature inside the oven is measured by e.g. a Platinum Resistant Thermometer (PRT). The shape of the Dynamic Mechanical Analyzer depends on the desired material response [69]. For example the Dynamic Mechanical Analyzer depicted in Figure 3.13 measures the flexural response of the sample (note the 3-point-bending configuration in the analyzer), while other Dynamic Mechanical Analyzers can measure the extensional or torsional response.

Normally DMA devices have a limited frequency range of 0.01-200Hz. However, this is fine for the composite tower's material, since its subjected to low frequencies. [84] In general DMA tends to be less suited for composites due to the high stiffness modulus [36]. However, according to Swaminathan [93] certain measurement guidelines can be applied in order to achieve valid results.
Using a DMA device the stress-strain hysteresis loop, seen in Figure 3.5, can be created as well [101]. As can be seen in Figure 3.5, the total area of the loop equals the total energy of one cycle, while the small section with the crossing lines equals the amount of dissipated energy. Subsequently Equation 3.17 can be used to calculate the specific damping capacity [21].

$$\psi = \frac{\Delta U}{U} \tag{3.17}$$

Here ΔU is the amount of dissipated energy and U is the stored energy. There are several definitions of U and as a result the specific damping capacity depends on the used definition [37]. In case U is defined as the energy stored in the purely elastic component of each damped material element, the specific damping capacity becomes as in Equation 3.18.

$$\psi = 2\pi tan(\phi) \tag{3.18}$$

Equation 3.18 is also the most common used equation for the specific damping capacity.
Another measure of damping is the damping loss factor. The damping loss factor represents the decay of energy in a certain material and can be described by Equation 3.19 [37], [99].

$$\eta = \frac{\psi}{2\pi} = \frac{\Delta U}{2\pi U} \tag{3.19}$$

Again the loss factor depends on how U has been defined. By substituting Equation 3.18 in Equation 3.19, the widely used Equation 3.20 has been derived.

$$\eta = tan(\phi) = \frac{E''}{E'} \tag{3.20}$$

Note that in general the damping loss factor can be converted into the damping ratio by Equation 3.21 [21], [70].

$$\zeta \approx \frac{\eta}{2} \tag{3.21}$$

3.6.2. Damping models

In literature there are several models present to estimate the damping capabilities of composite materials. Of all damping mechanisms, viscoelastic damping has been identified as the most dominant damping mechanism in undamaged polymer composites subjected to small amplitude vibrations [48]. Therefore, most models assume that the laminate is undamaged and the fiber-matrix interphase is perfectly bonded ($\eta_{interphase} = \eta_{matrix}$). In case the elastic behavior and viscous damping of the composite material are independent of the vibration amplitude, linear viscoelastic damping can be assumed. This assumption will lead to a simplification of the analysis.

Several models are capable of estimating the damping properties of a composite material, both on a microscopic and a macroscopic scale. Obviously, the damping capabilities of an entire laminate or an entire structure will be different than the damping capabilities of a single ply.
There are several micromechanical models able to determine the damping properties of a single unrotated ply by using the damping and stiffness properties of the fibers and the isotropic matrix. Examples of models are the Saravanos-Chamis Micromechanical model, Tsai model, Hashin model and Zhao-Weng model [25], [42], [110], [85]. The Saravanos-Chamis Micromechanical model is based on the rules of mixtures and can be considered as the most practical model [25], while the Zhao-Weng model can be considered as the most accurate and the most complex method. Also the Saravanos-Chamis Micromechanical model requires the basic material properties like the Young's modulus, Shear modulus and Poisson's ratio, while the Zhao-Weng model requires viscoelastic material properties like the storage and loss moduli.
The most general macromechanical models are the Ross-Kerwin-Ungar method [96], [62] and the Modal Strain Energy method [26], [25], [97], [2]. The Ross-Kerwin-Ungar method is a rough estimation of the damping loss factor of simple composite plates. In general the flexural damping of a certain plate can be calculated by using Equation 3.22, which is in reality the same as Equation 3.20.

$$\eta = \frac{Im(EI)}{Re(EI)} \tag{3.22}$$

Here, EI is the complex bending stiffness of the composite material.

The Modal Strain Energy method on the other hand, can both be applied on a micromechanical level and on a macromechanical level, however it requires a complex 3D Finite Element Analysis (FEA) in order to determine the damping loss factor on a structural level. The Modal Strain Energy method calculates the loss factor by means of the ratio seen in Equation 3.23

$$\eta = \frac{\sum_{i=1}^{n} \eta_{ij} U_{ij}}{\sum_{i=1}^{n} U_{ij}} = \frac{\sum_{i=1}^{n} \Delta U_{ij}}{\sum_{i=1}^{n} U_{ij}} \tag{3.23}$$

Here η_i is the damping loss factor of the element's material, U_{ij} is the strain energy of the element and ΔU_{ij} is the dissipated strain energy of one element.

Another macromechanical method is the one described by Chortis [31]. This method is capable of converting the damping properties of a composite ply into the damping properties of a hollow wind turbine blade by using a simple Finite Element Method (FEM). Both a wind turbine's tower and blades are tubular structures and therefore this method is also suitable for estimating the damping properties of a composite tubular tower. Besides, Chortis [31] has already validated this method and therefore this method can assumed to be reliable. Different than the Ross-Kerwin-Ungar method and the Modal Strain Energy method, Chortis' model requires damping loss factors of a composite ply and therefore an additional micromechanical model has to be used.

4

DMA measurements

As mentioned in the previous chapter, the tower's viscoelastic damping will be determined by its material constituents. Due to the viscoelastic nature of the matrix and other viscoelastic material constituents (e.g. a foam core), the tower's damping loss factor will be temperature, frequency and amplitude dependent.
Since little information is present about the damping loss factors of resins, composites and foam materials, measurements have to be performed. The magnitude of damping in a certain system can be determined by measuring the system's response. This response can be measured by means of strain gauges, accelerometers, lasers, etc. depending on the nature of the vibration and the required damping unit. Subsequently, by using the measured response, the amount of damping can be identified. Each damping identification method has its own limitations and defines damping differently. As a result, determining the damping capabilities of a system (comprising of specimen, sensors, mounting, etc.) is not straightforward and unambiguous.

During this research two different measurement methods have been performed. The first measurement method is a simple cantilever beam test. From the results of these tests can be concluded that this method is not suitable for any damping measurements. Despite the fact that a phase lag could be measured, this phase lag was most likely due to clamping effects and/or due to other time lags in the load cell and/or test bench. Small changes in the clamping block, for example after reclamping the sample, result in large differences in the time lag. Also at very low frequencies ($0.01 Hz$) a negative time lag could be measured, which is physically impossible. The results of these tests and the corresponding conclusions can be found in Appendix A.

The second method is DMA, which uses a similar configuration (3-point-bending) and is able to measure the same $\tan(\phi)$ as the simple bending tests. This method is far more accurate and is capable of measuring the temperature dependency of the material as well. The used DMA instrument is the Pyris Diamond DMA instrument of Perkin Elmer. In Figure 4.1, the entire test set-up (DMA instrument, computer and nitrogen container) is seen at the Aerospace Engineering faculty of the Delft University of Technology.

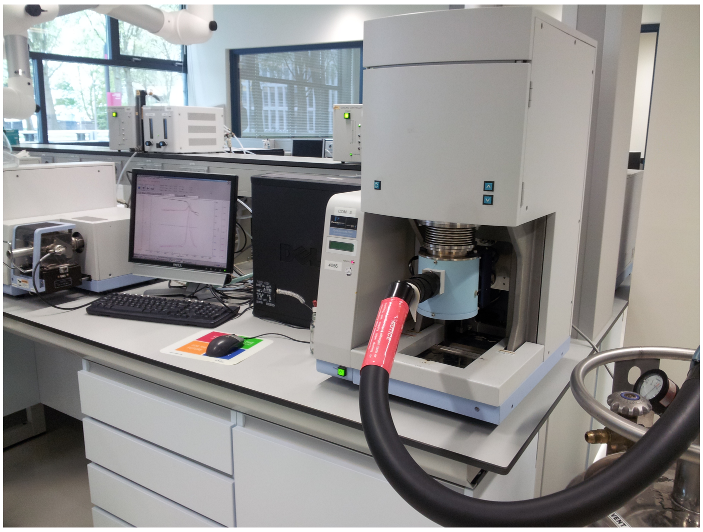

Figure 4.1: The DMA instrument at the Aerospace Engineering faculty.

This device has some important limitations. Due to the high stiffness of glass fibers, it is impossible to measure the damping of a 0° composite ply in axial direction. Therefore, it is impossible to use the axial configuration. Since these measurements can be conducted by a 3-point-bending configuration, this configuration has been used for all measurements.

The model presented in Chapter 5 requires the axial stiffness and damping of the material constituents. In case of a bending configuration, both the materials' stiffness and damping loss factor will be combinations of their tensile, compressive and shear components [111]. For now it is assumed that the compressive behavior of the material is similar to the tensile behavior. Subsequently, the effect of the shear component has to be determined. The damping loss factor can be defined as the percentage of strain energy that is dissipated from the system. Therefore the bending configuration can be divided into a strain energy component due to pure bending and a strain energy component due to pure shear. This division can be seen in Equation 4.1.

$$U_{tot} = U_s + U_b \tag{4.1}$$

Here, U_{tot} is the total strain energy, U_s is the strain energy due to shear and U_b is the strain energy due to pure bending.

During the measurements, it is preferred to measure only one damping component, which is the bending component. Therefore the ratio between the shear component and the bending component of the total strain energy should be lower than 10%. The definition of this ratio for a 3-point-bending configuration can be seen in Equation 4.2 and the derivation of this strain energy ratio can be found in Appendix D.

$$\frac{U_s}{U_b} = 4.8\frac{E}{G}\left(\frac{h}{L}\right)^2 \tag{4.2}$$

Subsequently the ratio between the bending component of the strain energy and the shear component of the strain energy can be calculated for most samples. The results can be seen in Table 4.1.

Table 4.1: Sample properties and the corresponding strain energy ratios.

type	$t\ [mm]$	$L\ mm$	$E\ [GPa]$	G $[GPa]$	$\frac{U_s}{U_b}$ [%]
High Modulus (HM) Vinylester resin	3	40	3.3 [78]	1.22	7.3
Low Modulus (LM) Epoxy resin	3	40	1.35 [80]	0.5	7.3
Glass Fiber Reinforced Vinylester (GFRV) 0°	1.5	40	37.9	3.17	8
GFRV 90°	1.5	40	8.51	3	1.9
Steel	1	40	200 [44]	76.9 [44]	0.8
Airex C70.75	3	40	85^* [27]	30 [27]	7.7

Here t is the sample thickness, L is the distance between the two supports of the 3-point-bending configuration, E is the Young's modulus, G is the Shear modulus, HM means High Modulus, LM means Low Modulus and GFRV stands for Glass Fiber Reinforced Vinylester. Note that the asterisk indicates that the Young's modulus is an average of the Compressive

modulus and the Tensile modulus. Also note that the calculation of the GFRVs' moduli can be found in Appendix C
Beside the samples seen in Table 4.1, also composite plies and PET foam samples have been tested. In case of the composite plies, the thickness is negligibly small compared to the sample's span and therefore the shear component of the strain energy will be neglected. In case of the anisotropic PET foams, the Young's modulus and Shear modulus differs in each direction. Nevertheless a similar result as for the Airex C70.75 is expected.
In general it can be concluded that the shear component of the total strain energy will only have a minor influence on the flexural damping loss factor and it can therefore be neglected.

Note that all samples, except for the composite plies, are tested by a 3-point-bending configuration, which is seen in Figure 4.3.

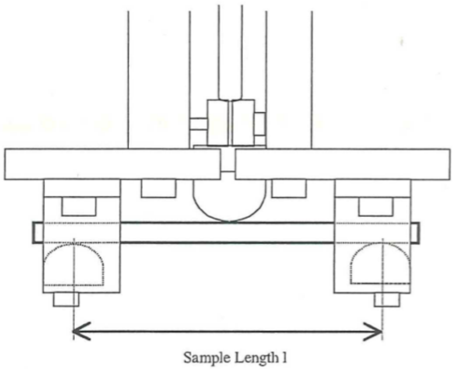

Figure 4.2: 3-point-bending configuration of the Pyris Diamond DMA instrument [50].

Note that for this configuration, the samples will only be pushed downwards. The dimensions of all samples are L (length) = 50mm and W (width) = 10mm. The thickness t is different for each sample, which can be seen in Table 4.1. As mentioned before, the composite plies have been tested with a different configuration than the other samples. This configuration is the 'general bending' mode, which can be seen in Figure 4.3 [50].

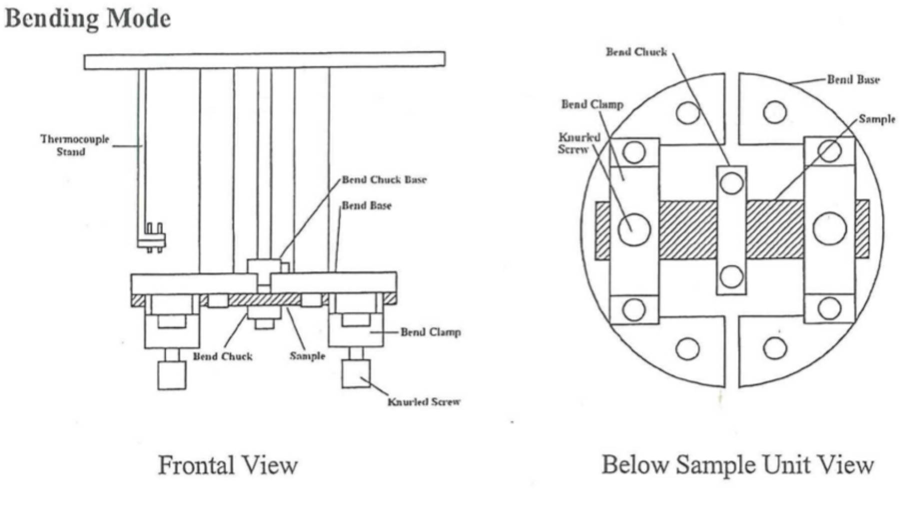

Figure 4.3: general bending configuration of the Pyris Diamond DMA instrument [50].

Note that this configuration requires the samples to be clamped at both ends, which secure the position of the thin composite plies. For this configuration the samples will both be pushed downwards and pulled upwards.

During all measurements, first the samples will be cooled to a temperature of $-50°C$ and subsequently the temperature will rise with a ramp of $2°C$ per minute until a temperature of $100°C$ has been reached. Each loading cycle has a certain frequency and is succeeded by a loading cycle with another frequency $(f_1 \rightarrow f_2 \rightarrow f_3 \rightarrow f_1 \rightarrow ...)$. Note that each sample is subjected to three different loading frequencies. The applied loading amplitude is $5\mu m$ in order to assure linear viscoelastic behavior.

4.0.3. Resin tests

As mentioned in Section 3.3, the resin is the main viscoelastic component of composite laminates and is therefore responsible for most of the composite's damping behavior.

Two different resin systems were tested, a low modulus Epoxy and a High modulus Vinylester. The latter one will be used for the composite wind turbine tower. The material properties of both resins can be found in Table 4.1. The Glass transition temperatures (T_g) of the resins are approximately $115^{\circ}C$ for the Vinylester and approximately $55^{\circ}C$ for the Epoxy [78], [80].

4.0.4. Results Vinylester

The Distitron VE370SC vinylester resin is a High modulus Vinylester. The exact composition of the tested samples is 97.7% Vinylester, 2% CHM50 hardener and 0.3% Cobalt. The manufacturing process of these samples can be found in Appendix B.

The results of the DMA measurements can be seen in Figure 4.4.

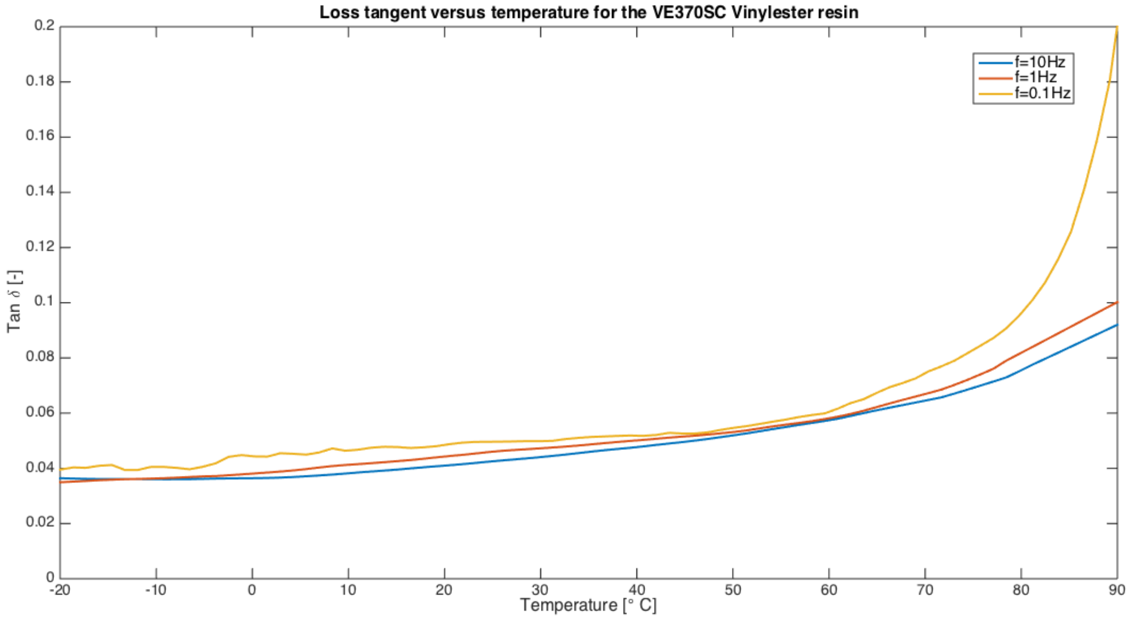

Figure 4.4: Loss factor versus temperature and frequency for the VE370SC vinylester.

Figure 4.4 shows that the damping loss factor depends on the frequency and the temperature. It is seen that at the tested frequencies, the damping behavior below approximately $60^{\circ}C$ is quite similar. Especially at the frequencies of $1Hz$ and $10Hz$ the loss factor can be assumed to be equal, which corresponds with literature [51]. At a frequency of $0.1Hz$ the damping is higher, probably due to the material's viscoelastic behavior. Above a temperature $60^{\circ}C$ the loss factor starts to become more frequency dependent. Especially at a $0.1Hz$ frequency, the loss factor starts to increase exponentially.

In Table 4.2 the average loss factors at room temperature for each frequency can be seen.

Table 4.2: Average loss factor at room temperature of the vinylester samples.

f $[Hz]$	$\tan\phi$ [-]	$N_{Samples}$
0.1	0.0493 ± 0.0039	2
1	0.0449 ± 0.0037	2
10	0.0415 ± 0.0038	2

4.0.5. Results Epoxy

The Ce-Sense 101 Epoxy resin is a low modulus Epoxy. The exact composition of the tested samples is 66.7% resin 101 and 33.3% hardener 113. The manufacturing process of the epoxy samples can be found in Appendix B as well. The epoxy resin shows a similar frequency response as the vinylester resin, which can be seen in Figure 4.4. Below a temperature of

$0°C$ the loss factor at $1Hz$ and $10Hz$ is exactly the same, while the loss factor at a frequency of $0.1Hz$ is higher. In Table 4.3 the average loss factors at room temperature for each frequency can be seen.

Table 4.3: Average loss factor at room temperature of the epoxy samples.

f $[Hz]$	$\tan\phi$ $[-]$	$N_{Samples}$
0.1	0.1311 ± 0.0042	2
1	0.1056 ± 0.0017	2
10	0.0913 ± 0.0008	2

In Figure 4.5 the comparison between the damping capabilities of both resin systems can be seen.

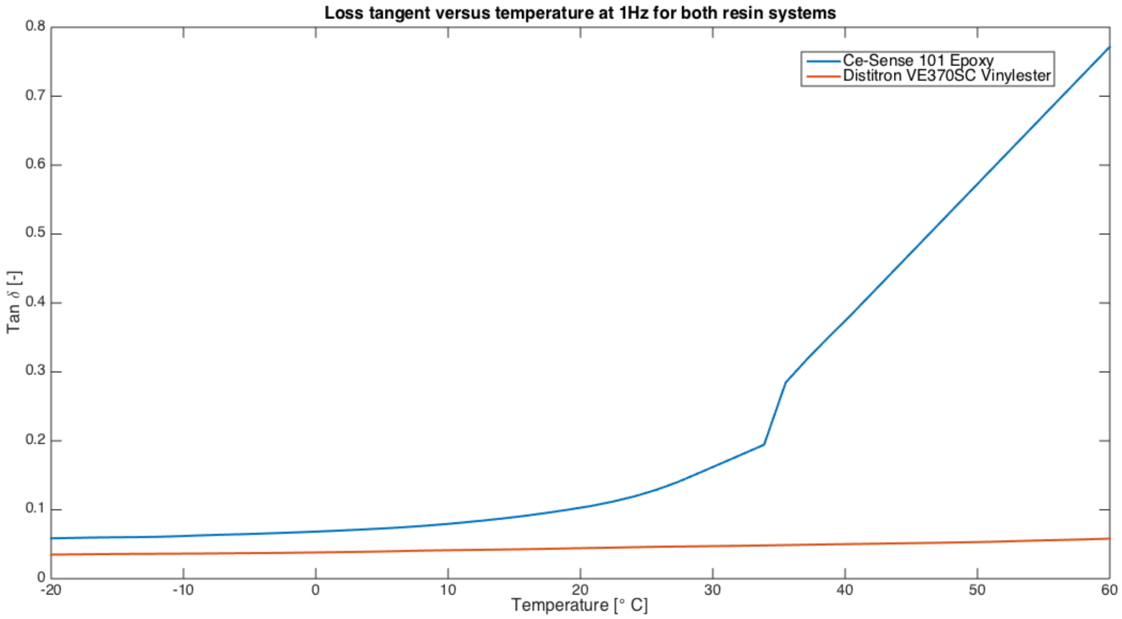

Figure 4.5: Loss factor versus temperature for both resin systems at a 1Hz loading frequency.

Obviously, the low modulus epoxy has better damping capabilities than the high modulus vinylester. This is both due to the epoxy's viscoelastic behavior as due to its lower glass transition temperature (T_g). The latter one is responsible for the exponential increase of the epoxy resin's damping loss factor.
In Table 4.4 a comparison between the loss factors of both resin systems at certain temperatures can be seen.

Table 4.4: Damping loss factors of the two resin systems at 1Hz and at room temperature.

Type	$\tan\phi$ at $-20°C$	$\tan\phi$ at $20°C$	$\tan\phi$ at $60°C$
Ce-Sense 101 Epoxy	0.0586 ± 0.00014	0.1056 ± 0.0017	0.7716 ± 0.1165
VE370SC Vinylester	0.0350 ± 0.0035	0.0446 ± 0.004	0.0577 ± 0.0052

4.1. Composite material

Composites are a combination of different types of materials and therefore the damping properties of a certain composite material will be a combination of the damping properties of the composite's material constituents as well. Several different composite materials have been tested by using two different configuration. Three types of composite laminates have been tested by the 3-point-bending configuration and four types of composite plies have been tested by the 'general' bending configuration.
The 3-point-bending configuration is less accurate compared to the 'general' bending configuration [50], however possible clamping effects are avoided and thicker samples can be tested.
The manufacturing process of all the composite samples can be found in Appendix B.

4.1.1. Composite laminates

The first three composite laminate types are vinylester samples with solely fibers in the lengthwise direction (0 degrees direction), vinylester samples with solely fibers in the transverse direction (90 degrees direction) and vinylester laminates with a $[45^\circ - 45^\circ - 45^\circ 45^\circ]$ lay-up. Note that all of these samples have a thickness of approximately $1.2mm$ to $1.4mm$. Also all of the composite samples contain polymeric stitches. Especially in the ±45° oriented laminates a significant amount of polymeric stitches in the 0° and 90° orientations are present.

In general the composite laminates show the exact same viscoelastic behavior as the vinylester resin (see Figure 4.6).

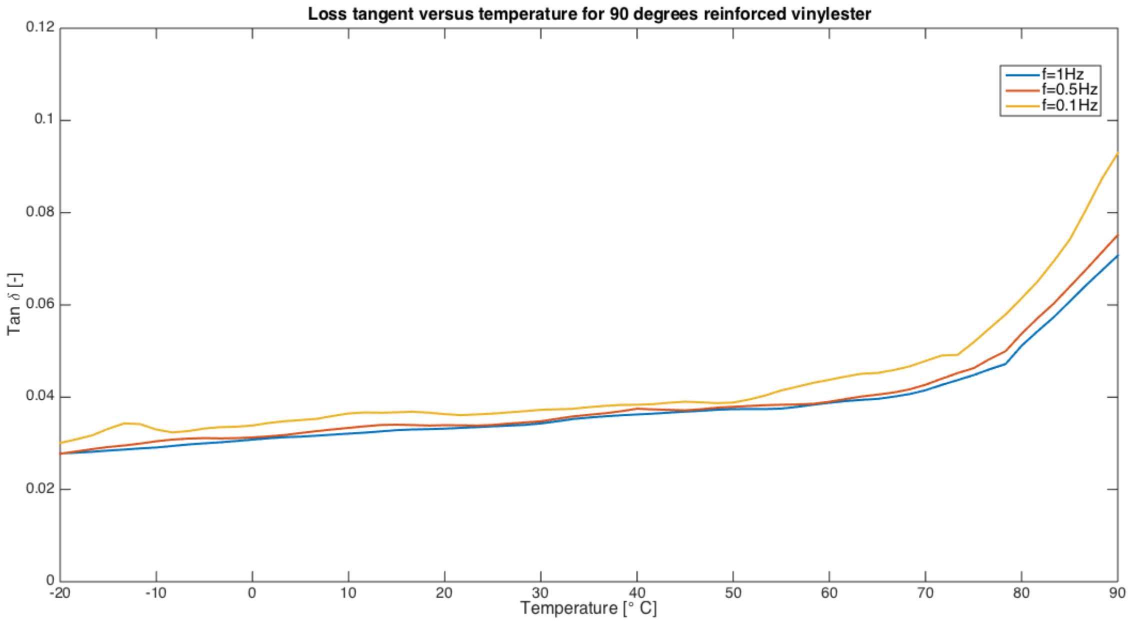

Figure 4.6: Loss factor versus temperature for the 90° GFRV laminates.

The ’0.5Hz’ curve has approximately the same damping values as the ’1Hz’ curve, which proves that in the frequency range 0.5Hz to 10Hz the composite material can be considered frequency independent. Again the ’0.1Hz’ curve shows higher values. In Table 4.5 some values of this measurement can be seen. Remarkably the damping loss factor is depending on the roughness of the samples. Each sample has been produced by vacuum infusion and therefore one side has a smooth surface while the other side has a very rough surface, which is due to the flow mesh. By placing the rough side on the supports, higher damping loss factors will be measured. This is probably due to the higher friction coefficient and/or the compression of the resin ’bumps’. One sample was fully sanded, which again resulted in a reduction of the damping loss factor.

Table 4.5: Measured damping loss factors of 90° GFRV laminates.

Description	Frequency $[Hz]$	$\tan\phi$ at $-20^\circ C$	$\tan\phi$ at $20^\circ C$	$\tan\phi$ at $60^\circ C$	$N_{samples}$
Rough side down	0.1	0.0393 ± 0.0007	0.0457 ± 0.0005	0.0625 ± 0.0065	2
Rough side up	0.1	0.0301 ± 0.0017	0.0363 ± 0.0001	0.0438 ± 0.00137	2
Sanded	0.1	0.0287	0.0308	0.0327	1
Rough side down	0.5	0.0362 ± 0.0022	0.0432 ± 0.0008	0.0548 ± 0.005	2
Rough side up	0.5	0.0277 ± 0.0005	0.0339 ± 0.0002	0.0390 ± 0.0004	2
Sanded	0.5	0.0273	0.0294	0.0315	1
Rough side down	1	0.0361 ± 0.0004	0.0429 ± 0.0012	0.0542 ± 0.0043	2
Rough side up	1	0.0278 ± 0.0003	0.0332 ± 0.0003	0.0388 ± 0.0006	2
Sanded	1	0.0279	0.0285	0.0318	1

In case of the 0° laminates the first tests have been done with the rough side up, while the second tests have been done with fully sanded samples. The results of those tests can be found in Table 4.6.

Table 4.6: Measured damping loss factors of 0° GFRV laminates.

Type	Frequencies $[Hz]$	$\tan\phi$ at $-20°C$	$\tan\phi$ at $20°C$	$\tan\phi$ at $60°C$	$N_{samples}$
Rough side up	0.1	0.0208 ± 0.0014	0.0241 ± 0.0005	0.0307 ± 0.0010	2
Sanded	0.1	0.0182 ± 0.0005	0.0187 ± 0.0011	0.0214 ± 0.0009	2
Rough side up	0.5	0.0198 ± 0.0006	0.0219 ± 0.0005	0.0276 ± 0.0006	2
Sanded	0.5	0.0179 ± 0.0008	0.0179 ± 0.0007	0.0204 ± 0.0001	2
Rough side up	1	0.0201 ± 0.0007	0.0218 ± 0.0006	0.0268 ± 0.0008	2
Sanded	1	0.0179 ± 0.0016	0.0179 ± 0.0008	0.0200 ± 0.0005	2

Note that the sanded samples show lower damping loss factors and therefore it can be concluded that the rough side of the samples interacts with the crosshead.

The last samples that were tested, were the sanded ±45° laminates. In Table 4.7 it is seen that in terms of damping the ±45° laminates perform better than the 0° laminates, but show at room temperature a similar result as the sanded 90° oriented sample. This is probably due to the fact that the bending-torsion coupling terms of a symmetrical ±45° laminate are non-zero. Also the polymeric stitches in the 0° and 90° orientations might have an influence on the damping loss factor.

Table 4.7: Measured damping loss factors of symmetrical ±45° GFRV laminates.

Frequencies $[Hz]$	$\tan\phi$ at $-20°C$	$\tan\phi$ at $20°C$	$\tan\phi$ at $60°C$	$N_{samples}$
0.1	0.0261 ± 0.0018	0.0300 ± 0.0011	0.0425 ± 0.0019	4
0.5	0.0240 ± 0.0018	0.0275 ± 0.0015	0.0377 ± 0.0013	4
1	0.0229 ± 0.0013	0.0268 ± 0.0018	0.0360 ± 0.0015	4

4.1.2. Composite plies

In total four types of composite plies have been tested using the general bending configuration. A reinforced (high modulus) vinylester and a reinforced (low modulus) epoxy ply with solely fibers in the lengthwise direction (0 degrees direction) and a reinforced vinylester and a reinforced epoxy ply with solely fibers in the transverse direction (90 degrees direction). All the composite ply samples have a thickness of approximately $0.5mm$.

In general the viscoelastic behavior of the composite plies is similar to the behavior of the composite laminates. Just as for the $0.5Hz$ frequency, the difference between the $10Hz$ frequency and the $1Hz$ frequency can be neglected. The behavior of the reinforced vinylester plies can be seen in Table 4.8.

Table 4.8: Average loss factor at room temperature for the reinforced vinylester samples.

f $[Hz]$	$\tan\phi$ at 0° orientation [-]	$\tan\phi$ at 90° orientation [-]	$N_{samples}$
0.1	0.0222 ± 0.0022	0.0325 ± 0.0006	2
1	0.0177 ± 0.0017	0.0268 ± 0.0009	2
10	0.0173 ± 0.0015	0.0239 ± 0.0009	2

Note that the damping loss factor at $1Hz$ of the 0° plies can be considered equal to the same damping loss factor of the sanded 0 degrees laminates, which indicates that the clamping effects are as severe as the friction between the samples and the supports of the 3-point-bending configuration. As can be seen, the damping loss factor at $1Hz$ in the 90° direction is similar to the same damping loss factor of the sanded 90° sample seen in Table 4.5.

If the reinforced (HM) vinylester plies are compared to the reinforced (LM) epoxy plies , some remarkable differences can be noticed. In Figure 4.7 both the differences between the 0° plies and the 90° plies can be seen.

Note that below a temperature of approximately $-20°C$ the damping loss factors of the two reinforced polymers can be considered to be the same. Below this temperature the damping loss factor is mainly determined by the stiff glass fibers. At higher temperatures the influence of the soft epoxy resin starts to increase exponentially.

The damping loss factors of the 90 degrees plies are highly dependent on the type of resin. Even below a temperature of $-20°C$ there is a significant difference in loss factor between the two reinforced polymers. In general the damping behavior of the 90 degrees plies can be compared to the damping behavior of the pure resins, which can be seen in Figure 4.5.

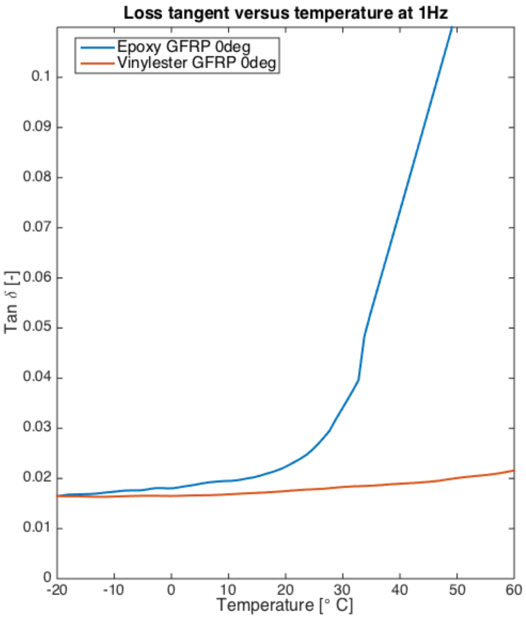
Loss tangent versus temperature at 1Hz
Epoxy GFRP 0deg
Vinylester GFRP 0deg
Tan δ [-]
0
0.01
0.02
0.03
0.04
0.05
0.06
0.07
0.08
0.09
0.1
-20
-10
0
10
20
30
40
50
60
Temperature [° C]
Loss tangent versus temperature at 1Hz
Epoxy GFRP 90deg
Vinylester GFRP 90deg
Tan δ [-]
Temperature [° C]

Figure 4.7: Loss factor versus temperature for a glass fiber reinforced vinylester and epoxy. In the left figure the composite materials have a 0° fiber orientation and in the right figure a 90° fiber orientation

In Table 4.9 a comparison between the two types of 0 degrees plies can be seen.

Table 4.9: Damping loss factors of the two reinforced (0 degrees orientation) resin systems at 1Hz and at room temperature.

Type	$\tan\phi$ at $-50°C$	$\tan\phi$ at $-20°C$	$\tan\phi$ at $20°C$	$\tan\phi$ at $60°C$
Ce-Sense 101 Epoxy	0.01531 ± 0.0003	0.0165 ± 0.0002	0.0227 ± 0.0002	0.1135 ± 0.0417
VE370SC Vinylester	0.01466 ± 0.0035	0.0165 ± 0.0017	0.0175 ± 0.0015	0.0201 ± 0.0014

4.1.3. Composite materials versus steel

In order to compare the composite wind turbine's material damping with the material of the current wind turbines, also steel samples have been tested using the 3-point-bending configuration. The manufacturing process of the steel samples can be found in Appendix B.
Compared to the composite material, steel cannot be considered a viscoelastic. This is seen in Figure 4.8.
As can be seen, the damping loss factor of steel can be considered frequency independent for a frequency range of $0.1Hz$ to $1Hz$. The $0.1Hz$ curve appears to be different from the other two curves, however this difference can be neglected. Beside the frequency, also the temperature does not have a significant effect on the damping loss factor. Note that the damping loss factor decreases with an increasing temperature. The internal friction or damping of steel alloys depends on the steel's composition and microstructure [45]. Probably the higher damping loss factor at $-20°C$ is due to the formation of kink-pairs in the edge dislocations [45].
In Table 4.10 the damping loss factors at several temperatures and at several loading frequencies can be seen.

Table 4.10: Average loss factors of steel.

f $[Hz]$	$\tan\phi$ [-] at $-20°C$	$\tan\phi$ [-] at $20°C$	$\tan\phi$ [-] at $60°C$	$N_{samples}$
0.1	0.0148 ± 0.0006	0.0139 ± 0.0012	0.0131 ± 0.0008	3
0.5	0.0141 ± 0.0003	0.0133 ± 0.001	0.0130 ± 0.0009	3
1	0.0143 ± 0.0004	0.0134 ± 0.0008	0.0129 ± 0.001	3

Finally a comparison can be made between the composite laminates, vinylester resin and steel samples. This comparison can be seen in Figure 4.9.

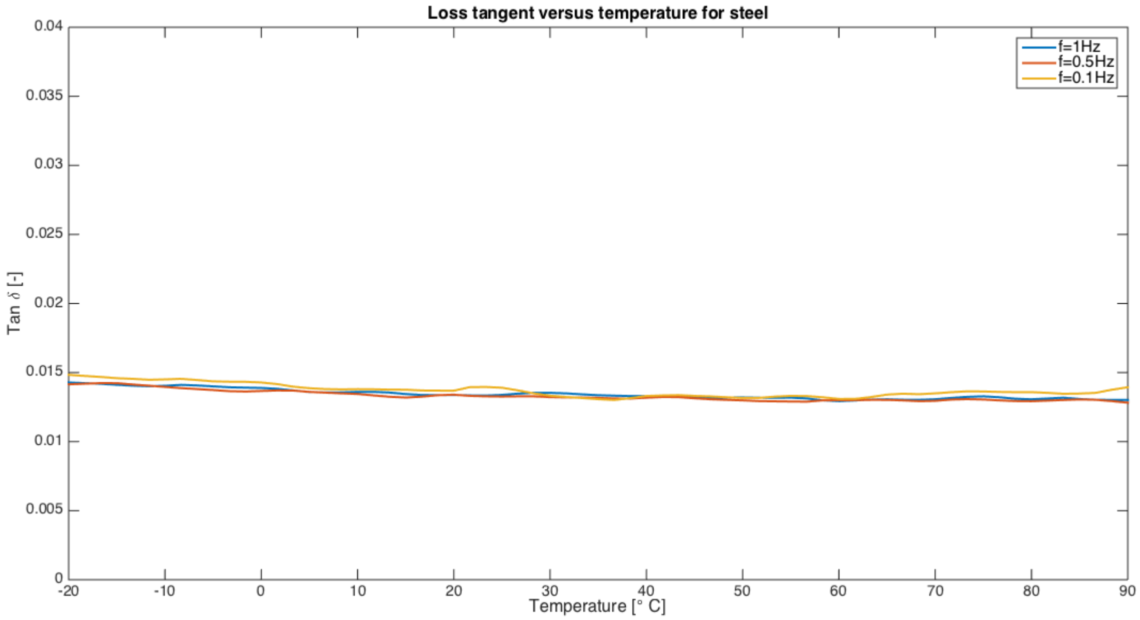

Figure 4.8: Loss factor versus temperature for steel.

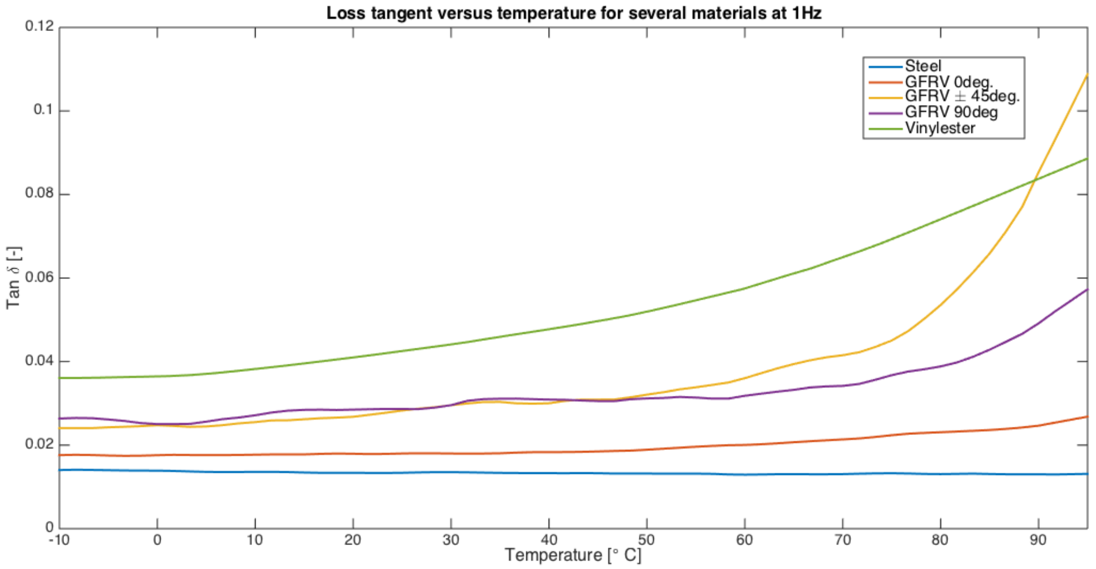

Figure 4.9: Loss factor versus temperature for several kinds of material. Note that GFRV stands for glass fiber reinforced vinylester.

It can be seen that steel has the worst damping behavior. As expected, the damping behavior of the 0 degrees composite laminate is not much better than that of steel. In the 0 degrees direction the damping loss factor is mainly determined by the glass fibers. In the 90 degrees direction on the other hand, the damping behavior of the vinylester is dominant. The $\pm 45^\circ$ laminates show a remarkable behavior. Up till a temperature of approximately $50^\circ C$ the damping behavior is similar to the damping behavior of the 90° laminates. Above this temperature, the damping loss factor of the $\pm 45^\circ$ laminates start to increase drastically and above a temperature of $90^\circ C$ the damping loss factor even exceeds the damping loss factor of the vinylester resin. This is probably due to an increasing influence of the bending-torsion coupling terms.

4.2. Foam material

Foams are quite odd materials when compared to solid materials. Due to their irregular cell structure, foams cannot be seen as a standard viscoelastic material. Therefore measuring the damping loss factor, might result in ambiguous values.

In general, foams can be divided in two types.

- Open-cell foams: Foams composed of windowless cells connected by strands of approximately triangular cross-section. Due to the fact that the gas inside the voids can move in and out of the material, deformations of the material will result in pneumatic effects. These pneumatic effects will result in extra internal energy dissipation. [60], [23]
- Closed-cell foams: Foams composed of dodecahedral voids with binding pentagonal interfaces of the voids composed of the base polymer. Due to their closed nature, no pneumatic effects occur. In general the lower the density of the foam, the larger the dodecahedral voids. In general closed-cell foams have better mechanical and insulation properties than open-cell foams and are water resistant. [23]

In case of structural foams, the foams are composed of closed-cells since they require good mechanical properties and have to be water resistant. In terms of damping, they perform better than composite plies and high modulus thermoset resins. Two common structural foams are Polyvinyl Chloride (PVC) foams and Polyethylene terephthalate (PET) foams. Unfortunately, the damping properties of PET and PVC foams are quite unexplored fields.

In general the mechanical properties of foams are determined by both the foam's base material as the foam's closed cell structure or foam density. However, the $\tan\phi$ or damping loss factor of foams can be considered relatively independent of the foam density if the density is greater than $75\frac{kg}{m^3}$ [51]. Therefore the damping loss factor can be estimated by assuming Equation 4.3.

$$\tan\phi = \tan\phi_s \tag{4.3}$$

Here $\tan\phi$ is the damping loss factor of the foam material, while $\tan\phi_s$ is the damping loss factor of the foam's base polymer.

Note that all foam samples have a thickness of approximately $3mm$. The manufacturing process of these samples can be found in Appendix B.

4.2.1. PVC foam

There exist two types of PVC foams i.e. linear (thermoplastic) PVC foams and (lightly) cross-linked PVC foams. Data on the damping properties of these foams are scarce. Kanny et al. have measured the viscoelastic behavior of the lightly cross-linked foams of DIAB by doing 3-point-bending DMA measurements. The results of these measurements can be found in Table 4.11 [51].

Table 4.11: Damping loss factors of the various foams at a frequency of 3Hz and at room temperature [51].

Type	$\rho\left[\frac{kg}{m^3}\right]$	$\tan\phi$ [-]
R75	75	0.081 ± 0.004
H130	130	0.067 ± 0.003
R260	260	0.047 ± 0.001
R300	300	0.045 ± 0.009

Obviously, the lower the foam's density the higher the damping loss factor and the more the damping loss factor will deviate from the base material's damping loss factor. This contradicts Equation 4.3. In case of the C-tower project a possible PVC foam is the C70.75 ($\rho = 80kg/m^3$) foam of Airex. In order to check whether the damping loss factor of this foam is similar to the damping loss factor of DIAB's R75 foam, the viscoelastic behavior of this foam has been measured. The measured loss factor depends on the temperature and frequency and can be seen in Figure 4.10.

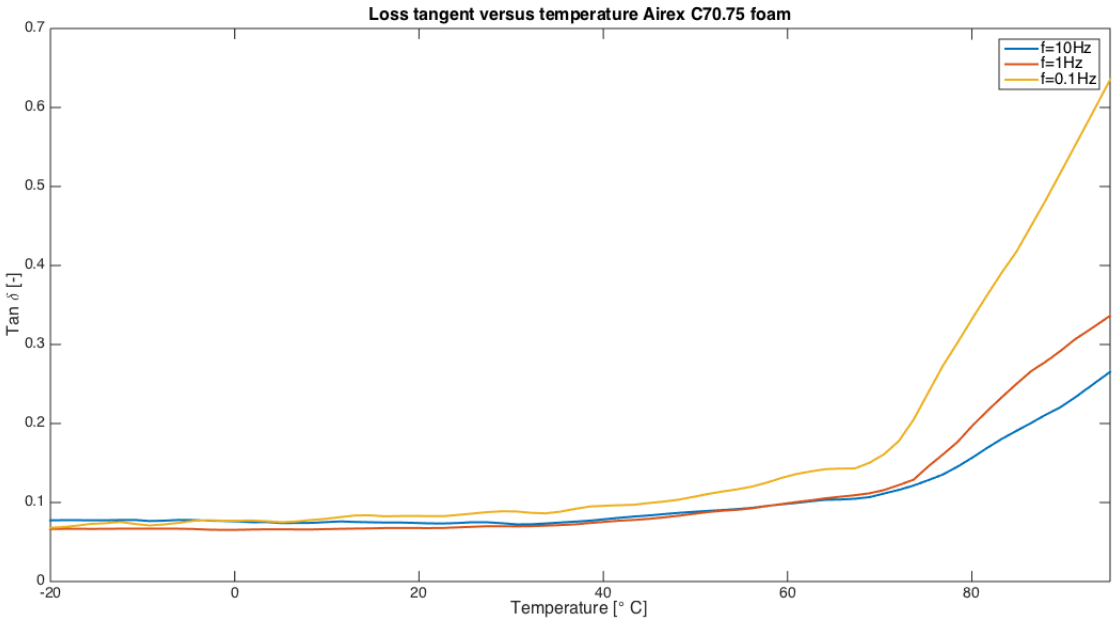

Figure 4.10: Loss tangent versus frequency and temperature for the C70.75.

As can be seen in Figure 4.10, the damping loss factor depends on the frequency and the temperature. Note that below the material's T_g a frequency of $10Hz$ results in a higher damping loss factor than a frequency of $1Hz$. This is quite remarkable, since a frequency of $0.1Hz$ results in a higher damping loss factor as well. Probably two mechanisms are influencing the damping loss factor. The first one is the aforementioned viscoelastic behavior of the bulk material and the second one is the foam's cell structure. Probably the bigger the cells and the thinner the cell walls, the higher the influence of the cell structure on the material's damping loss factor. Also due to the fact that the cells are large with respect to the sample thickness, pneumatic effects might occur.

Table 4.12: Average loss factors for the Airex C70.75.

f $[Hz]$	$\tan\phi$ [-] at $-20°C$	$\tan\phi$ [-] at $20°C$	$\tan\phi$ [-] at $60°C$
0.1	0.0679 ± 0.0085	0.081 ± 0.007	0.1360 ± 0.0119
1	0.0664 ± 0.0098	0.068 ± 0.01	0.1005 ± 0.009
10	0.0773 ± 0.0122	0.074 ± 0.007	0.0995 ± 0.0082

Note that the values in Table 4.12 deviate from the values in Table 4.11. This can be due to a large number of reasons. For example the measurement set-up could be different, the sample quality could be different, the chemical composition could be different, etc. Nevertheless, the measured values are still quite comparable to the value of the R75 foam seen in Table 4.11.

4.2.2. PET foam

PET foams are semi-crystalline thermoplastic foams and are due to their manufacturing process anisotropic in nature. Typically PET foams are manufactured by extrusion and therefore they show often a honeycomb pattern, which can be seen in Figure 4.11. Due to the extrusion process, the cells are oriented in the extrusion direction and therefore the foam material has a higher stiffness in this direction. The stiffness in the other two directions is lower and approximately equal to each other.

After the production, the pieces of PET foam are welded together, which results in weld lines. These weld lines are made of pure PET and therefore are much stiffer than the surrounding material and result in a fully anisotropic foam material.

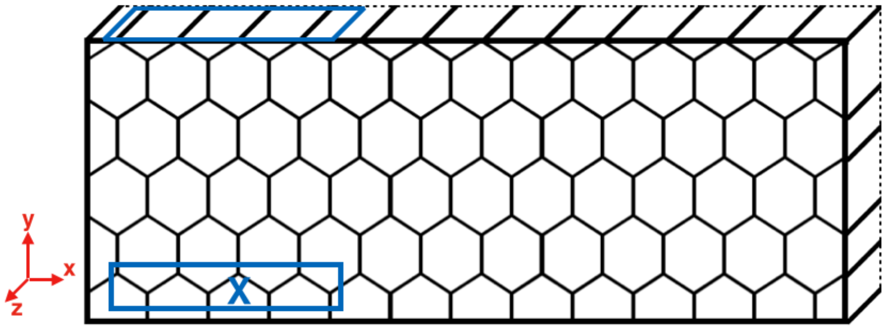

Figure 4.11: Extruded honeycomb structure of the PET foams. Note that direction z corresponds with the extrusion direction and the blue rectangles indicate the different kind of samples.

Compared to the amount of available data on the damping properties of PVC foams, the data on the damping properties of PET foams is even scarcer. Therefore more DMA measurements are required. In order to limit the amount of tests that have to be done, the foam samples are cut around the weld lines. Therefore the damping properties of two different directions will be tested, which can be seen in Figure B.1 as well. The samples with their thickness in the extrusion direction are marked with the letter X.
The results of the DMA tests can be found in Figure 4.12.

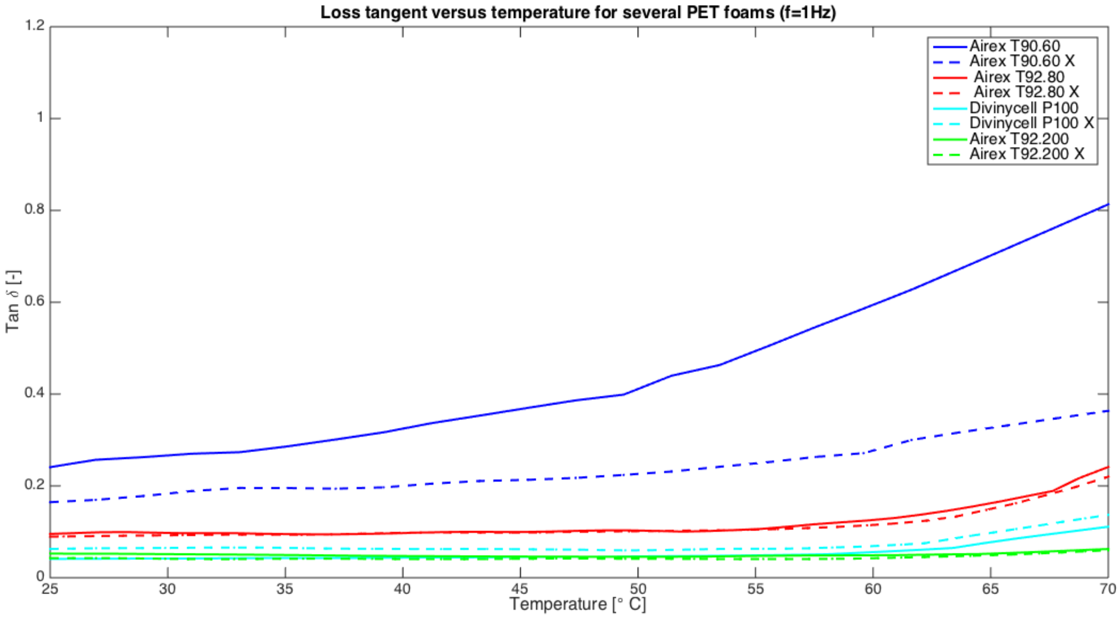

Figure 4.12: Lost factor versus temperature for several PET foams.

Figure 4.12 shows that the damping behavior of PET foams is density dependent as well. In general the higher the foam density, the lower the loss factor. The corresponding loss factors at room temperature can be found in Table 4.13.

Table 4.13: Damping loss factors of the various PET foams at a frequency of 1Hz and at room temperature.

Type	ρ $\left[\frac{kg}{m^3}\right]$	$\tan\phi$ [-]	$N_{samples}$	$\tan\phi_X$ [-]	$N_{samplesX}$
Airex T90.60	65	0.2277 ± 0.0730	3	0.1537 ± 0.0194	2
Airex T92.80	85	0.0839 ± 0.0091	3	0.0866 ± 0.0110	4
Divinycell P100	110	0.041 ± 0.006	4	0.0627 ± 0.0150	4
Airex T92.200	210	0.0520 ± 0.0013	4	0.0427 ± 0.0130	3

Due to the irregular cell structure there is a non-linear difference between the damping loss factors of the two different directions. Especially the Divinycell P100 and the Airex T90.60 show a large difference between the two directions. Any difference between the DivniycellI and the other PET foams can be due to the fact that it is produced by a different manufacturer. For example both the chemical composition as the production process might be different. In case of the T90.60, the closed cells are large compared to the amount of material that is present. The loss factor of this type of foam will mainly be determined by the cell structure and probably some pneumatic effects. This results in loss factors which are much higher compared to the loss factors of the other foams. In case of the Airex T92.80, the difference between the two directions can be neglected.

Just as PVC foams, Pet Foams are both temperature and frequency dependent. In Figure 4.13, the influence of the frequency and temperature on the Airex T92.200 and the Airex T92.80 can be seen.

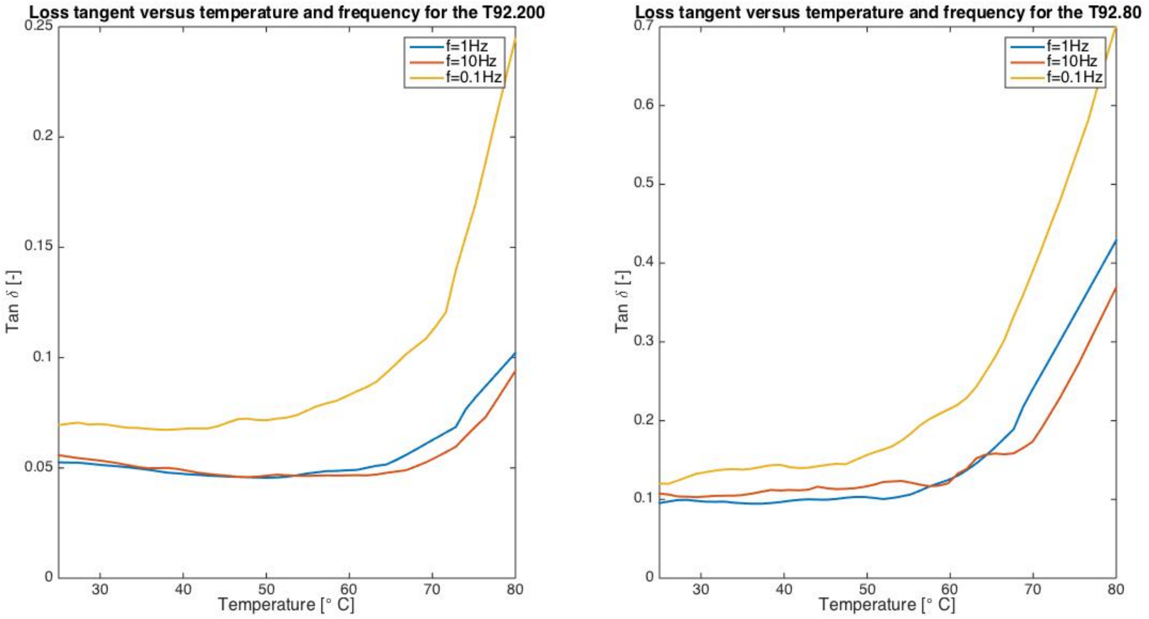

Figure 4.13: The influence of the frequency and temperature on the Airex T92.200 and the Airex T92.80.

Note that below the material's T_g, the '10Hz curve' equals the '1Hz curve' for the T92.200 foam. The Divinycell P100 shows a similar behavior, while the T92.80 shows a different behavior. Apparently a 10Hz frequency results in a higher damping loss factor below the material's T_g. The T90.60X samples show a similar behavior as the T92.80 samples. Since the Airex T92.80 is a likable option for the C-Tower project, an overview of the loss factors at several temperatures and frequencies is presented in Table 4.14 and Table 4.15.

Table 4.14: Average loss factors of the Airex T92.80 samples.

$f\ [Hz]$	$\tan\phi$ [-] at $-20°C$	$\tan\phi$ [-] at $20°C$	$\tan\phi$ [-] at $60°C$	$N_{samples}$
0.1	0.0886 ± 0.0225	0.107 ± 0.0159	0.1977 ± 0.0381	5
0.5	0.0606 ± 0.0139	0.0825 ± 0.0091	0.1290 ± 0.02	5
1	0.0665 ± 0.0101	0.0863 ± 0.0115	0.1237 ± 0.0196	3
10	0.0825 ± 0.003	0.0996 ± 0.0136	0.1327 ± 0.0218	2

Table 4.15: Average loss factors of the Airex T92.80X samples.

$f\ [Hz]$	$\tan\phi$ [-] at $-20°C$	$\tan\phi$ [-] at $20°C$	$\tan\phi$ [-] at $60°C$	$N_{samples}$
0.1	0.0808 ± 0.0170	0.118 ± 0.0134	0.2386 ± 0.0399	4
0.5	0.0758 ± 0.0110	0.0873 ± 0.0141	0.1363 ± 0.0094	4
1	0.0681 ± 0.0067	0.0882 ± 0.0099	0.1185 ± 0.0097	4

Note that the values in Table 4.13 and Figure 4.13 are based on three T92.80 samples which were subjected to the $1Hz$, $0.5Hz$ and $0.1Hz$ frequencies, while the values in Table 4.14 are based on 5 samples of which three samples were subjected to the $1Hz$, $0.5Hz$ and $0.1Hz$ frequencies and two samples to the $1Hz$, $0.1Hz$ and $10Hz$ frequencies.
During the DMTA measurements, each cycle with a certain frequency is followed by another cycle with a different frequency. Probably these succeeding cycles with different frequencies affect each other. Therefore the values of the three samples which were subjected to the $1Hz$, $0.5Hz$ and $0.1Hz$ frequencies will be slightly different than those of the two samples which were subjected to $1Hz$, $0.1Hz$ and $10Hz$ frequencies. As a result both the mean value and the standard deviation presented in Table 4.14 are higher than those presented in Table 4.13.

4.3. Sandwich structured composites

In case of the composite wind turbine tower, the used material will not be a pure composite laminate but a sandwich structured composite material. It will exist of two Glass Fiber Reinforced Vinylester (GFRV) face sheets, which are separated by a low weight T92.80 (PET) foam core. Therefore the final damping loss factor will probably be a combination of those two materials.

In order to research the influence of the foam material on the sandwich structured GFRVs, a couple of DMA tests have been performed. The sandwich structured composite samples have dimensions of $L = 50mm$, $W \approx 9mm$ and $t \approx 3.4mm$. The thickness of the foam material is $\approx 2mm$ and the thickness of the 0° GFRV face sheets is $\approx 0.5mm$ per face sheet. This means that the adhesive layer is $\approx 0.2mm$ per face sheet. Also a large number of the core material's voids are filled with resin. The manufacturing process of the sandwich samples can be found in Appendix B.
The resulting damping loss factors of these DMA measurements can be found in Table 4.16.

Table 4.16: Average loss factors of the sandwich structured GFRV.

f $[Hz]$	$\tan\phi$ [-] at $-20°C$	$\tan\phi$ [-] at $20°C$	$\tan\phi$ [-] at $60°C$	$N_{samples}$
0.1	0.0267 ± 0.0025	0.0280 ± 0.0011	0.0684 ± 0.0074	3
0.5	0.0237 ± 0.0022	0.0251 ± 0.0013	0.0506 ± 0.0042	3
1	0.0232 ± 0.0019	0.0243 ± 0.0006	0.0464 ± 0.0026	3

As can be seen, the difference between the loss factors measured at a $1Hz$ frequency and at a $0.5Hz$ frequency can be neglected and at a $0.1Hz$ frequency the damping loss factors are higher. The same behavior can be observed for both the tested composite laminates and foams. At a $60°C$ temperature the damping loss factors have been increased significantly. The difference in behavior between the sandwich structured 0° GFRVs and the 0° GFRV laminates can be seen in Figure 4.14.

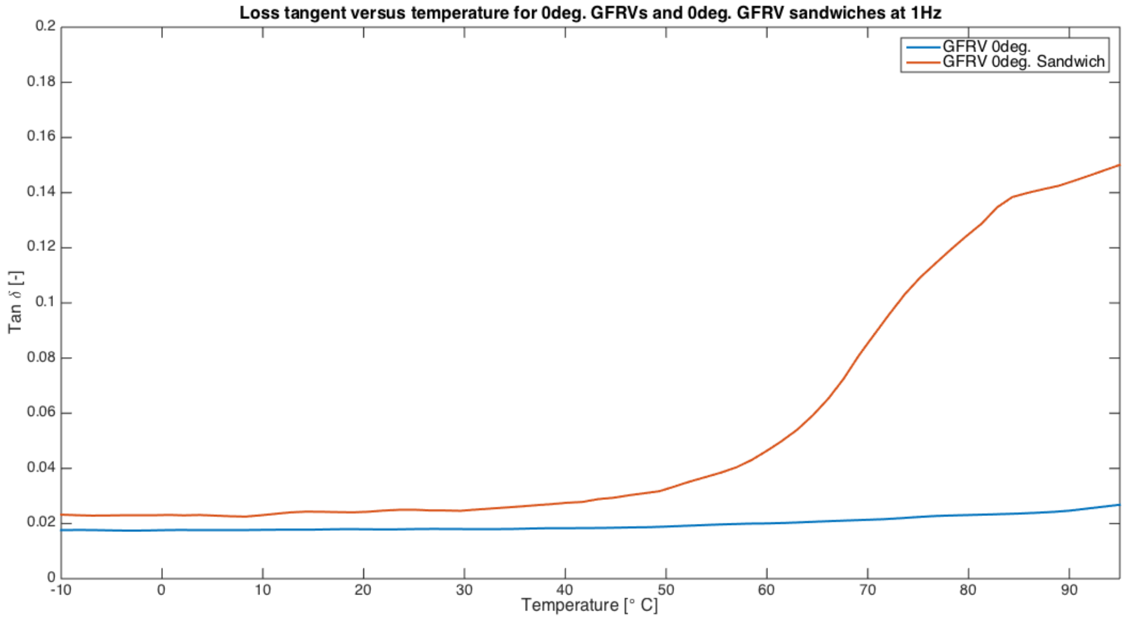

Figure 4.14: The influence of the frequency and temperature on a sandwich structured GFRV.

The corresponding values for the damping loss factors and the damping loss factors of the T92.80 foam can be found in Table 4.17.

Table 4.17: Damping loss factors of the various PET foams at a frequency of 1Hz and at room temperature.

Type	$\tan\phi$ [-] at $-10°C$	$\tan\phi$ [-] at $20°C$	$\tan\phi$ [-] at $60°C$
GFRV 0°	0.0176 ± 0.0016	0.0179 ± 0.0008	0.0200 ± 0.0006
Sandwich	0.0232 ± 0.0019	0.0243 ± 0.0006	0.0464 ± 0.0026
T92.80 foam	0.0696 ± 0.0077	0.0882 ± 0.0099	0.1185 ± 0.0097

Up till a temperature of $30°C$, the difference between the 0° GFRV laminates and the sandwich structured 0° GFRVs is not drastically high. For example the difference between the 0° GFRV laminates and the ±45° GFRV laminates is more significant. This means that the damping behavior of the sandwich material is mainly determined by the damping behavior of the composite face sheets. Above a temperature of $30°C$, the foam material is starting to reach its T_g and therefore the damping loss factor starts to increase exponentially.

The initial difference between the 0° GFRVs and the sandwich structured 0° GFRVs can be explained by several factors. For example during the 3-point-bending tests the soft foam material between the face sheets is compressed / sheared, which results in a higher influence on the sandwich materials damping loss factor. Also the relatively thick adhesive layers and the foam material's resin filled voids are probably influencing the overall damping loss factor.

4.4. Validation of the DMA measurements

In order to validate the DMA measurements, the measured loss factors have to be compared with the loss factors found in literature. In Table 4.18 a small list can be found with the damping loss factors and with the corresponding references. Note that MDM stands for Modal Damping Measurements (see Appendix A).

Table 4.18: Loss factors of several composite material and one resin

Method	Configuration	Material	f [Hz]	η_{11} [%]	η_{22} [%]	Source
MDM	Single cantilever	UD Glas fiber / Epoxy	50	0.35	1.3	[15]
MDM	Unknown	UD Glas fiber / Epoxy	-	0.371	0.898	[31]
Unknown	Unknown	UD Glass fiber / Epoxy	-	≈ 0.22	≈ 1.38	[12]
Unknown	Unknown	Epoxy	-	≈ 1.5	≈ 1.5	[12]
DMA	Single cantilever	UD Glass fiber / Epoxy	1	≈ 1.3	-	[32]
DMA	Single cantilever	Epoxy	1	≈ 1.5	≈ 1.5	[32]
DMA	3-point-bending	UD Glass fiber / Epoxy	1	≈ 4	-	[94]
DMA	3-point-bending	UD Glass fiber / Polyester	1	≈ 4.3	-	[71]
DMA	3-point-bending	Polyester	1	≈ 5.4	≈ 5.4	[71]
DMA	3-point-bending	UD Glass fiber / Vinylester	1	1.79	2.78	Own work
DMA	3-point-bending	Vinylester	1	4.49	4.49	Own work

Here f is the frequency, η_{11} is the damping loss factor in fiber direction and η_{22} is the damping loss factor in transverse direction.

Each measurement method tends to measure a different damping loss factor for similar materials. In general the DMA measurements result in a large diversity of different values, although the values can be considered to have the same magnitude. This proofs that the type of machine, sample quality, configuration, etc. are all influencing the measured damping loss factor. Compared to the DMA measurements, the MDM methods measure a much lower damping loss factor.

According to Alijani and Amabili [4], any kind of clamping conditions results in faulty measurement values. Even at simply supported conditions frictional interactions between the sample and the supports / crosshead result in a significant amount of parasitic damping. By improving the surface quality of the samples and by reducing the contact surfaces of the crosshead and supports, this parasitic damping will be reduced significantly [9]. Also performing the measurements in a vacuum will improve the test results, since the surrounding air always results in some parasitic damping [9].

4.5. Conclusion

Apparently both resin systems, all tested composite materials and the high density foams can be considered frequency independent in the range of $0.5Hz$ to $10Hz$. In case of the low density foams this range will be much smaller, however still they can be considered frequency independent in the range of $0.5Hz$ to $1Hz$. This means that for most of the tower's loading frequencies, the damping loss factor will hardly change.
At a $0.1Hz$ frequency the damping loss factor will be higher, however for the vinylester and reinforced vinylester laminates this increase is less than 10%. Steel on the other hand can be considered frequency independent in the range of $0.1Hz$ to $1Hz$.

In case of the tested laminates, it can be concluded that the damping behavior of the 0° oriented laminates is mainly determined by the damping behavior of the glass fibers, while for the 90° oriented laminates the damping behavior is mainly determined by the resin. In case of the ±45° oriented laminates, the torsion-bending coupling terms probably result in an increase of the damping loss factor.

The temperature dependency is more complicated. It depends on both the material's damping capabilities as the material's T_g. In general viscoelastic materials tend to show an increasing damping loss factor with an increasing temperature, while an elastic material like steel hardly shows any thermal response in a temperature range of $-20°$ C to $120°C$. As a matter of fact, steel even shows a slight decrease in damping loss factor at elevated temperatures. In case of the ±45° oriented laminates, the temperature will probably have an effect on the torsion-bending coupling terms as well.

In case of the structural foams, some other conclusions with respect to the foam density can be made. In general the higher the foam density, the higher the damping loss factor. This is probably due to the fact that structural foams cannot be considered as solid materials. The lower the density, the more the damping loss factor is determined by the foam's structure instead of by the foam's material. On the other hand the damping loss factor of high density foams can be considered close to the loss factor of the foam's base material. In case of the anisotropic PET foams, different directions have different loss factors. Due to the cell structure of the PET foams, transverse isotropy can be assumed and therefore the damping loss factor will differ in two different directions. In case of the T92.80 the difference in damping between the two directions can be neglected.

The damping capabilities of sandwich structured composites is mainly determined by the damping capabilities of the face sheets. Below the foam's T_g, the damping loss factors are only a bit higher than the damping loss factors of the face sheets. Probably this difference is due to the microscopic compressing and/or shearing of the core material. Also the thick relatively thick adhesive layer and the resin filled voids of the core material might have an effect on the sandwich material's damping behavior. In case the temperature reaches the foam core's T_g, the sandwich material's damping loss factor starts to increase exponentially.
When comparing the measured damping loss factors with the damping loss factors found in literature, one finds that for similar materials and similar configurations a large diversity of damping loss factors has been measured. Apparently the measured damping loss factor is influenced by the amount of parasitic damping, which is dependent on, among others, the type of measurement, sample quality and the type of configuration. Therefore the validity of the measured damping loss factors is questionable. Nevertheless, the measured values will serve as an input for the wind turbine's damping model.

5

Damping Model

The total damping of the tower can be described by several types of damping loss factors. The tower's for-aft motion is mainly damped by aerodynamic damping, while the side-to-side motion is mainly damped by the structure itself [102]. The aerodynamic damping in the side-to-side direction is small compared to the structural damping and it will therefore be neglected [6]. Due to the non-linearity and complexity of the damping due to the bolted connections, only the material damping will be considered.

The model of Chortis describes, as most damping models, the material damping loss factor as in Equation 5.1. [31]

$$\eta = \frac{1}{2\pi}\frac{W_d}{H} \tag{5.1}$$

Where W_d is the total amount of dissipated energy and H is the total amount of stored energy.
In order to determine the material damping loss factor of a composite tower, the damping properties of the material constituents have to be translated to the damping properties of a circular cross-section and subsequently to the damping properties of a full scale tower. In Figure 5.1 the several steps that have to be taken in order to translate the damping properties from ply level to structural level can be seen.

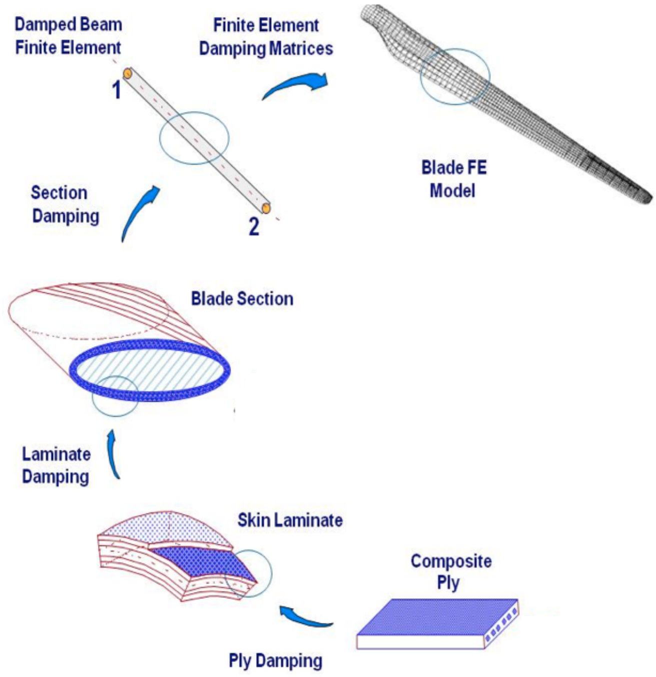
Damped Beam
Finite Element
Finite Element
Damping Matrices
1
2
Blade FE
Model
Section
Damping
Blade Section
Laminate
Damping
Skin Laminate
Composite
Ply
Ply Damping

Figure 5.1: Schematic overview of all translation steps that have to be taken. [31]

Note that for now linear viscoelastic properties will be assumed and hence the damping loss factor will be assumed to be independent of the load amplitude.

5.1. Ply damping

The damping behavior of a composite structure can be computed by assuming that each composite ply has viscoelastic material properties. Using the Kevin-Voigt model, the viscoelastic behavior of the material can be estimated. Hence, the stress behavior of the composite ply can be estimated by Equation 5.2 [31].

$$\sigma_c = \big([Q_c] + i[Q_c]\eta_c\big)\epsilon_c \tag{5.2}$$

Here σ_c is the stress matrix, Q_c is the stiffness matrix, η_c is the damping loss factor matrix and ϵ_c is the strain matrix. The damping loss factor matrix is represented by Equation 5.3. [31]

$$\eta_c = R^T \eta_l R^{-T} \tag{5.3}$$

Here R is the full rotation matrix and η_l is the unrotated damping matrix. The latter can be represented by Equation 5.4. [86]

$$\eta_l = diag(\eta_{11}, \eta_{22}, \eta_{33}, \eta_{23}, \eta_{13}, \eta_{12}) \tag{5.4}$$

Note that η_{33} is assumed to be negligible small [31]. Also it is assumed that $\eta_{13} = \eta_{12}$.

The damping behavior of a single ply is determined by the damping properties of its material constituents (i.e. matrix and fibers) and the orientation of the fibers. The translation from the material constituents to a composite ply is done by using the Saravanos-Chamis micromechanical model, which is described in Appendix F. In order to determine the damping behavior of a single ply, a couple of assumptions have been made.

- Only viscoelastic damping is present.
- Room temperature has been assumed.
- A loading frequency of 1Hz has been assumed.
- The axial damping loss factor equals the flexural damping loss factor.
- The axial damping loss factor of the vinylester matrix is assumed to be equal to the shear damping loss factor.
- The axial damping loss factor of the vinylester matrix is assumed to be equal to the value measured during the DMA tests.
- The glass fibers are assumed to be isotropic.
- The cross-section of the glass fibers is assumed to be circular.
- The axial damping loss factors of the glass fibers is determined by using the Saravanos-Chamis model, in such a way, that the damping loss factor in the fiber direction of the composite ply equals the same damping loss factor measured during the DMA tests.
- Since the influence of the glass fibers' shear damping on the tower's damping loss factor is negligible small, the glass fibers' shear damping loss factors are assumed to be zero.

The damping loss factors of the martial constituents and the composite ply can be seen in Table 5.1. Note that the damping loss factors of the composite ply are calculated by using the Saravanos-Chamis micromechanical model.

Table 5.1: The damping loss factors of the material constituents and the composite ply at $1Hz$.

Material	η_{11} [-]	η_{22} [-]	η_{23} [-]	η_{13} [-]	η_{12} [-]
Vinylester resin	0.0449	0.0449	0.0449	0.0449	0.0449
E-glass fibers	0.0166	0.0166	0	0	0
Composite ply	0.0178	0.0353	0.0321	0.0343	0.0343

As can be seen in Table 5.1, the Saravanos-Chamis micromechanical model overestimates η_{22}. The η_{22} measured during the DMA tests is approximately 0.0285, which is approximately 20% lower than the value seen in Table 5.1. The reason for this overestimation is currently unknown and it could be due to several reasons. For example the polymeric stitches that are bonding the glass fibers together and are oriented in the 0° direction could have a significant effect. Also, it is possible that the Saravanos-Chamis micromechanica modell is not accurate enough in the resin dominated directions.
In order to prevent an overestimation of the tower's damping loss factor, all resin dominated directions will be multiplied by a reduction factor of 0.8. The resulting damping loss factors can be seen in Table 5.2.

Table 5.2: Reduced damping loss factors of the composite ply at $1Hz$.

Material	η_{11} [-]	η_{22} [-]	η_{23} [-]	η_{13} [-]	η_{12} [-]
Composite ply	0.0178	0.0285	0.0257	0.0274	0.0274

Subsequently the obtained damping loss factor matrix of the composite ply can be rotated by applying Equation 5.3. In Figure 5.2 the influence of the rotation matrix on the damping loss factor matrix can be seen.

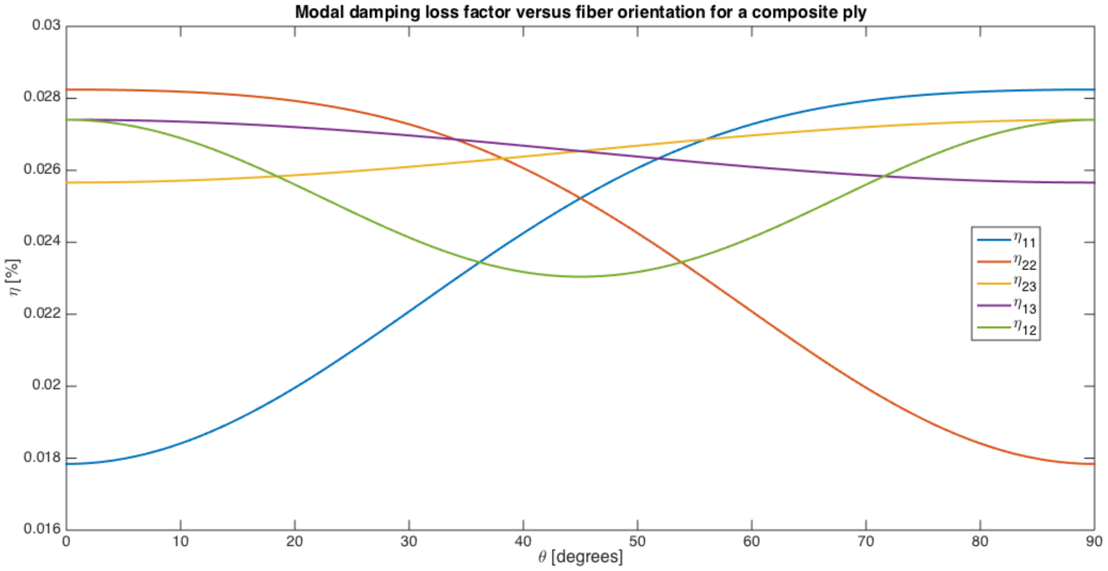

Figure 5.2: The effect of the rotation matrix on the composite ply's damping loss factors.

Note that the rotated damping loss factors do not equal the actual loss factors of a rotated ply. The actual damping loss factors depend on the rotating material stiffness matrix as well.

5.2. Laminate and cross-sectional damping

The next step is translating the damping properties of the individual ply to the damping properties of the entire sandwich-structured material and subsequently of the entire cross-section.

This translation is done by constructing the regular ABD-matrix of the laminate, which is a measure of the laminate's stiffnesses, and the damping ABD-matrix, which is a measure of the laminate's dissipated energy. The calculation of the ABD-matrix can be found in Appendix E and the definitions of the damping ABD-matrix can be seen in Equation 5.5, Equation 5.6 and Equation 5.7 [31], [86]. Due to the low stiffness of the core material and due to the large thickness of the sandwich material, the plane stress conditions cannot be assumed.

$$A_{dij} = \sum_{k=1}^{n} \left(\left[R^{(k)} \right] \eta_l Q_{c\theta}^{(k)} \left[R^{(k)} \right]^T \right) (z_k - z_{k-1}) \tag{5.5}$$

$$B_{dij} = \frac{1}{2} \sum_{k=1}^{n} \left(\left[R^{(k)} \right] \eta_l Q_{c\theta}^{(k)} \left[R^{(k)} \right]^T \right) (z_k^2 - z_{k-1}^2) \tag{5.6}$$

$$D_{dij} = \frac{1}{3} \sum_{k=1}^{n} \left(\left[R^{(k)} \right] \eta_l Q_{c\theta}^{(k)} \left[R^{(k)} \right]^T \right) (z_k^3 - z_{k-1}^3) \tag{5.7}$$

Subsequently both these ABD matrices have to be converted to the ABD matrices of a tubular cross-section. In Figure 5.3 an overview of such a tubular beam cross-section and the corresponding coordinate systems can be seen [31].

In general the ABD-matrix of this kind of cross-section will look like the ABD-matrix seen in Equation 5.8 [31]. Note that the superscript 0 indicates that the terms of the ABD-matrix are those of the cross-section.

$$[\mathbf{A^0}] = \begin{bmatrix} A_{11}^0 & A_{15}^0 & A_{16}^0 \\ A_{51}^0 & A_{55}^0 & A_{56}^0 \\ A_{61}^0 & A_{65}^0 & A_{66}^0 \end{bmatrix} \quad [\mathbf{B^0}] = \begin{bmatrix} B_{11}^0 & B_{12}^0 & B_{16}^0 \\ B_{51}^0 & B_{52}^0 & B_{56}^0 \\ B_{61}^0 & B_{62}^0 & B_{66}^0 \end{bmatrix} \quad [\mathbf{D^0}] = \begin{bmatrix} D_{11}^0 & D_{12}^0 & D_{16}^0 \\ D_{21}^0 & D_{22}^0 & D_{26}^0 \\ D_{61}^0 & D_{62}^0 & D_{66}^0 \end{bmatrix} \tag{5.8}$$

Note that the definitions of all the terms of the ABD-matrix can be found in Appendix G. In case of the composite wind turbine tower and the tower's composite laminate, which is symmetrical and balanced, most terms will be zero, therefore the tower's ABD-matrix will look like the ABD-matrix seen in Equation 5.9.

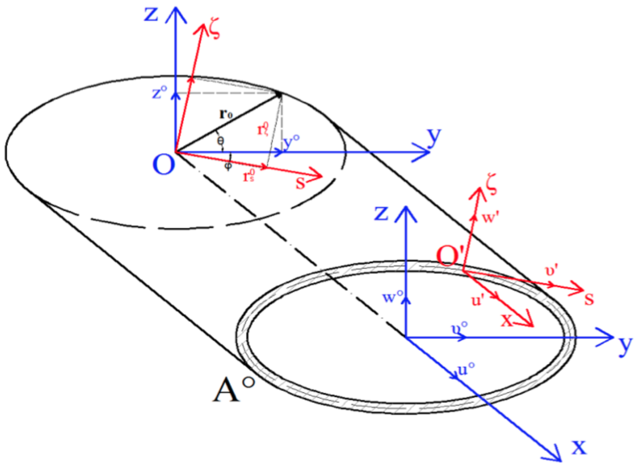

Figure 5.3: A simple representation of a typical tubular beam cross-section geometry and coordinate systems. [31]

$$\mathbf{ABD^0} = \begin{bmatrix} A_{11}^0 & 0 & 0 & 0 & 0 & 0 \\ 0 & A_{55}^0 & 0 & 0 & 0 & 0 \\ 0 & 0 & A_{66}^0 & 0 & 0 & 0 \\ 0 & 0 & 0 & D_{11}^0 & 0 & 0 \\ 0 & 0 & 0 & 0 & D_{22}^0 & 0 \\ 0 & 0 & 0 & 0 & 0 & D_{66}^0 \end{bmatrix} \tag{5.9}$$

The corresponding stiffness terms can be seen in the equations below. The derivation of those terms can be found in Appendix G as well.

$$A_{11}^0 = 2\pi R A_{11} \tag{5.10}$$

$$A_{55}^0 = A_{66}^0 = \pi R A_{66} + \pi R A_{55} \tag{5.11}$$

$$D_{11}^0 = D_{22}^0 = \pi R^3 A_{11} + \pi R^3 D_{11} \tag{5.12}$$

$$D_{66}^0 = 2\pi R (A_h^2 A_{66} + 4 D_{66}) \tag{5.13}$$

Here, R is the tower's radius, the A_{ij} and D_{ij} are the stiffness terms of the composite laminate and $A_h = R$.
The damping ABD-matrix is determined by using the exact same equations, however instead of the using the terms of the laminate's general ABD matrix, the terms of the laminate's damping matrix have to be used.

5.3. Tower Damping

In order to determine the viscoelastic damping properties of the current tower design, the material properties (stiffness ABD and damping ABD matrices) on a cross-sectional level have to be converted into the damping properties on a structural level.
The material damping loss factor of the entire tower can be estimated by Equation 5.14 [31].

$$\eta_m = \frac{\int_L \delta W_d^{sec} dx}{\int_L \delta H^{sec} dx} \tag{5.14}$$

Here,

$$\delta W_d^{sec} = \{\delta \epsilon^{\mathbf{0T}}, \delta \kappa^{\mathbf{0T}}\} \begin{bmatrix} [\mathbf{A_d^0}] & [\mathbf{B_d^0}] \\ [\mathbf{B_d^0}]^T & [\mathbf{D_d^0}] \end{bmatrix} \begin{Bmatrix} \delta \epsilon^{\mathbf{0T}} \\ \delta \kappa^{\mathbf{0T}} \end{Bmatrix} \tag{5.15}$$

$$\delta H^{sec} = \{\delta \epsilon^{\mathbf{0T}}, \delta \kappa^{\mathbf{0T}}\} \begin{bmatrix} [\mathbf{A^0}] & [\mathbf{B^0}] \\ [\mathbf{B^0}]^T & [\mathbf{D^0}] \end{bmatrix} \begin{Bmatrix} \delta \epsilon^{\mathbf{0T}} \\ \delta \kappa^{\mathbf{0T}} \end{Bmatrix} \tag{5.16}$$

Where $\epsilon = \{\epsilon_{\mathbf{x}}, \epsilon_{\mathbf{xy}}, \epsilon_{\mathbf{xz}}\}$ and $\kappa = \{\kappa_{\mathbf{xy}}, \kappa_{\mathbf{xz}}, \kappa_{\theta}\}$ represent the equivalent strain and curvature of a certain section respectively.

The modal damping loss factor η_m can also be described by Equation 5.17, which depends on the system stiffness matrix $[K_s]$ and system damping matrix $[C_s]$ [86], [31].

$$\eta_m = \frac{\mathbf{U_m^T}[C_s]\mathbf{U_m}}{\mathbf{U_m^T}[K_s]\mathbf{U_m}} \tag{5.17}$$

Here U_m are the modal displacements along the center line of the tower.

K_s and C_s are estimated by assuming the entire tower structure as a 2D beam. Subsequently the cross-sectional properties are assigned to the corresponding tower section. By dividing the tower in a certain amount of beam elements, the damping properties of the tower can be calculated by using a finite element based method.
Note that for each element the following assumptions have been made.

- For each element a constant tower radius has been assumed, which is the average radius of the corresponding tower section.
- For each element a constant wall thickness has been assumed, which is the average thickness of the corresponding tower section.
- It is assumed that the 0° direction of the element's laminate is in the lengthwise direction of the tower. In reality the fiber orientations are tapered due to the conical shape of the tower. This means that the laminate's 0° direction is not oriented in the lengthwise direction of the tower.

In Figure 5.4 the translation from a circular tube to a two-node 2D beam element can be seen.

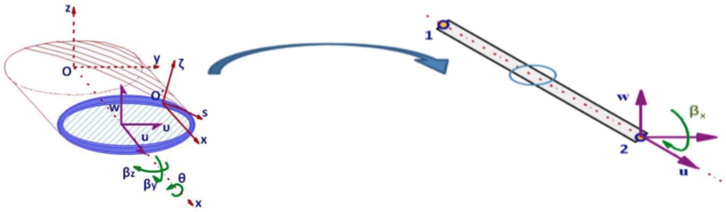

Figure 5.4: The conversion from 3D tubular structure to 2D beam element.

Each beam element has 6 DOFs at each node (and therefore 12 DOFs for a two-node beam element), which are described by Equation 5.18 [31].

$$\mathbf{U_e^i} = \left\{\mathbf{u^{0i}}, \mathbf{v^{0i}}, \mathbf{w^{0i}}, \beta_{\mathbf{y}}^{\mathbf{i}}, \beta_{\mathbf{z}}^{\mathbf{i}}, \theta^{\mathbf{i}}\right\} \tag{5.18}$$

These DOFs can be seen in Figure G.1. Subsequently these DOFs are converted into the total displacements of the tower's center line by Equation 5.19.

$$\begin{aligned} &u^0(x) = \textstyle\sum_{i=1}^n N^i(x)u^{0i} \quad && v^0(x) = \textstyle\sum_{i=1}^n N^i(x)v^{0i} \quad && w^0(x) = \textstyle\sum_{i=1}^n N^i(x)w^{0i} \\ &\beta_y(x) = \textstyle\sum_{i=1}^n N^i(x)\beta_y^i \quad && \beta_z(x) = \textstyle\sum_{i=1}^n N^i(x)\beta_z^i \quad && \theta(x) = \textstyle\sum_{i=1}^n N^i(x)\theta^i \end{aligned} \tag{5.19}$$

Here $N^i(x)$ is the continuous nodal interpolation function.

The relations between the DOFs of a certain beam element and the local strain can be described by Equation 5.20 [31].

$$\begin{gathered} \epsilon_x^0 = u_{,x}^0 = N_{,x}^i(x)u^{0i} \\ \gamma_{xy}^0 = v_{,x}^0 + \beta_z = N_{,x}^i(x)v^{0i} + N^i(x)\beta_z^i \\ \gamma_{yz}^0 = w_{,x}^0 + \beta_z = N_{,x}^i(x)w^{0i} + N^i(x)\beta_y^i \\ \kappa_y = \beta_{y,x} = N_{,x}^i(x)\beta_y^i \\ \kappa_z = \beta_{z,x} = N_{,x}^i(x)\beta_z^i \\ \kappa_\theta = \theta_{,x} = N_{,x}^i(x)\theta^i \end{gathered} \tag{5.20}$$

Subsequently these relations can be rewritten as Equation 5.21 [31]. Here the right-hand side matrix is called the total strain shape function (R^i_{tot}).

$$\begin{bmatrix} \epsilon^0_x \\ \gamma^0_{xy} \\ \gamma^0_{xz} \\ \kappa^0_y \\ \kappa^0_z \\ \kappa^0_\theta \end{bmatrix} = \begin{bmatrix} N^i_{,x}(x) & 0 & 0 & 0 & 0 & 0 \\ 0 & 0 & N^i_{,x}(x) & N^i(x) & 0 & 0 \\ 0 & N^i_{,x}(x) & 0 & 0 & N^i(x) & 0 \\ 0 & 0 & 0 & N^i_{,x}(x) & 0 & 0 \\ 0 & 0 & 0 & 0 & N^i_{,x}(x) & 0 \\ 0 & 0 & 0 & 0 & 0 & N^i_{,x}(x) \end{bmatrix} \begin{bmatrix} u^{0i} \\ v^{0i} \\ w^{0i} \\ \beta^i_y \\ \beta^i_z \\ \theta^i \end{bmatrix} \tag{5.21}$$

For a two-node linear beam element (with 12 DOFs) the nodal interpolation function can be described by Equation 5.22 [31].

$$\begin{gathered} N^1(x) = 1 - \tfrac{x}{L_e} \\ N^2(x) = \tfrac{x}{L_e} \end{gathered} \tag{5.22}$$

Here L_e is the beam element length and x is the global coordinate. The superscripts 1 and 2 indicate the nodes of the beam element. The derivatives of these functions can be found in Equation 5.23.

$$\begin{gathered} N^1_{,x}(x) = -\tfrac{1}{L_e} \\ N^2_{,x}(x) = \tfrac{1}{L_e} \end{gathered} \tag{5.23}$$

Normally these shape functions refer to the local coordinate system of a certain element. In case of the beam finite element this local coordinate system is defined by ξ, which can be seen in Equation 5.24 [31].

$$\xi = \frac{2}{x_2 - x_1}(x - x_1) - 1 \tag{5.24}$$

According to this local coordinate system, $\xi = -1$ is located at node 1 and $\xi = 1$ is located at node 2. Obviously the center of the beam element is located at $\xi = 0$. In Figure 5.5 both the global as the local coordinate systems can be seen.

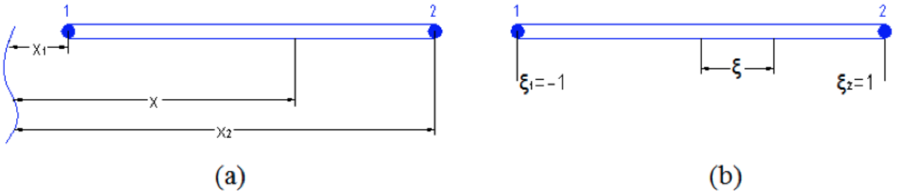

Figure 5.5: A typical two-node beam element. a) the global coordinate system. b) the local coordinate system. [31]

The local coordinate system is used to define the shape functions, which are used for interpolating the unknown displacement field within an element. By assuming that x_1 (the global coordinate of node 1 equals zero and subsequently by substituting Equation 5.24 into Equation 5.22, the local shape functions become as in Equation 5.25.

$$\begin{gathered} N^1(\xi) = \tfrac{1-\xi}{2} \\ N^2(\xi) = \tfrac{1+\xi}{2} \end{gathered} \tag{5.25}$$

These linear shape functions can be seen in Figure 5.6
The derivatives of the shape functions in the global coordinate system are constants, which can be seen in Equation 5.23, and therefore they will be equal to the derivatives of the local coordinate system.

Subsequently the shape functions can be used to determine the element stiffness matrix $[K]$ and the element damping matrix $[C]$, which are defined by Equation 5.26 and Equation 5.27 respectively [31].

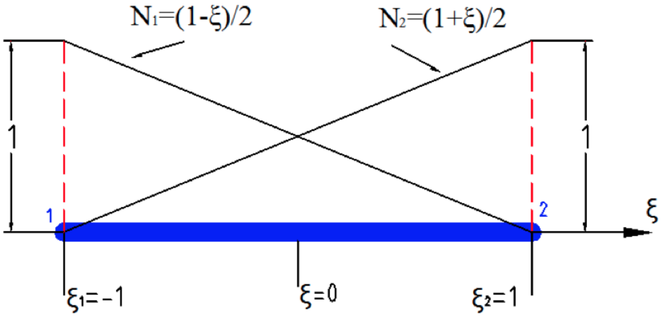

Figure 5.6: The linear shape functions of a two-node beam finite element [31].

$$[K_e]^{ij} = \int_{L_e} \left(\left[R^i_{tot}\right]^T \begin{bmatrix} [\mathbf{A^0}] & [\mathbf{B^0}] \\ [\mathbf{B^0}]^T & [\mathbf{D^0}] \end{bmatrix} \left[R^j_{tot}\right] \right) dx \tag{5.26}$$

$$[C_e]^{ij} = \int_{L_e} \left(\left[R^i_{tot}\right]^T \begin{bmatrix} [\mathbf{A^0_d}] & [\mathbf{B^0_d}] \\ [\mathbf{B^0_d}]^T & [\mathbf{D^0_d}] \end{bmatrix} \left[R^j_{tot}\right] \right) dx \tag{5.27}$$

Where $i, j = 1, 2$ are the element nodes

The calculation of the integrals presented, which is seen in Equation 5.26 and Equation 5.27, takes place in the local coordinate system. The global coordinate system can be transformed to the local coordinate system by applying Equation 5.28 and by applying different integration limits.

$$dx = \frac{L_e}{2} d\xi \tag{5.28}$$

As a result the calculations of $[K_e]$ and $[C_e]$ in the local coordinate system become as in Equation 5.29 and Equation 5.30.

$$[K_e]^{ij} = \int_{-1}^{1} \left(\left[R^i_{tot}\right]^T \begin{bmatrix} [\mathbf{A^0}] & [\mathbf{B^0}] \\ [\mathbf{B^0}]^T & [\mathbf{D^0}] \end{bmatrix} \left[R^j_{tot}\right] \right) \frac{L_e}{2} d\xi \tag{5.29}$$

$$[C_e]^{ij} = \int_{-1}^{1} \left(\left[R^i_{tot}\right]^T \begin{bmatrix} [\mathbf{A^0_d}] & [\mathbf{B^0_d}] \\ [\mathbf{B^0_d}]^T & [\mathbf{D^0_d}] \end{bmatrix} \left[R^j_{tot}\right] \right) \frac{L_e}{2} d\xi \tag{5.30}$$

Subsequently the line integrals are calculated by using the Gauss integration method, which is seen in Equation 5.31 [31].

$$[K_e]^{ij} = \sum_{k=1}^{n} H_k \left(\left[R^i_{tot}(\xi(k))\right]^T \begin{bmatrix} [\mathbf{A^0}] & [\mathbf{B^0}] \\ [\mathbf{B^0}]^T & [\mathbf{D^0}] \end{bmatrix} \left[R^j_{tot}(\xi(k))\right] \right) \frac{L_e}{2} \tag{5.31}$$

Here, the index number k indicates the Gauss integration points and H_k indicates the corresponding weights. In order to avoid the shear locking of the beam, the stiffness and damping matrices are calculated at just one integration point [31]. The final stiffness and damping matrices of each beam finite element will have a square form with dimensions 12x12. The final stiffness matrix can be seen in Equation 5.32.

$$[K_e]^{ij}_{12x12} = \begin{bmatrix} [K_e]^{11}_{6x6} & [K_e]^{12}_{6x6} \\ [K_e]^{21}_{6x6} & [K_e]^{22}_{6x6} \end{bmatrix} \tag{5.32}$$

Finally the element matrices of each element have to be substituted in one system matrix. In case of 12 DOFs per element and a total number of nodes of $n = 100$ the system stiffness and damping matrices $[K_s]$ and $[C_s]$ wil have dimensions 606x606.
Finally the modal viscoelastic damping of the tower can be calculated by solving Equation 5.17.

5.4. Model sensitivity

As can be seen in the previous sections, the model depends on a large amount of variables like the basic material properties, laminate architecture and tower architecture. Of all these variables, the basic material properties like the damping loss factors and stiffnesses of the material constituents are the most important and form the baseline of the tower's modal damping loss factor.

In order to assure that the ABD matrices are calculated correctly, the ABD matrices calculated by the model are compared to the ABD matrices calculated by Kolibri. Also the FEM part of the model has been validated. This validation process can be seen in Appendix H.

5.4.1. The influence of the composite laminate's architecture

Obviously the laminate's architecture will have a significant influence on the tower's damping loss factor. Factors that influence the damping loss factor are among others the fiber volume fraction, fiber orientation, the stacking sequence and the thickness distribution. The fiber volume fraction depends on the production technique and according to tests done by Jules Dock, this fraction is approximately 50% for the composite tower. Other material properties like the poisson's ratio do have an influence on the tower's damping loss factor, however this effect is negligible.

In general the higher the thickness of a certain layer, the higher the flexural and axial rigidity of that layer and therefore the higher the influence of that layer's damping capabilities on the overall modal damping loss factor of the tower. In case of the stacking sequence, a more outward position of a certain layer with respect to the neutral line of the composite laminate will result in a larger influence of that layer on the laminate's flexural damping capabilities and therefore the tower's flexural modal damping loss factor. These are standard effects, which follow from the classical laminate theory.

The influence of the fiber orientation on the composite tower's modal damping loss factor is more complicated. In Figure 5.7 the effect of the fiber orientation on the tower's damping loss factor can be seen for two different modes.

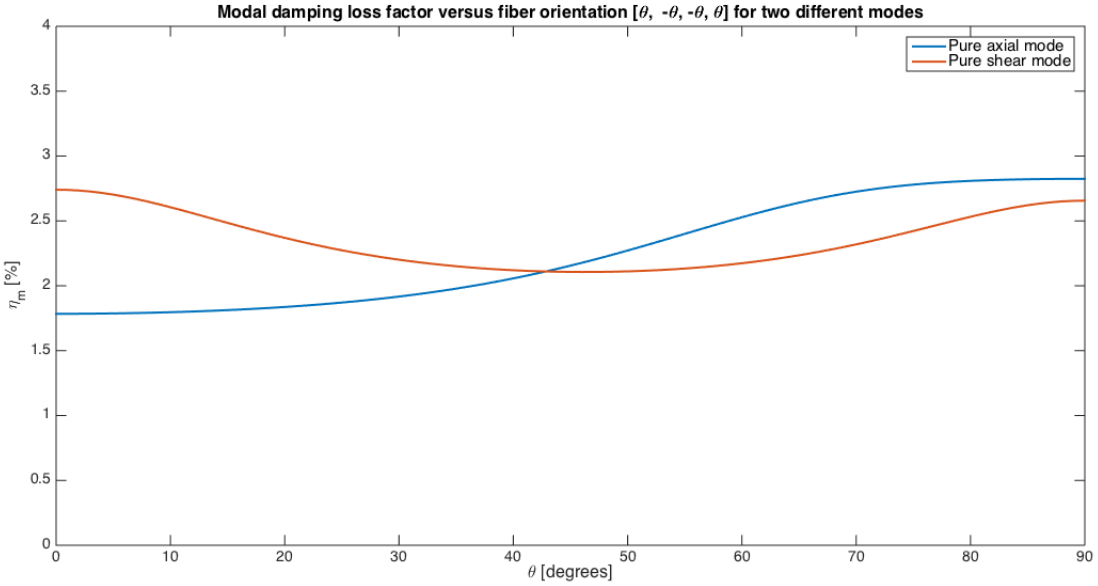

Figure 5.7: The effect of the fiber orientation on the tower's damping loss factor for two different modes.

In case the tower subjected to an axial motion, a fiber orientation of 90° will result in the maximum damping loss factor, while a fiber orientation of 0° will result in the minimum damping loss factor. In case the tower is subjected to a shearing motion, local maxima can be found at 0° and 90°, while the damping loss factor is at its minimum at a fiber orientation of 45°. This difference in response can be explained by Figure 5.8.

Note that the circular ring in Figure 5.8 is assumed to be subjected to a load in the x-direction for a shearing motion and a load in the y-direction for an axial motion. For both motions, the damping loss factor is globally determined by the two sections indicated by the red dashed rectangles.

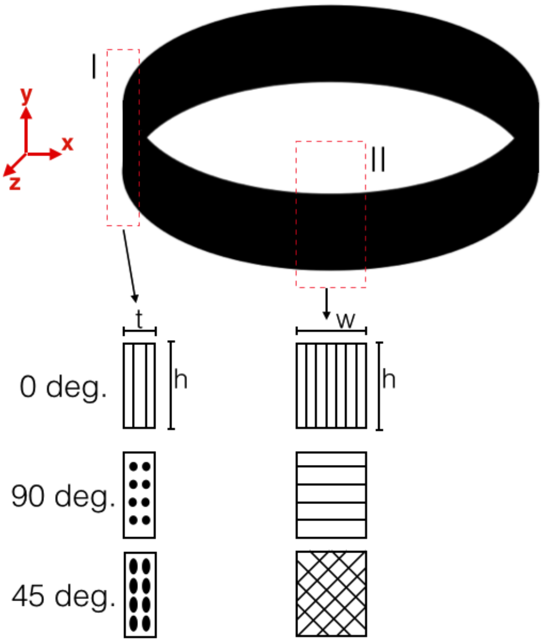

Figure 5.8: Ring shaped section of the composite tower with corresponding detailed views of several local laminates. Section I is the front view at the area indicated by the left red dashed rectangle and coincides with the cross-section of the laminate. Section II is the front view at the area indicated by the right red rectangle. Both sections show the local fiber orientation.

In case of a pure bending motion, the damping loss factor will be a combination of the axial and shear responses, since a certain rotation at a certain node will result in both a shear displacement as a certain curvature. As a result a ratio between the shear strain energy and the bending strain energy can be determined, which is in Equation 5.33. Note that the derivation of this ratio can be found in Appendix D.

$$\frac{U_s}{U_b} = 3\frac{E}{G}\left(\frac{R}{L}\right)^2 \tag{5.33}$$

Here E is the Young's modulus, G is the shear modulus, R is the radius of the thin-walled cylinder and L is the length of the cylinder.

According to this ratio, the tower's architecture will influence the modal damping loss factor of the bending modes and will determine the effect of the fiber orientation on this factor.

5.4.2. The influence of the tower's architecture

The variables concerning the tower's architecture, like the tower's radii, the tower's wall thicknesses and the length of the tower, have in general no influence on the tower's axial, shear or torsional damping. During these modes, the modal damping is mainly determined by the material properties and the laminate's architecture. On the other hand, they have a significant influence on the modal damping of the tower's bending modes.

For example, the influence of the tower's radius can be seen in Figure 5.9.

Note that at $R = 1m$ the axial damping of the tower prevails, while at $R = 25$ the shear damping starts to be dominant. The tower length will have a similar influence. In general the smaller the length of the tower in combination with a certain radius, the higher the influence of the shear damping. A larger wall thickness on the other hand will result in a larger influence of the shear damping in the fiber orientation range $0°$ to $30°$. Nevertheless its influence on the tower's modal damping is insignificant and can be neglected. For wall thicknesses smaller than $1m$ the influence can be considered to be non-existent, which confirms the thin-walled assumption.

The exact effect of the tower length and the wall thickness can be seen in Appendix I.

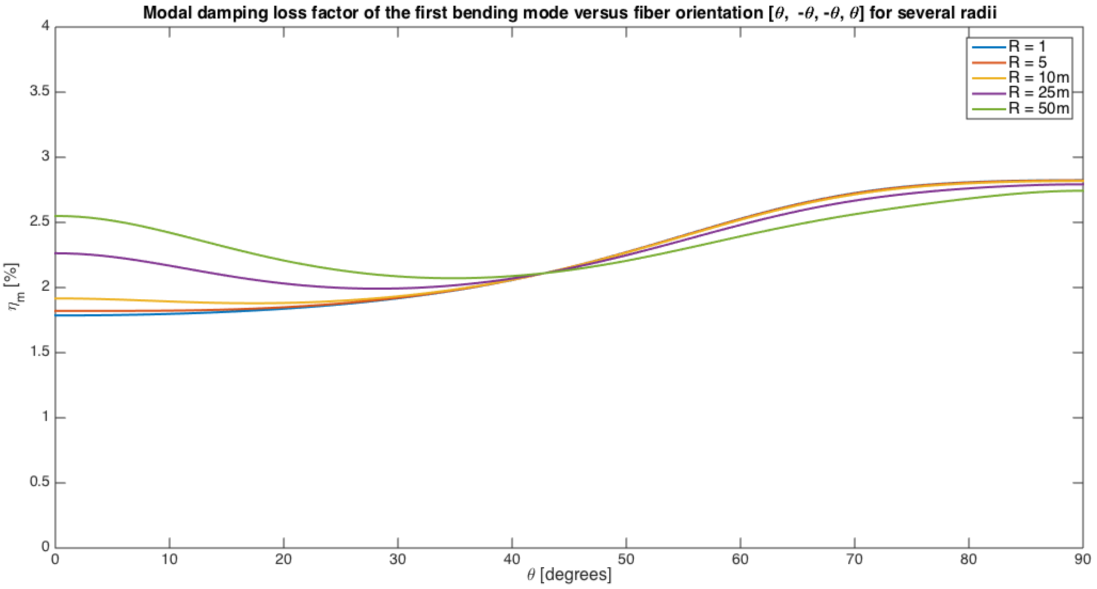

Figure 5.9: The influence of the fiber orientation and tower's radius on the modal damping loss factor of the first bending mode. Note that the tower's element length is $1m$ and the tower's wall thickness is $100mm$

5.4.3. The influence of a core

In case of a circular composite tower, a core material can be used. The main reason for using a core material in the composite tower's laminate is to prevent local buckling [102]. A thicker laminate can be chosen in order to increase the local bending stiffness, however choosing a light core material is far more efficient and results in a far lighter design. Therefore it is required to know the influence of a core material on the modal damping loss factor of the tower.

There are three variables that influence the tower's modal damping loss factor. These variables are the core stiffness, the core's damping loss factors (η_{core} and the core thickness.

In Figure 5.10 the influence of the core stiffness and the fiber orientation on the tower's modal damping loss factor can be seen.

As can be seen, the influence of the core on the tower's modal damping loss factor can be increased by increasing its stiffness with respect to the laminate's stiffness. This same effect is described by Lakes [58] Note that a low modulus foam like the Airex T92.80 does not have a significant effect on the tower's modal damping loss factor, even if the core's loss factor and core thickness are increased drastically. The biggest impact is seen at a fiber orientation of 90°, since at this orientation the difference between the stiffness of the composite material and the stiffness of the core material is at its minimum. The exact effect of the core's damping loss factor and the core's thickness can be seen in Appendix J.

It can be concluded that the core material will only have a significant influence on the tower's modal damping loss factor if the core's stiffness is sufficiently high compared to the overall thickness of the composite material. Note that the current model assumes a thin-walled structure and therefore it ignores local shear effects. As a result, it might be possible that in reality the contribution of the core material on the tower's modal damping loss factor is much higher.

5.4.4. Mode dependency

As discussed in Section 3.1 a wind turbine has several eigenmodes / motions. The most important motions for a cylindrical tower are the first and second bending mode, which correspond with the bending of a cantilever beam and a 3-point-bending configuration respectively. For both bending modes the modal damping will be a combination of the tower's axial damping and the tower's shear damping. The less important motions are the torsional and axial mode, whose modal damping loss factors are depending on pure shear damping and pure axial damping respectively. In Figure 5.11 modal damping loss factors of the first two bending modes can be seen. As can be seen, the shear damping is more dominant at the second bending mode than at the first bending mode. Therefore each mode results in a different ideal laminate lay-up.

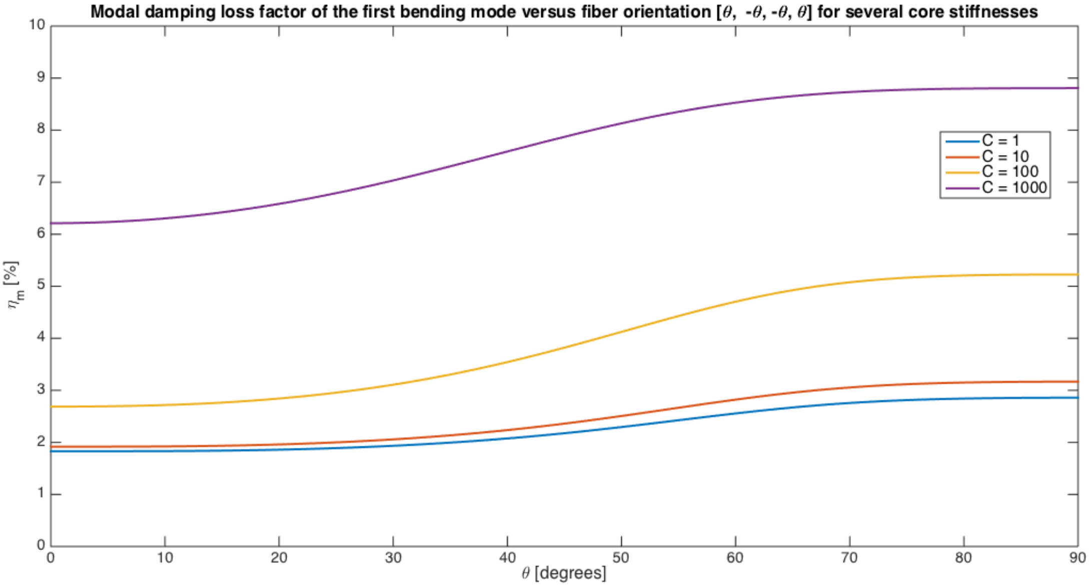

Figure 5.10: The influence of the fiber orientation and the core stiffness on the modal damping loss factor of the first bending mode. The symbol C represents the multiplification factor, which is multiplied by both the core's tensile//compressive modulus and the core's shear modulus. Both moduli are equal to the moduli of the Airex T92.80 foam material, which can be seen in Appendix C. Note that the tower's radius is $5m$, the tower's element length is $1m$ and the total thickness of the face sheets is $100mm$. The core has a thickness of $100mm$ as well and a loss factor of 0.1 for both axial and shear damping.

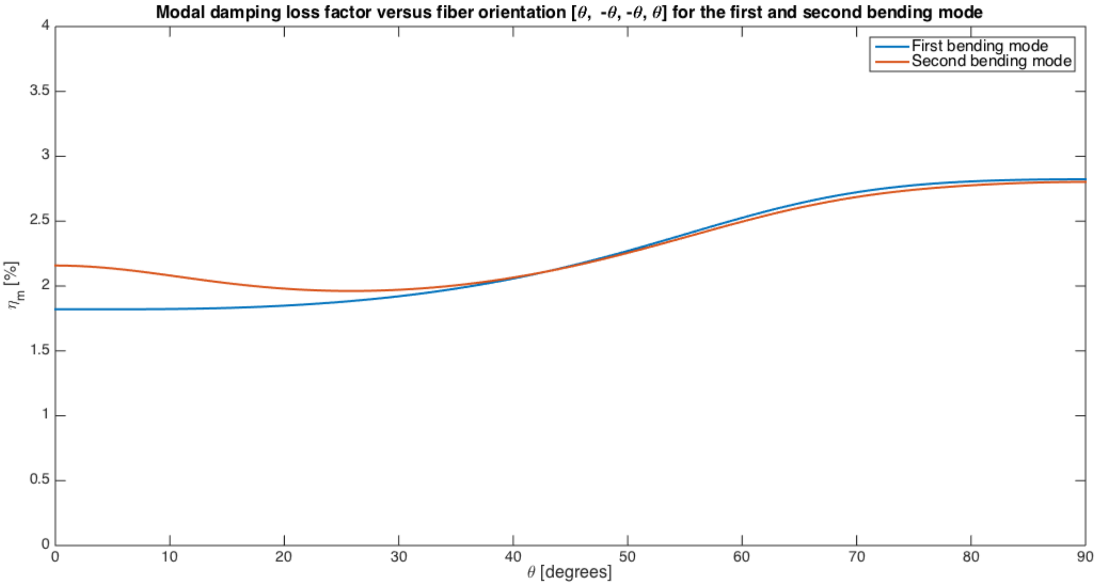

Figure 5.11: The influence of the fiber orientation and tower's wall thickness on the modal damping loss factor of the first two bending modes. Note that the circular tower's radius is $5m$, the wall thickness is $100mm$ and the element length is $1m$.

5.5. Model implementation and results

The current design of the composite 10MW wind turbine tower is an approximately 104m high conical shell. The used composite material is a fiber reinforced vinyl ester laminate with an Airex T92.80 core. The design of the tower faced two major challenges. The first challenge was that the tower should have enough strength to withstand the dynamic loads. The second challenge was that the tower should be flexible enough in order for the first eigenfrequency to be beneath the 1P frequency band.

Due to these challenges, the final design can be considered as unusual, since the thickness is varying significantly and the bottom thickness is much thinner than the top thickness.

The sandwich material has a constant core thickness along the entire tower, while the laminates differ in thickness. At the bottom and the top of the tower the applied laminate is a 2m high solid laminate without a core. These pieces of solid laminate are required to mount the tower to the support structure and to mount the nacelle to the tower. The mounting will be done by means of T-bolts.

In Table 5.3 the global dimensions of the current design can be seen [103].

Table 5.3: Table with design parameters

Parameter	**Value**	**Description**
L	$104.13m$	Tower height
D_{top}	$5,5m$	Top diameter
D_{bottom}	$8,02m$	Bottom diameter
D_{40m}	$6.99m$	Diameter at 40m
t_{top}	$241mm$	Top skin thickness
t_{bottom}	$203mm$	Bottom skin thickness
t_{40m}	$186mm$	Skin thickness at 40m
$L_{mounting}$	$2m$	Length of solid top and bottom laminate.
t_{core}	$106mm$	Thickness of the core.

The material properties of the various materials can be seen in Appendix C.

The tower's composite laminate is symmetrical and balanced and consists of 3% 0° oriented plies, approximately 52% 90° oriented plies and approximately 45% ±45° oriented plies. Other design parameters like the actual lay-up and the tower's exact thickness distribution are classified and therefore these will not be discussed in this report.

5.5.1. Implementation of the current design

Subsequently these parameters can be used to calculate the modal damping loss factors of the first two bending modes. Note that all the stiffnesses have been assumed to be frequency and temperature independent. The modal loss factors of the first bending mode for three different frequencies can be seen in Table 5.4. Note that according Equation 3.21, the tower's damping loss factor can be converted to the damping ratio by dividing the loss factor by a factor two.

Table 5.4: Modal damping loss factors of the first bending mode for three different frequencies.

frequency $[Hz]$	η_{m1} $[-]$	η_{m2} $[-]$
10	0.0226	0.0225
1	0.0238	0.0236
0.1	0.0254	0.0252

As can be seen, the tower can be considered frequency independent for a frequency range of $0.1Hz$ to $10Hz$. Also the difference in modal damping between the first and second bending mode can be neglected, which means that the modal damping loss factor can be considered equal for the most important low frequency motions.

Beside the loading frequency and mode, the modal damping loss factor is also dependent on the surrounding temperature. In Figure 5.12 the influence of the temperature on the modal damping loss factor can be seen.

The average air temperature on the North Sea ranges from $0°C$ to $4°C$ in January and from $13°C$ to $18°C$ in July [3]. This means that on an average the damping loss factor will range from approximately 2.13% in January to approximately 2.26% in July, which is approximately a difference of 6%. This means that on an average, the change in modal damping loss factor due to the temperature can be neglected and therefore it can assumed that the tower is temperature independent.

Note that the materials' moduli are assumed to be frequency and temperature independent and therefore the actual modal damping loss factors might differ a bit from the calculated values.

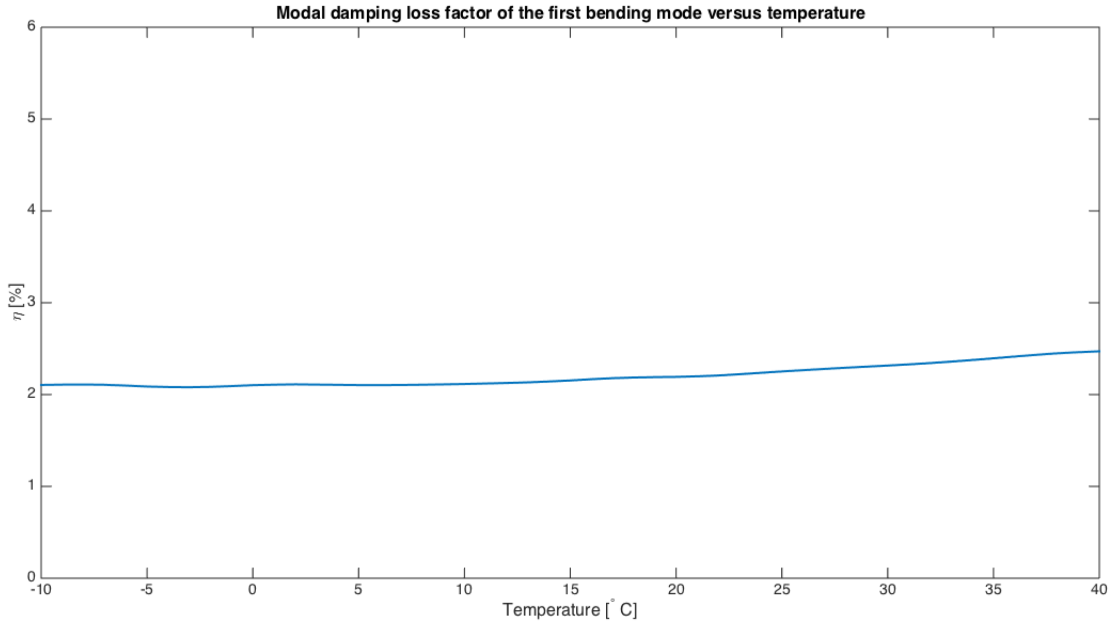

Figure 5.12: The influence of the temperature on the tower's modal damping loss factor.

5.5.2. Comparison with a steel design

In order to validate whether or not the composite design has a better damping performance than a steel design, the material properties of the current design are substituted with the properties of steel. The assumed material properties of steel can be seen in Table 5.5. Note that the shear damping of steel is unknown, therefore it is assumed to be twice the axial damping.

Table 5.5: Material properties of steel.

Property	Value
E [GPa]	200 [44]
G [GPa]	97 [44]
v [$-$]	0.3 [44]
η_t [$-$] at 1Hz	0.0134
η_s [$-$] at 1 Hz	0.0268

Here η_t is the axial damping loss factor and η_s is the shear damping loss factor.

Subsequently in Table 5.6 the comparison between the modal damping loss factors of the first two bending modes of the composite design, the composite design with and the steel tower design can be seen. Note that according Equation 3.21, the tower's damping loss factor can be converted to the damping ratio by dividing the damping loss factor by a factor two.

Table 5.6: Comparison of the modal damping loss factors of the current composite design and a steel design.

Material	η_{m1} [$-$]	η_{m2} [$-$]
Composite	0.0238	0.0236
Steel	0.0135	0.0142

According to the current model, the modal damping loss factors of the first two bending modes are approximately 71% higher than the damping loss factors of the assumed steel tower. According to Equation 3.8, a 71% increase of the damping ratio, results in an approximately 71% reduction of the time that a certain excitation requires to return to its steady-state. This means that the amplitude will return faster to zero and that the system is subjected to less loading cycles. The fatigue life of the material will therefore be increased as well.
As mentioned before, the damping loss factor is approximately twice the damping ratio. Hence, the damping ratio shows a 71% increase as well.

5.5.3. Optimization of the current design for damping

The current tower design has been optimized in order to sustain a certain strength and to have certain eigenfrequencies, however the tower has not been optimized for damping. This means that a much higher damping loss factor can be achieved by altering e.g. the fiber orientation, tower architecture, thickness distribution, stacking sequence, etc. The current lay-up exists of primarily ±45° plies and 90° plies. For the first bending mode it is beneficial to have solely 90° plies, since this lay-up results in the highest possible axial damping. It will result in the lowest possible bending strength and bending stiffness as well and therefore most of the time it is required to have plies with other fiber orientations.

For the second bending mode the influence of the shear damping is higher and therefore the 0° plies result in a higher damping loss factor than the ±45° degrees plies. By applying 0° plies instead of the ±45° plies, the damping loss factor of the second mode can be increased while the stiffness is not drastically decreased.

In case of the stacking sequence, by placing the 90° plies as far from the laminate's neutral line as possible, a higher flexural damping loss factor is achieved. It will lead to a decreased bending stiffness and strength as well. The same can be concluded for the laminate's thickness distribution.

Another way to increase the tower's modal damping loss factor is by applying a stiffer core material. The core material will store a larger amount of strain energy and therefore a larger amount of energy will be dissipated by the core material.

6

Conclusion and Recommendations

6.1. Conclusion

Jules Dock's current composite wind turbine design uses a structural damping ratio, which is common for steel tower designs. In order to have a better prediction of the tower's fatigue life, the composite tower's damping capabilities have to be researched. Also by increasing this design's structural damping ratio with 10%, already several years can be added to the fatigue life of the composite structure. The structural damping of a wind turbine can be divided in the damping due to structural connections and material damping. Of those two, only the material damping will be considered, since the damping due to the structural connections is complex and non-linear.
The resulting research question of this thesis is:

What is the material damping of a flexible composite tower, made of a fiber reinforced sandwich-structured composite, and in which way are the tower's damping capabilities affected by the loading frequency and temperature?

The material damping of composite materials can be divided in five damping mechanisms of which one is relevant for the composite tower. This damping mechanism is viscoelastic damping and depends mainly on the loading frequency, loading amplitude and temperature. In case low strains are assumed, the viscoelastic damping can be considered amplitude independent.
There are several methods capable of determining the viscoelastic damping ratio of the structure, however most are limited to small and simple composite beams and structures. The most suitable micro mechanical model is the Saravanos-Chamis model due to its practicality. The most suitable macro mechanical model is the FEM model described by Chortis. Since little information is present about the damping loss factors of resins, composites and foam materials, measurements have been performed. Note that each damping identification method has its own limitations and defines damping differently. As a result, determining the damping capabilities of a system (comprising of specimen, sensors, mounting, etc.) is not straightforward and unambiguous.

During this research two different measurement methods have been performed. The first measurement method is a simple cantilever beam test. From the results of these tests can be concluded that this method is not suitable for any damping measurements. Despite the fact that a phase lag could be measured, this phase lag was most likely due to clamping effects and/or due to other time lags in the load cell and/or test bench.
The second method is DMA, which uses a similar configuration (3-point-bending) and is able to measure the same $\tan(\phi)$ as the simple bending tests. This method is far more accurate and is capable of measuring the temperature dependency of the material as well.

During the DMA measurements, several materials have been tested. These materials are two resin systems, steel, several composite materials and several foam materials. Apparently both resin systems, all tested composite materials and the high density foams can be considered frequency independent in the range of $0.5Hz$ to $10Hz$. In case of the low density foams this range will be much smaller, however still they can be considered frequency independent in the range of $0.5Hz$ to $1Hz$. This means that for most of the tower's loading frequencies, the damping loss factor will not change.
At a $0.1Hz$ frequency the damping loss factor will in general be higher, however for the vinylester and reinforced vinylester laminates this increase is less than 10%. Steel on the other hand can be considered frequency independent in the range of $0.1Hz$ to $1Hz$.
The temperature dependency is more complicated. It depends on both the material's damping capabilities as the material's T_g. In general viscoelastic materials tend to show an increasing damping loss factor with an increasing temperature, while an elastic material like steel hardly shows any thermal response in a temperature range of $-20°$ C to $120°C$.

In case of the structural foams, some other conclusions with respect to the foam density can be made. In general the higher the foam density, the higher the damping loss factor. This is probably due to the fact that structural foams cannot be considered as solid materials. The lower the density, the more the damping loss factor is determined by the foam's structure instead of by the foam's material. In case of the anisotropic PET foams, different directions have different loss factors. In case of the Airex T92.80 the difference in damping loss factor between the two directions can be neglected.
The damping capabilities of sandwich structured composites is probably mainly determined by the damping capabilities of the face sheets. Below the foam's T_g, the damping loss factors are only a bit higher than the damping loss factors of the face sheets.
When comparing the measured damping loss factors with the damping loss factors found in literature, one finds that for similar materials and similar configurations a large diversity of damping loss factors has been measured. Apparently the measured damping loss factor is influenced by the amount of parasitic damping, which is dependent on, among others, the type of measurement, sample quality and the type of configuration. Therefore the validity of the measured damping loss factors is questionable. Nevertheless, the measured values will serve as an input for the wind turbine's damping model.

The resulting damping behavior of the tower can be considered frequency independent in a frequency range of $0.1Hz$ to $10Hz$. Also the difference in modal damping between the first and second bending mode can be neglected, which means that the modal damping loss factor can be considered equal for the most important low frequency motions. Also the tower can be considered temperature independent on an average. The modal damping loss factors of the first two bending modes are approximately 71% higher than the damping loss factors of a steel tower with the same dimensions. Since the damping loss factor is approximately twice the damping ratio, the damping ratio will show a 71% increase as well. This 71% increase of the damping ratio, results in an approximately 71% reduction of the time that a certain excitation requires to return to its steady-state. This means that the amplitude will return faster to zero and that the system is subjected to less loading cycles. The fatigue life of the material will therefore be increased as well.
By optimizing the tower for damping, the damping loss factor can be increased even further. However, due to this optimization, the tower's strength and stiffness will suffer. Also wind turbine tower's eigenfrequencies might shift in the 1P and 3P loading frequency range.

In the end the research question and all the corresponding subquestions and goals, which are stated in Chapter 2, are answered. Still this is achieved by making several assumptions, which might have affected the accuracy of the measurements and the model.
The most important assumptions are:

- Only viscoelastic damping is present.
- The axial damping loss factor equals the flexural damping loss factor.
- The axial damping loss factor of the matrix is assumed to be equal to the shear damping loss factor.
- The axial damping loss factor of the matrix is assumed to be equal to the value measured during the DMA tests.
- The glass fibers are assumed to be isotropic.
- The cross-section of the glass fibers is assumed to be circular.
- the axial damping loss factors of the glass fibers is determined by using the Saravanos-Chamis model in such a way that the damping loss factor of the composite ply in fiber direction equals the same damping loss factor measured during the DMA tests.
- Since the influence of the glass fibers' shear damping on the tower's damping loss factor is negligible small, the glass fibers' shear damping loss factors are assumed to be zero.
- The tower is assumed to be thin-walled.
- The matrix' moduli are assumed to be frequency and temperature independent.
- For each element a constant tower radius has been assumed, which is the average radius of the corresponding tower section.
- For each element a constant wall thickness has been assumed, which is the average thickness of the corresponding tower section.
- It is assumed that the 0° direction of the element's laminate is in the lengthwise direction of the tower.

6.2. Recommendations

In order to improve the accuracy of the current model, several topics should be addressed in a follow-up research.
Those topics are:

- **Measuring damping at low loading frequencies**: The damping loss factors, which were measured during the DMA measurements, are different when compared to the damping loss factors found in literature. Probably the parasitic damping induced by the friction between the sample and the supports and crosshead is significant. Also the DMA machine's structure could induce some extra damping. Whether or not the resulting damping loss factors are accurate is therefore still questionable. There are several ways to reduce the parasitic damping, e.g. by reducing the contacting surfaces between the supports/crosshead and the sample or by using the modal damping measurements described in Appendix A. Whether these improvements are sufficient enough or suitable for low frequency vibrations is still unknown. A follow-up research should therefore focus primarily on this topic.
- **Damping due to structural connections**: The structural damping of a wind turbine is a combination of the material damping and the damping due to the structural connections. Since the latter one could be the most dominant damping mechanism, it probably cannot be neglected. An estimation of the damping due to structural connections should be one of the main topics in a follow-up research.
- **Local damping effects** The current 2D wire model might neglect several local effects and as a result the used model might be conservative. In order to take these effects into account, a 3D FEM model has to be made. Also other local effects like damping due to fiber-matrix interphase, viscoplastic damping, thermoelastic damping and damping due to damage could be considered.
- **A better estimation of the damping capabilities of the composite plies**: In order to estimate the damping loss factors of the composite plies more accurately, Zhao-Weng's model could be used. This model requires dynamic properties like the storage moduli and loss moduli of the resin and the fibers. Also this model takes the actual shape of the rovings into account. Besides, the damping properties of a ply can be determined, by measuring the damping loss factor in all directions (η_{11}, η_{22}, η_{23}, η_{13} and η_{12}).
- **Damping of structural foams and sandwiches**: Only little is known about the damping behavior of foam materials and therefore also about the damping behavior of sandwich structured composites. In general foams show a different damping behavior than solid materials, which is primarily due to their random cell structure. Also the exact influence of the foam material on the overall damping behavior of the sandwich structured composite is still unknown. A thorough research on the damping behavior of foam material like PVC and (anisotropic) PET foams and the damping behavior of sandwich structured composites, might result in an improvement of the current damping model.
- **Non-linear damping**: The current damping model takes only the linear viscoelastic behavior of the tower into account, which means that the tower's damping behavior is amplitude independent. In case the strains cannot be considered smallI. The current damping model should be converted into a non-linear model. This non-linear model is described by Chortis [31].
- **Scale model tests**: In order to validate the current model, a scale model should be tested. Chortis [31] already validated this model, however during a scale model test other damping mechanisms like the damping due to the structural connections will be measured as well.
- **Prepregs**: In a follow-up research prepregs should be used to manufacture the composite laminates. The dry fiber fabrics used for the vacuum infused composite laminates contain often polymeric stitches, which are most of the time absent in prepregs. Also during the placing of the vacuum bag, the dry fiber fabrics may shift, which will result in less accurate results.
- **Improve FEA model**: Jules Dock's current model is based on a FEA model with a beam element length of $1m$. A more accurate damping loss factor can be achieved by decreasing the element length while the length of the tower is kept constant. Also the taper of the tower's laminate should be taken into account.

Another topic that should be considered in a follow-up research is:

- **Exact relation between the structural damping and the fatigue life**: As mentioned in this report, a higher damping loss factor decreases the number of loading cycles, which is beneficial for the fatigue life of the structure. The exact relation between the composite tower's structural damping and the entire wind turbine's fatigue life is, however, still unknown. For example damage (e.g. matrix cracking, fiber-matrix debonding and delaminations) and cyclic heating are fatigue related phenomena that will influence both the tower's structural damping and the tower's fatigue life. By estimating the relation between the structural damping and the fatigue, a better estimation of the fatigue life can be made.

A

Measuring Damping

There are several methods to measure damping. A common way to measure the modal damping of a certain material is by using a shaker/stinger or an impact hammer in order to subject the sample to a certain vibration and a laser vibrometer in order to measure the modal response and damping of the sample [15], [4]. A large variety of experimental set-ups are possible (e.g. the sample can have fixed or free boundary conditions). In Figure A.1 an example of this method can be seen [4].

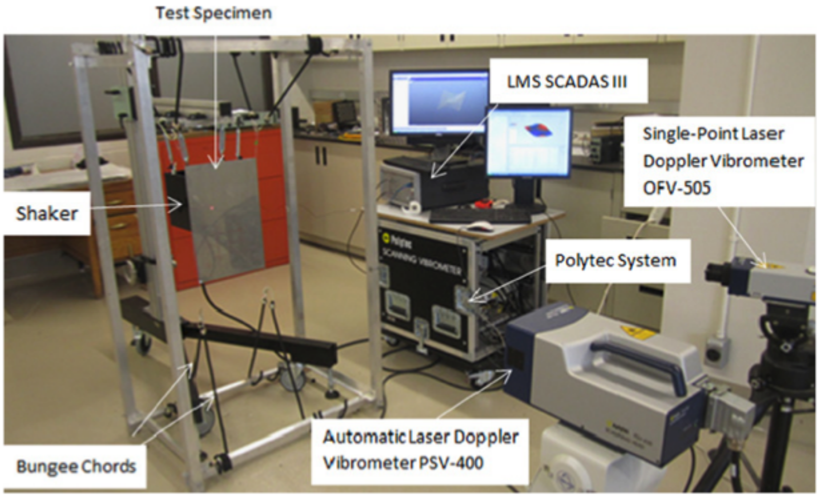
Test Specimen
LMS SCADAS III
Single-Point Laser
Doppler Vibrometer
OFV-505
Shaker
Polytec System
Automatic Laser Doppler
Vibrometer PSV-400
Bungee Chords

Figure A.1: Example of an experimental set-up [4].

In general these methods are meant for real vibrations and are most of the time unsuitable for low frequency vibrations like the slow oscillating movements of the composite wind turbine tower. In order to measure the damping, two methods have been tested of which the first method is described in this appendix. The first method is a simple bending test using a 20kN Zwick test bench. The test set-up of this method can be seen in Figure A.2.

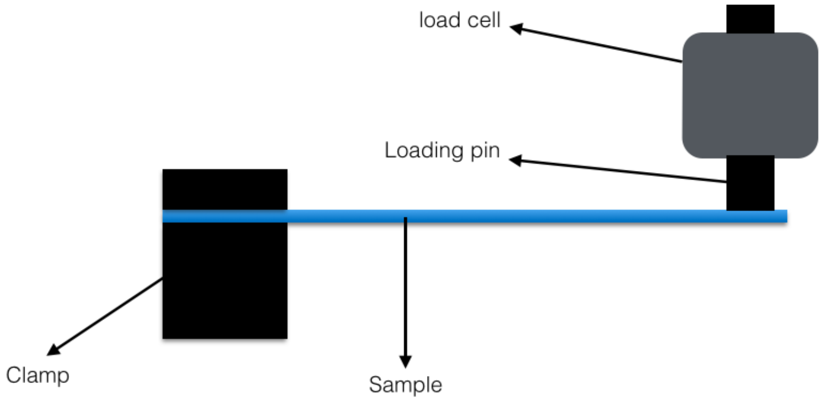

Figure A.2: Test set-up of the simple bending test.

The main goal of this test was to measure the phase lag between the applied force and the displacement, which can be seen in Figure A.3 [94].

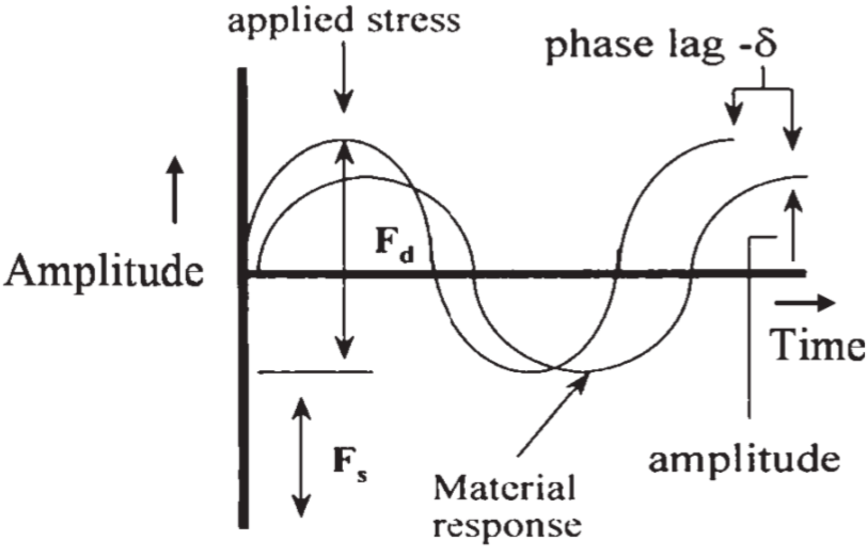

Figure A.3: Stress-strain response of a certain material / structure [94].

Subsequently this phase lag can be converted into the damping loss factor by using Equation A.1 [106].

$$\eta = \tan(\phi) = tan(2\pi f \Delta t) \tag{A.1}$$

Here, f is the loading frequency and Δt is the time lag. According to this equation, when the frequency increases by approximately a factor 10, the phase lag should decrease approximately by a factor 10 in order to achieve a similar damping loss factor.

Two measurement series have been performed. During the first series 0 degrees vinylester laminates and 90 degrees laminates have been tested using a 10N load cell. Note that the composite laminates are made of glass fiber reinforced vinylester and are produced by means of vacuum infusion. During the second measurement series, a steel plate and a 0 degrees laminate have been tested using a 1kN load cell. Note that each sample is subjected to three loading cycles. Also each sample has a size of $L = 300mm$ and $W = 100mm$. The thickness varies with each sample.

A.0.1. First measurement tests using the 10N load cell

During the first measurement series, two 0 degrees laminates, two 0 degrees laminates with a thickening at one end and two 90 degrees laminates have been tested.

The 0 degrees laminates exists of 3 layers of glass fibers impregnated by a high modulus vinylester resin. Due to the manufacturing process the laminates have a fiber volume content of 50%. Note that one side of the laminate is very rough and therefore has a thickness of approximately $1.5mm$. In Table A.1 and Table A.2 the measured phase lags of two 0 degrees laminate samples can be seen. Note that each phase lag is the average phase lag of three cycles.

Table A.1: Average phase lags measured at certain frequencies and amplitudes. Note that the $*$ sign indicates that the sample has been removed and subsequently reclamped prior to testing and a ! indicates that each cycle has a incomparable phase lag.

	$f = 0.1Hz$	$f = 0.1Hz^*$	$f = 0.01Hz$	$f = 0.01Hz^*$
$A = 2.5mm$	$\approx 13ms$	-	$-13ms!$	-
$A = 5mm$	$\approx 30ms$	$\approx 20ms$	$\approx 13ms$	$\approx 20ms$
$A = 10mm$	$\approx 57ms$	-	$\approx 63ms$	-
$A = 15mm$	-	-	$\approx 67ms$	-
$A = 20mm$	$\approx 63ms$	-	$\approx 97ms$	-
$A = 25mm$	$\approx 80ms$	-	-	-

Table A.2: Average phase lags measured at a 0.1Hz frequency and several amplitudes for the second 0 degrees laminate sample.

	$f = 0.1Hz$
$A = 5mm$	$37ms!$
$A = 10mm$	$\approx 33ms$
$A = 15mm$	$\approx 77ms$
$A = 20mm$	$\approx 93ms$
$A = 25mm$	$\approx 90ms$

It can be seen that the phase lags of both samples differ quite much. The phase lags even differ when the same sample is tested after reclamping it, which means that the results are irreproducible. This is probably due to the contact interactions between the clamp and the sample. Also at an amplitude of $2.5mm$ and a frequency of $0.01Hz$ a negative phase lag can be observed, which is physically impossible. This is probably due to inaccuracies in the load cell and/or test bench. The amplitude seems to have an influence as well, since an increasing amplitude results in an increasing phase lag. This could be due to the material's viscoelastic behavior, however it could also be an effect caused by the clamping conditions. Remarkably, the average phase lags at a $0.1Hz$ frequency is quite comparable with the phase lags at a $0.01Hz$ frequency. This means that the difference in damping loss factor between the two frequencies is almost a factor 10, which should not be the case.

Subsequently, two 90 degrees laminates were tested in order to verify this behavior. The results of these tests can be found in Table A.3 and Table A.4 Note that these samples have the same dimensions as the 0 degrees laminates.

Table A.3: Average loss factors for the Airex T92.80.

	$f = 1Hz$	$f = 0.5Hz^*$	$f = 0.1Hz$	$f = 0.1Hz^*$	$f = 0.01Hz$
$A = 5mm$	$\approx 7ms$	$\approx 10ms$	$\approx 30ms$	$\approx 57ms$	$\approx 40ms$
$A = 10mm$	-	-	$\approx 47ms$	$\approx 87ms$	$\approx 53ms$
$A = 15mm$	-	-	$\approx 43ms$	$\approx 90ms$	$123ms!$
$A = 20mm$	-	-	$\approx 47ms$	-	$\approx 60ms$

Table A.4: Average loss factors for the Airex T92.80.

	$f = 1Hz$	$f = 0.5Hz^*$	$f = 0.1Hz$	$f = 0.01Hz$
$A = 5mm$	$\approx 67ms!$	$\approx 37ms$	$\approx 43ms$	$\approx 17ms$
$A = 10mm$	-	-	$\approx 60ms$	$\approx 70ms$
$A = 15mm$	-	-	$\approx 90ms$	$\approx 100ms$
$A = 20mm$	-	-	$\approx 90ms$	$\approx 110ms$

Again the same kind of behavior can be observed as for the 0 degrees laminates. At the current configuration (cantilever beam) the maximum strains are located at the mouth of the clamp. According to Baur and Kulik [10], this results in irreproducible perturbations, probably due to the inadvertent prestrain in the clamped part of the sample, which is caused during the sample mounting.

In order to reduce this inadvertent strain distribution, the maximum stress has to be located far from the clamp. Various methods are possible, however the easiest method is by thickening one end of the sample and subsequently placing this end inside the clamping block. The thickness distribution of these samples can be seen in Figure A.4. Note that in reality the thickness jump seen in Figure A.4 is less severe.

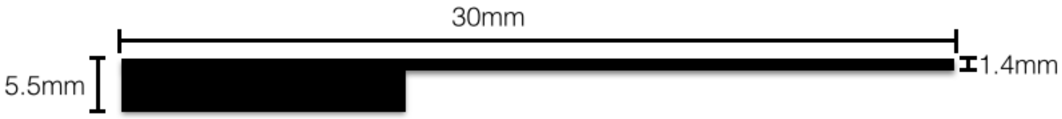

Figure A.4: Thickness distribution of the thickened samples.

Subsequently, two of these samples were tested. The results of these tests can be found in Table A.5 and A.6.

Table A.5: Average loss factors for the Airex T92.80.

	$f = 1Hz$	$f = 0.5Hz^*$	$f = 0.1Hz$	$f = 0.01Hz$
$A = 2.5mm$	$\approx 27ms$	$\approx 20ms$	$\approx 13ms$	$-7ms!$
$A = 5mm$	$\approx 27ms$	$\approx 23ms$	$\approx 30ms$	$\approx 20ms$
$A = 10mm$	-	-	$\approx 43ms$	$\approx 57ms$
$A = 15mm$	-	-	$\approx 60ms$	$\approx 67ms$

Table A.6: Average loss factors for the Airex T92.80.

	$f = 1Hz$	$f = 0.5Hz^*$	$f = 0.1Hz$	$f = 0.01Hz$
$A = 2.5mm$	$\approx 23ms$	$\approx 20ms$	$\approx 13ms$	$-7ms!$
$A = 5mm$	$\approx 27ms$	$\approx 30ms$	$\approx 20ms$	$\approx 0ms$
$A = 10mm$	-	-	$\approx 30ms$	$\approx 27ms$
$A = 15mm$	-	-	$\approx 30ms$	$\approx 37ms$

As can be seen, the values are quite similar at the lower amplitudes, which means that for these amplitudes the results seem to be reproducible. At higher amplitudes, the effect of the prestrain is probably significant again. Nevertheless, still a negative phase lag can be observed at an amplitude of $2.5mm$ and a frequency of $0.01Hz$. This means that the other measured values are still irreproducible and unreliable.

A.0.2. Tests using the 1kN load cell

During the second measurement series, one steel sample and one 0 degrees composite sample have been tested using a 1kN load cell. The results of these measurements are found in Table A.7 for the steel sample and in Table A.8 for the composite sample.

Table A.7: Average loss factors for the Airex T92.80.

	$f = 1Hz$	$f = 0.5Hz^*$	$f = 0.1Hz$	$f = 0.1Hz^1$	$f = 0.1Hz^2$	$f = 0.1Hz^3$	$f = 0.1Hz^*$	$f = 0.01Hz$
$A = 2.5mm$	$\approx 37ms$	$\approx 40ms$	$\approx 40ms$	-	-	$23ms!$	$13ms!$	$60ms!$
$A = 5mm$	$\approx 40ms$	$30ms$	$\approx 27ms$	$\approx 23ms$	$\approx 37ms$	$\approx 47ms$	$97ms!$	$36ms!$
$A = 10mm$	-	-	$\approx 30ms$	$\approx 37ms$	-	$20ms$	$\approx 67ms$	$\approx 80ms$
$A = 15mm$	-	-	$\approx 43ms$	$\approx 53ms$	$\approx 53ms$	$\approx 57ms$	$\approx 63ms$	$\approx 90ms!$
$A = 20mm$	-	-	$\approx 73ms$	-	-	-	$\approx 83ms$	-

Table A.8: Average loss factors for the Airex T92.80.

	$f = 1Hz$	$f = 0.5Hz^*$	$f = 0.1Hz$	$f = 0.1Hz^1$	$f = 0.1Hz^2$	$f = 0.1Hz^3$	$f = 0.1Hz^*$	$f = 0.01Hz$
$A = 2.5mm$	$\approx 40ms$	$\approx 20ms$	$\approx 33ms$	-	-	$10ms$	$-27ms!$	$3ms!$
$A = 5mm$	$\approx 30ms$	$30ms$	$\approx 23ms$	$\approx 23ms$	$\approx 37ms$	$\approx 20ms$	-	$53ms!$
$A = 10mm$	-	-	$\approx 43ms$	$\approx 37ms$	$\approx 37ms$	$30ms$	$\approx 80ms$	$\approx 27ms$
$A = 15mm$	-	-	$\approx 40ms$	$\approx 40ms$	-	$\approx 53ms$	$\approx 50ms$	$\approx 80ms$
$A = 20mm$	-	-	$\approx 67ms$	-	-	-	$\approx 87ms$	-

It can be seen that the measured phase lags for the steel and the composite samples are remarkably similar. On the other hand, the measured phase lags of the 0 degrees laminate are not comparable with the phase lags of the same sample, which were measured using the 10N load cell. This can both be due to a difference in clamping conditions or due to a difference in accuracy between the two load cells. Even if a sample with the exact same clamping conditions is tested (the test has been run multiple times in a row), already small variations in the average phase lag can occur. This is probably caused by external vibrations.

It can be concluded that this method is not trustworthy and therefore not suitable for any damping measurement. First of all, the measured phase lags should differ significantly at different frequencies, which is not the case. Second, at a $0.01Hz$ frequency often a negative phase lag is measured. And third, small variations in the clamping conditions and a different load cell results in significant differences in the measured phase lags. Therefore, this method will not be researched any further.

B

Production of samples

B.1. Resin Samples

Two types of resin samples have been made, i.e. High Modulus Vinylester resin samples and Low Modulus Epoxy resin samples. The exact composition of the vinylester samples is 97.7% Distitron VE370SC vinylester, 2% CHM50 hardener and 0.3% Cobalt. The exact composition of the epoxy samples is 66.7% Ce-sense 101 Epoxy resin and 33.3% Ce-sense hardener 113.

The resin samples are manufactured by mixing the various components and subsequently by pouring the composition in a simple bathtub like mold. The first resin samples were degassed at a vacuum of -0.97 bar in order to lose most of the dissolved air. The vacuum had an adverse effect on the samples, since it initiated a significant amount of 'bubbles' of which a small part did not dissolve after curing. Even if the vacuum is released before the gelation of the resins. This is probably due to the lack of a proper nucleation material and due to the short gelation time of the vinylester resin. As a result, the new resin samples were not degassed at all, which resulted in glass like samples.

When the samples were fully cured (24 hours at $24°C$ and 2 hours at $100°C$ for the vinylester samples and 24 hours at room temperature for the epoxy resins), the samples were cut in the right size and subsequently sanded and polished.

B.2. Foam and steel samples

Both the foam and steel samples were easy to manufacture and therefore they are both discussed briefly.

B.2.1. Foam samples

All the foam samples were carefully cut from larger foam plates by using a sharp Stanley knife. In case of the PET foams, samples were cut in two different directions and around the weld lines. This can be seen in Figure B.1

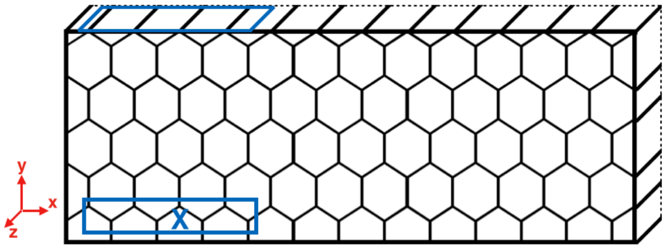

Figure B.1: Extruded honeycomb structure of the PET foams. Note that direction z corresponds with the extrusion direction and the blue rectangles indicate the different kind of samples.

B.2.2. Steel samples

In case of the steel samples, the samples are cut from a larger plate by using a guillotine. The guillotine results in 'sharp' edges, which could affect the measurements. Therefore, these 'sharp' edges are sanded.

B.3. Composite samples

Two types of composite samples have been produced, i.e. simple composite laminates and plies and sandwich structured laminates.

B.3.1. Composite laminates and plies

All composite laminate samples and composite ply samples have been manufactured by means of vacuum infusion. Note that the applied vacuum is approximately $-0.97 bar$. All the production steps are:

- Clean a smooth plate with aceton.
- Apply a release agent on a certain area.
- Surround this certain area with tacky tape
- Apply glassfiber fabrics, compoflex (flow mesh and peel ply), compomat (flow retarder), PE spirals and PE tubes (connected by PE spirals by a small T-shaped tube).
- Apply vacuum bag.
- Close the PE tube at the input (by means of a clamp and/or by folding the PE tube).
- Attach the PE tube at the output to a vacuum pump.
- Apply vacuum.
- Check for leaks.
- Prepare resin.
- Put the end of the PE tube at the input into the resin and open it.
- At the end of the infusion the PE tube at the input is closed again and the vacuum is increased to -0.7 bar (in order to reduce the size of any ’bubble’).
- Remove the vacuum bag and release the composite part after approximately 24 hours.

The simplified vacuum infusion set-up can be seen in Figure B.2.

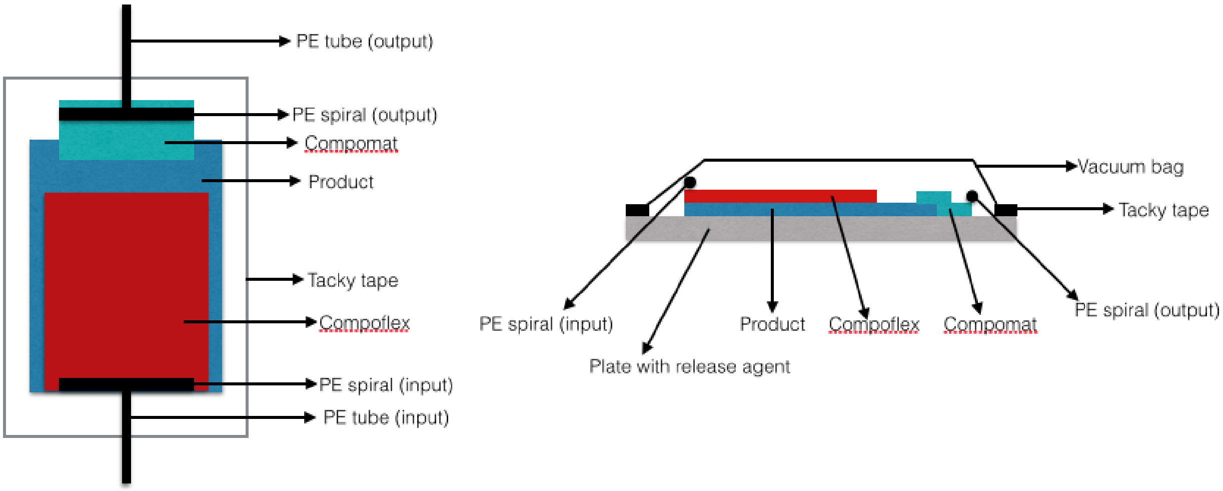
PE tube (output)
PE spiral (output)
Compomat
Product
Tacky tape
Compoflex
PE spiral (input)
PE tube (input)
Vacuum bag
Tacky tape
PE spiral (input)
Plate with release agent
Product
Compoflex
Compomat
PE spiral (output)

Figure B.2: Simplified representation of the vacuum infusion set-up.

All the manufactured composite samples can be found in Table B.1. Note that the indicated resins have the same composition.

Table B.1: Table with all types of manufactured samples

Type of composite	**Glass fiber fabric**	**Number of fiber layers**	**Resin**	**Test**
0° GFRV laminate	$600 gr/m^2$ Unidirect.	3	VE370SC	DMA & SCB
90° GFRV laminate	$600 gr/m^2$ Unidirect.	3	VE370SC	DMA & SCB
0° GFRV laminate	$600 gr/m^2$ Unidirect.	3 + 9 extra (See Figure A.4)	VE370SC	SCB
90° GFRV laminate	$600 gr/m^2$ Unidirect.	3 + 9 extra (See Figure A.4)	VE370SC	SCB
±45° GFRV laminate	$600 gr/m^2$ Biax	4	VE370SC	DMA
0° GFRV plies	$600 gr/m^2$ Unidirect.	1	VE370SC	DMA
90° GFRV plies	$600 gr/m^2$ Unidirect.	1	VE370SC	DMA
0° GFRE plies	$600 gr/m^2$ Unidirect.	1	Ce-Sense 101	DMA
90° GFRE plies	$600 gr/m^2$ Unidirect.	1	Ce-Sense 101	DMA

Note that Unidirect. is the abbreviation of unidirectional and SCB the abbreviation of Simple Cantilever Beam. In Figure B.3 a picture of several vacuum infused plates can be seen.

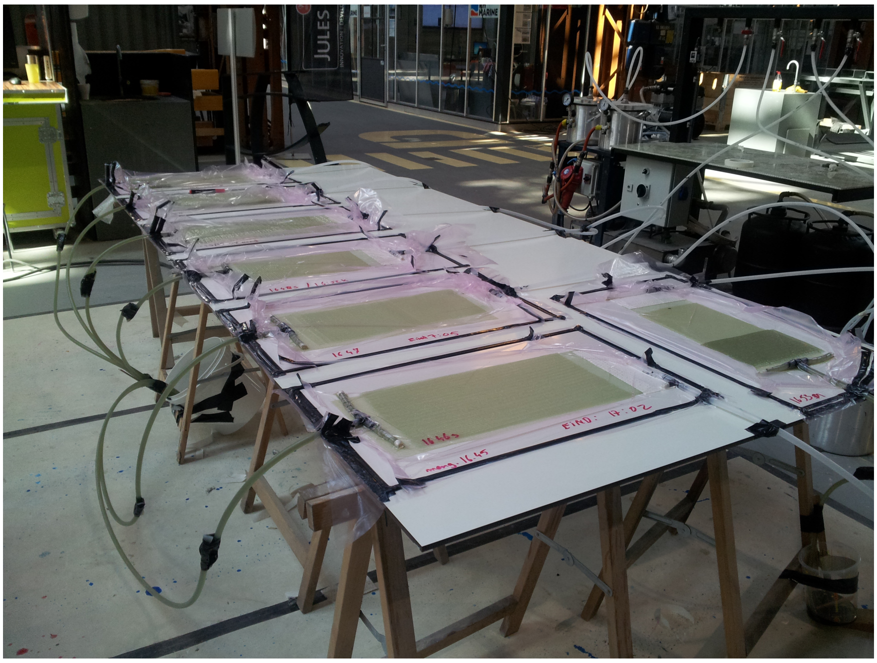

Figure B.3: Picture of several vacuum infused plates.

After approximately 24 hours the resin is cured and the composite part can be released from the vacuum bag. Before the reinforced vinylester plates can be cut into the required size, first the plates have to be post-cured at $100°C$ for two hours. Subsequently the composite laminates are cut into the required size by using a water cooled diamond cutting wheel. The composite plies are cut by using a sharp Stanley knife.

In Figure B.4 a picture with several of the samples can be seen.

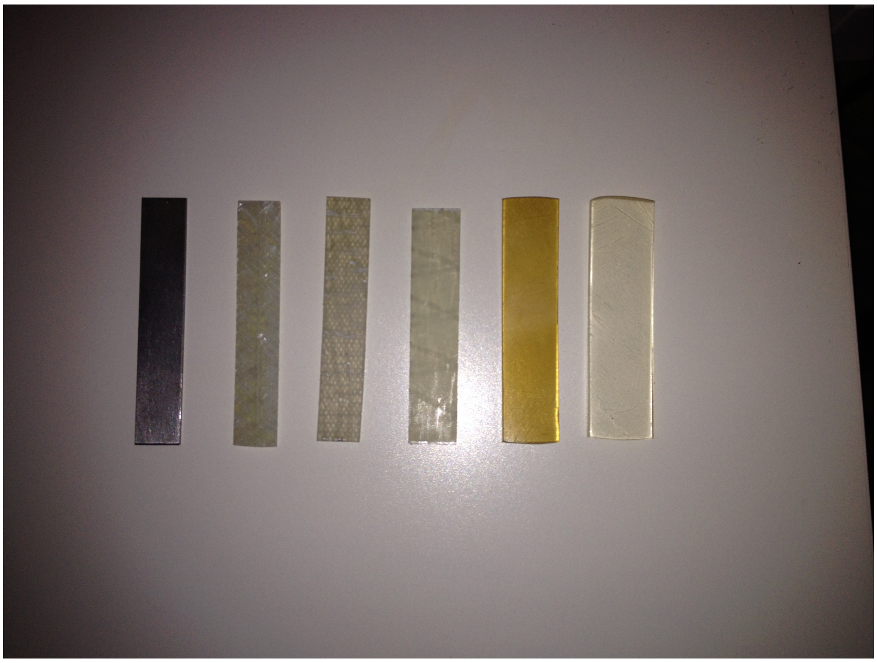

Figure B.4: A picture of several samples. From left to right: Epoxy sample, Vinylester sample, 0° GFRV laminate, 90° GFRV laminate, ±45° GFRV laminate and a steel sample.

B.3.2. Sandwich structured composite

Besides composite laminate samples, sandwich structured laminate samples were manufactured as well. Each face sheet is made of one $0° GFRV ply$ and manufactured by means of vacuum infusion. The core material is a $2mm$ thick Airex T92.80 foam. Due to low strength of the core material, it is impossible to reduce the thickness of a large foam plate by means of grinding or cutting without deforming the material. Also the minimum thickness that the foam's manufacturer could deliver is approximately $3mm$ [28]. Therefore both the face sheets and the core material are carefully cut by means of a sharp Stanley knife.

The manufacturing steps are:

- Produce facesheets.
- Cut the face sheets in the required size.
- Cut foam material carefully in the required size. Note that the foam material is slightly thicker than it should be.
- Prepare resin / adhesive.
- Apply the resin on the rough side of one of the face sheets and on one side of the core material.
- Place a plate and a small weight on top of the face sheet in order to have a equally distributed adhesive layer.
- After 24 hours, sand the core material (with on one side a face sheet) until the required thickness is reached.
- Apply the resin on the rough side of the other face sheet and on the other side of the core material.
- Place a plate and a small weight on top of the sandwich.
- After 24 hours, sand the edges of the sandwich structured composite.
- Place the samples in the oven for two hours at $100°C$.

The final appearance of the sandwich structured composite samples can be seen in Figure B.5.

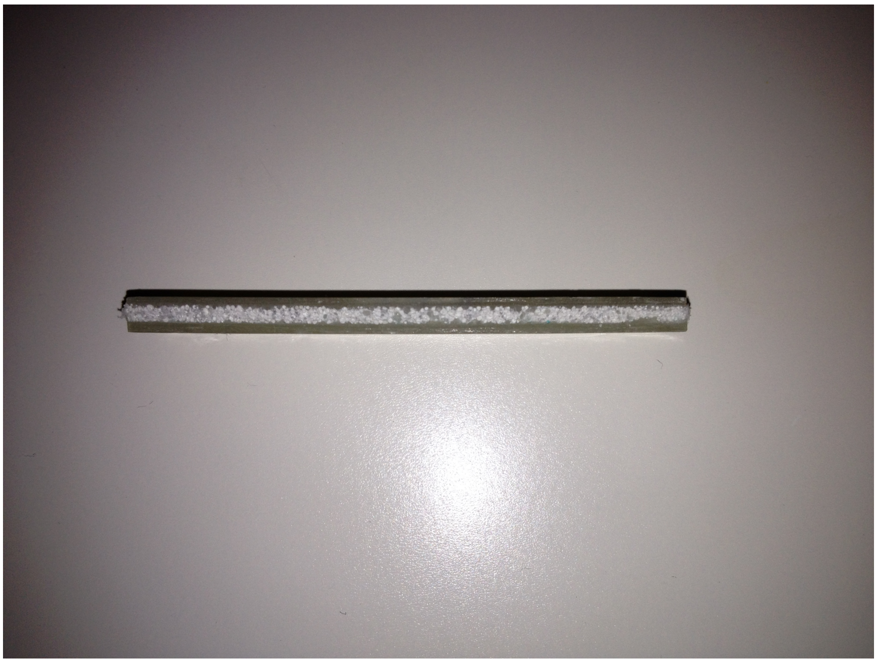

Figure B.5: The final appearance of the sandwich structured composite samples.

C

Used material properties

In order to be able to calculate the modal damping loss factor of the composite wind turbine tower, it is required to know the properties of all the material constituents. The material constituents are the E-glass fibers, the VE370SC vinylester resin and the Airex T92.80 foam. In Table C.1 [41] and Table C.2 [78] the material properties of the glass fibers and the vinylester resin can be found respectively. Note that both the glass fibers and the vinylester resin are assumed to be isotropic. Hence, $G = \frac{E}{2(1+v)}$ and the Young's modulus, Shear modulus and Poisson's ratio are equal in all directions.

Table C.1: Table with the material properties of E-glass fibers [41].

Parameter	**Value**	**Description**
E_{f11}	$72GPa$	Young's modulus in fiber direction
E_{f22}	$72GPa$	Young's modulus in the transverse direction
G_{f12}	$35GPa$	In-plane shear modulus
v_{12}	0.22	Poisson's ratio
v_{23}	0.22	Poisson's ratio

Table C.2: Table with the material properties of VE370SC vinylester resin [78].

Parameter	**Value**	**Description**
E_m	$3.4GPa$	Tensile modulus
E_{mf}	$3.3GPa$	Flexural modulus
G_m	$1.65GPa$	Shear modulus
v_m	0.3	Poisson's ratio

These material properties are used to calculate the required material properties of the composite material. This is done by means of Equation C.1 for the Young's modulus in the fiber direction, Equation C.2 for the Young's modulus perpendicular to the fiber direction and Equation C.3 for the in-plane shear components [25].

$$E_{11} = V_f E_{f11} + (1 - V_f) E_m \tag{C.1}$$

$$E_{22} = \left(1 - \sqrt{(V_f)}\right) E_m + \frac{\sqrt{(V_f)} E_m}{1 - \sqrt{((1 - V_f)}\left(1 - \frac{E_m}{E_{f22}}\right))} \tag{C.2}$$

$$G_{12} = \left(1 - \sqrt{(V_f)}\right) G_m + \frac{\sqrt{(V_f)} G_m}{1 - \sqrt{((1 - V_f)}\left(1 - \frac{G_m}{G_{f12}}\right))} \tag{C.3}$$

Here V_f is the fiber volume fraction.
In case a circular fiber cross-section is assumed, the laminate will be transverse isotropic and therefore the inplane shear modulus will be equal to the inter laminar shear modulus (see Equation C.4.

$$G_{13} = G_{12} \tag{C.4}$$

Also it is assumed that the transverse shear modulus (G_{23}) will be equal to Equation C.5.

$$G_{23} = \frac{E_{22}}{2(1+\upsilon_{23})} \tag{C.5}$$

And here,

$$\upsilon_{23} = \frac{\upsilon_m}{\left(1 - V_f \upsilon_m\right)} + V_f \left(\upsilon_{f23} - \frac{(1-V_f)\upsilon_m}{(1-V_f\upsilon_m)}\right) \tag{C.6}$$

The resulting material properties for the fiber reinforced vinylester ply can be found in Table C.3

Table C.3: Table with the material properties of a fiber reinforced vinylester ply

Parameter	**Value**	**Description**
V_f	50%	Fiber volume fraction
E_{11}	$37.7GPa$	Young's modulus in fiber direction
E_2	$8.5GPa$	Young's modulus in transverse direction
G_{12}	$3.3GPa$	In-plane shear modulus
G_{13}	$3.3GPa$	In-plane shear modulus
G_{23}	$3.1GPa$	In-plane shear modulus

Beside the material properties of the composite material, also the material properties of the Airex T92.80 core have to be known. These can be found in Table C.4.

In Table C.4 the used material properties of the anisotropic Airex T92.80 core can be seen [28].

Table C.4: Table with the material properties of the Airex T92.80 core.

Parameter	**Value**	**Description**
E_t	$80MPa$	Tensile modulus
E_c	$60MPa$	Compresssive modulus
G_{12}	$19.5MPa$	Shear modulus
ρ	$85\frac{kg}{m^3}$	Density
υ	0.3	Poisson's ratio

D

Shear energy distribution

In order to determine the ratio between the shear strain energy and the bending strain energy, each strain energy component has to be determined. The ratio between the shear strain energy and the bending strain energy has been determined for two different configurations. The first configuration is a 3-point-bending configuration with a simple rectangular beam. The second configuration is a cantilever beam with a tubular cross-section.

D.0.3. Three-point-bending configuration

In Figure D.1 the Free Body Diagram (FBD) of the 3-point-bending configuration can be seen. In order to solve the FBD, the beam has to be divided into two equal sections with an equal length of $\frac{L}{2}$.

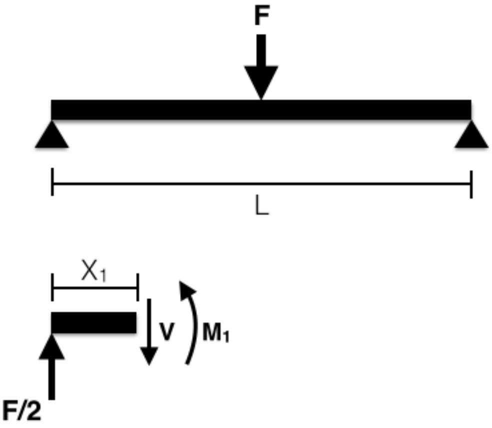

Figure D.1: Free body diagram of the entire 3-point-bending configuration and of a small section.

The first strain energy component that will be determined is the one due to pure bending. The definition of the pure bending strain energy can be seen in Equation D.1. [44]

$$U_b = \int_0^L \frac{M^2 dx}{2EI} \tag{D.1}$$

Here M is the bending moment, L is the length of the beam and EI is the beam's bending stiffness. The bending moment of the small section, seen in Figure D.1, can be defined by Equation D.2.

$$M_1 = \frac{F}{2} x_1 \tag{D.2}$$

Here F is a certain force, x_1 is a certain section length and M_1 is a certain moment. Subsequently the bending moment of this small section can be substituted into Equation D.1. The resulting equation can be seen in Equation D.3.

$$U_b = \int_0^{\frac{L}{2}} \frac{\left(\frac{F}{2} x_1\right)^2 dx}{2EI} = \frac{F^2 L^3}{192EI} \tag{D.3}$$

Subsequently the bending stiffness of a simple rectangular cross-section can be defined by Equation D.13.

$$EI = E\frac{bh^3}{12} \tag{D.4}$$

Here b is the width of the beam and h the height/thickness. Subsequently this definition of the bending stiffness can be substituted in Equation D.3. The total bending strain energy of the entire beam can be seen in Equation D.5

$$U_{b,tot} = \frac{F^2L^3}{8Ebh^3} \tag{D.5}$$

The same kind of calculation can be done for the shear strain energy component. The general definition of the shear strain energy can be seen in Equation D.6 [44]

$$U_s = \int_0^L \frac{f_s V^2 dx}{2GA} \tag{D.6}$$

Here f_s is the shape factor, which equals $\frac{6}{5}$ for a rectangular cross-section, V is the shear force, G is the material's shear modulus and A is the cross-sectional area. The shear force of the small section, seen in Figure D.1, can be defined by Equation D.7.

$$V_1 = \frac{F}{2} \tag{D.7}$$

Subsequently the shear force of this small section can be substituted into Equation D.6. The resulting definition for the shear strain energy can be seen in Equation D.8.

$$U_s = \int_0^{\frac{L}{2}} \frac{\frac{6}{5}\left(\frac{F}{2}\right)dx}{2GA} = \frac{6F^2L}{20GA} \tag{D.8}$$

Finally the definition of the total shear strain energy of the entire beam can be seen in Equation D.9. Note that $A = bh$.

$$U_{s,tot} = \frac{6F^2L}{10Gbh} \tag{D.9}$$

At last the ratio between the shear strain energy and the bending strain energy can be derived by dividing Equation D.9 by Equation D.5. The resulting ratio can be seen in Equation D.10

$$\frac{U_s}{U_b} = 4.8\frac{E}{G}\left(\frac{h}{L}\right)^2 \tag{D.10}$$

D.0.4. cantilever beam configuration

In Figure D.1 the Free Body Diagram (FBD) of the cantilever beam configuration can be seen.

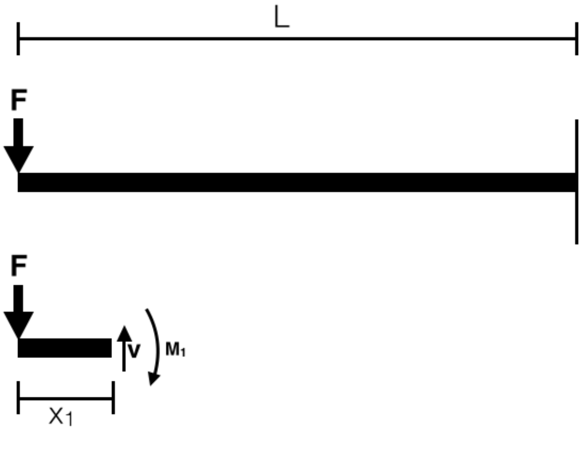

Figure D.2: Free body diagram of the entire cantilever beam configuration and of a small section.

The bending moment of the small section, seen in Figure D.2, can be defined by Equation D.11.

$$M_1 = Fx_1 \tag{D.11}$$

Here F is a certain force, x_1 is a certain section length and M_1 is a certain moment. Subsequently the bending moment of this small section can be substituted into Equation D.1. The resulting equation can be seen in Equation D.12.

$$U_b = \int_0^L \frac{\left(Fx_1\right)^2 dx}{2EI} = \frac{F^2 L^3}{2EI} \tag{D.12}$$

Subsequently the bending stiffness of a thin walled tubular cross-section can be defined by Equation D.13.

$$EI = E\pi R^3 t \tag{D.13}$$

Here R is the average radius of the cross-section and t is the wall thickness. Subsequently this definition of the bending stiffness can be substituted in Equation D.12, which results in the expression seen in Equation D.14

$$U_{b,tot} = \frac{F^2 L^3}{6E\pi R^3 t} \tag{D.14}$$

The same kind of calculation can be done for the shear strain energy component. The general definition of the shear strain energy can be seen in Equation D.6 [44] The shear force of the small section, seen in Figure D.2, can be defined by Equation D.15.

$$V_1 = F \tag{D.15}$$

Subsequently the shear force of this small section can be substituted into Equation D.6. Note that the form factor $f_s = 2$ and $A = 2\pi R t$ for a thin walled tubular cross-section [34]. The resulting definition for the shear strain energy can be seen in Equation D.16.

$$U_s = \int_0^L \frac{2F dx}{2GA} = \frac{F^2 L}{GA} = \frac{F^2 L}{2G\pi R t} \tag{D.16}$$

At last the ratio between the shear strain energy and the bending strain energy can be derived by dividing Equation D.16 by Equation D.14. The resulting ratio can be seen in Equation D.17

$$\frac{U_s}{U_b} = 3\frac{E}{G}\left(\frac{R}{L}\right)^2 \tag{D.17}$$

E

Classical laminate theory

Composites are anisotropic or quasi-isotropic materials and therefore they show different material properties in different directions. Due to the elastic nature of the fibers and the fact that the strain of fiber reinforced composites is generally limited by the fibers, the elastic behavior of composites can be described by Hooke's law (see Equation E.1). [52], [106]

$$\sigma = E\epsilon \tag{E.1}$$

Here E is the elastic modulus, ϵ the strain and σ the stress. Due to the anisotropic nature of composites the stress-strain behavior will be different in each direction. However, composite plies can be assumed to be orthotropic, since they possess two axes of symmetry. Therefore Equation E.1 can be represented as Equation E.2.[52]

$$\begin{bmatrix} \sigma_x \\ \sigma_y \\ \sigma_z \\ \tau_{yz} \\ \tau_{xz} \\ \tau_{xy} \end{bmatrix} = \begin{bmatrix} Q_{11} & Q_{12} & Q_{13} & 0 & 0 & 0 \\ Q_{12} & Q_{22} & Q_{23} & 0 & 0 & 0 \\ Q_{13} & Q_{23} & Q_{33} & 0 & 0 & 0 \\ 0 & 0 & 0 & G_{44} & 0 & 0 \\ 0 & 0 & 0 & 0 & G_{55} & 0 \\ 0 & 0 & 0 & 0 & 0 & G_{66} \end{bmatrix} \begin{bmatrix} \epsilon_x \\ \epsilon_y \\ \epsilon_z \\ \gamma_{yz} \\ \gamma_{xz} \\ \gamma_{xy} \end{bmatrix} \tag{E.2}$$

Of course a ply containing a different fiber orientation will have different stiffnesses in the x and y direction. The stiffness matrix of such a ply can easily be obtained by applying Equation E.3 [52].

$$Q_{c\theta} = RQ_{c\theta=0}R^T \tag{E.3}$$

Here $Q_{c\theta=0}$ is the unrotated stiffness matrix and R is the full rotation matrix. The latter can be seen in Equation E.4 [81].

$$[R] = \begin{bmatrix} \cos^2\theta & \sin^2\theta & 0 & 0 & 0 & -2\sin\theta\cos\theta \\ \sin^2\theta & \cos^2\theta & 0 & 0 & 0 & 2\sin\theta\cos\theta \\ 0 & 0 & 1 & 0 & 0 & 0 \\ 0 & 0 & 0 & \cos\theta & \sin\theta & 0 \\ 0 & 0 & 0 & -\sin\theta & \cos\theta & 0 \\ \sin\theta\cos\theta & -\sin\theta\cos\theta & 0 & 0 & 0 & (\cos^2\theta - \sin^2\theta) \end{bmatrix} \tag{E.4}$$

Here, θ is the fiber orientation.
The full compliance matrix can be determined by Equation E.5;

$$Q_{c\theta=0} = \mathbf{S^{-1}} \tag{E.5}$$

Here S is the full stiffness matrix and can be seen in Equation E.6.

$$\mathbf{S} = \begin{bmatrix} \frac{1}{E_x} & -\frac{\upsilon_{xy}}{E_x} & -\frac{\upsilon_{xz}}{E_x} & 0 & 0 & 0 \\ -\frac{\upsilon_{xy}}{E_x} & \frac{1}{E_y} & -\frac{\upsilon_{yz}}{E_y} & 0 & 0 & 0 \\ -\frac{\upsilon_{xz}}{E_x} & -\frac{\upsilon_{yz}}{E_y} & \frac{1}{E_z} & 0 & 0 & 0 \\ 0 & 0 & 0 & G_{yz} & 0 & 0 \\ 0 & 0 & 0 & 0 & G_{xz} & 0 \\ 0 & 0 & 0 & 0 & 0 & G_{xy} \end{bmatrix} \tag{E.6}$$

In case the laminate is transverse isotropic (the cross-section of the fibers is circular), Equation E.6 can be simplified by applying Equation E.7 and Equation E.8.

$$E_z = E_y \tag{E.7}$$

$$G_{xz} = G_{xy} \tag{E.8}$$

Since a composite ply can be considered thin walled compared to the rest of the structure, plane stress can be assumed. Therefore all stresses regarding the thickness direction of the ply becomes zero and subsequently Equation E.2 can be rewritten as Equation E.9. [52]

$$\begin{bmatrix} \sigma_x \\ \sigma_y \\ \tau_{xy} \end{bmatrix} = \begin{bmatrix} Q_{11} & Q_{12} & 0 \\ Q_{21} & Q_{22} & 0 \\ 0 & 0 & G_{66} \end{bmatrix} \begin{bmatrix} \epsilon_x \\ \epsilon_y \\ \gamma_{xy} \end{bmatrix} \tag{E.9}$$

Subsequently the stress-strain conversion matrix can be rewritten in terms of the elastic moduli and poisson ratios of the material. The resulting matrix can be seen in Equation E.10. [52]

$$Q_{c\theta=0} = \begin{bmatrix} \frac{E_x}{1-\upsilon_{xy}\upsilon_{yx}} & \frac{\upsilon_{xy}E_y}{1-\upsilon_{xy}\upsilon_{yx}} & 0 \\ \frac{\upsilon_{xy}E_y}{1-\upsilon_{xy}\upsilon_{yx}} & \frac{E_y}{1-\upsilon_{xy}\upsilon_{yx}} & 0 \\ 0 & 0 & G_{xy} \end{bmatrix} \tag{E.10}$$

Here, E_x is the ply's Young's modulus in fiber direction, E_y is the ply's Young's modulus in transverse direction, G_{xy} is the in-plane shear modulus, υ_{xy} is the Poisson's ratio of the contraction in transverse direction due to an extension in fiber direction and υ_{yx} is the Poisson's ratio of the contraction in fiber direction due to an extension in transverse direction. Both Poisson's ratios are related to each other by Maxwell's equation, which can be seen in Equation E.11. [52]

$$\frac{\upsilon_{ji}}{E_j} = \frac{\upsilon_{ij}}{E_i} \tag{E.11}$$

This relation also proves that $Q_{ij} = Q_{ji}$.
The corresponding reduced rotation matrix can be seen in Equation E.12.

$$R = \begin{bmatrix} \cos^2\theta & \sin^2\theta & 2\sin\theta\cos\theta \\ \sin^2\theta & \cos^2\theta & -2\sin\theta\cos\theta \\ -\sin\theta\cos\theta & \sin\theta\cos\theta & (\cos^2\theta - \sin^2\theta) \end{bmatrix} \tag{E.12}$$

The next step is determining the elastic properties of the entire laminate. A representation of the elastic properties of the laminate is the ABD matrix, which serves as a connection between the strains and the applied forces.The ABD matrix can be seen in Equation E.13. [52]

$$\begin{bmatrix} N_x \\ N_y \\ N_{xy} \\ M_x \\ M_y \\ M_{xy} \end{bmatrix} = \begin{bmatrix} A_{11} & A_{12} & A_{16} & B_{11} & B_{12} & B_{16} \\ A_{12} & A_{22} & A_{26} & B_{12} & B_{22} & B_{26} \\ A_{16} & A_{26} & A_{66} & B_{16} & B_{26} & B_{66} \\ B_{11} & B_{12} & B_{16} & D_{11} & D_{12} & D_{16} \\ B_{12} & B_{22} & B_{26} & D_{12} & D_{22} & D_{26} \\ B_{16} & B_{26} & B_{66} & D_{16} & D_{26} & D_{66} \end{bmatrix} \begin{bmatrix} \epsilon_x \\ \epsilon_y \\ \gamma_{xy} \\ \kappa_x \\ \kappa_y \\ \kappa_{xy} \end{bmatrix} \tag{E.13}$$

Here the A_{ij} components describe the laminate's extensional stiffness, the D_{ij} components the laminate's bending stiffness and the B_{ij} components the laminate's extension-bending couplings.
The A, B and D matrices are calculated by Equation E.14, Equation E.15 and Equation E.16. [52]

$$A_{ij} = \sum_{k=1}^{n} Q_{c\theta}^{(k)}(z_k - z_{k-1}) \tag{E.14}$$

$$B_{ij} = \frac{1}{2}\sum_{k=1}^{n} Q_{c\theta}^{(k)}(z_k^2 - z_{k-1}^2) \tag{E.15}$$

$$D_{ij} = \frac{1}{3}\sum_{k=1}^{n} Q_{c\theta}^{(k)}(z_k^3 - z_{k-1}^3) \tag{E.16}$$

Here $Q_{c\theta}$ is the stiffness matrix of a ply and $z_(k)$ is the distance between the neutral plane of a ply and the neutral plane of the entire laminate.

F

Saravanos-Chamis Micromechanical model

This method assumes unified micromechanics for a square unit cell and considers the stress/strain uniform throughout the composite material. Therefore, the damping loss factors of the composite can easily be solved by the Rule of Mixtures. The damping loss factor in fiber direction can be calculated by applying Equation F.1 [25], [85], [14].

$$\eta_{11} = \eta_{f11} V_f \frac{E_{fll}}{E_{11}} + \eta_m (1 - V_f) \frac{E_m}{E_{11}} \tag{F.1}$$

Here V_f is the fiber volume, E_{f11} is the stiffness modulus of the fibers in fiber direction, η_{f11} is the loss factor of the fibers in fiber direction, E_{11} is the stiffness modulus of the composite in fiber direction, η_m is the loss factor of the matrix and E_m is the stiffness modulus of the matrix.
A similar equation can be applied for the damping loss factor in the transverse direction (see Equation F.2) [25], [85], [14].

$$\eta_{22} = \eta_{f22} \sqrt{V_f} \frac{E_{22}}{E_{f22}} + \eta_m (1 - \sqrt{V_f}) \frac{E_{22}}{E_m} \tag{F.2}$$

Here E_{f22} is the stiffness modulus of the fibers in the transverse direction, η_{f22} is the loss factor of the fibers in transverse direction and E_{22} is the stiffness modulus of the composite in transverse direction.

In case circular fibers and the fiber spacing in the thickness direction is equal to the fiber spacing in the transverse direction, transverse isotropy can be assumed and therefore Equation F.3 is valid [25], [85], [14].

$$\eta_{33} = \eta_{22} \tag{F.3}$$

For all shear damping factors, Equation F.4 can be used [25], [14].

$$\eta_{ij} = \eta_{fij} \sqrt{V_f} \frac{G_{ij}}{G_{fij}} + \eta_{msh} (1 - \sqrt{V_f}) \frac{G_{ij}}{G_m} \tag{F.4}$$

Here η_{ij} is the shear damping loss factor in the i and the j direction, G_{ij} is the composite's shear modulus in the i and the j direction, G_{fij} is the fiber's shear modulus in the i and the j direction, η_{msh} is the shear damping loss factor of the matrix and G_m is the shear modulus of the matrix. As mentioned, the subscript ij indicates the direction. For example η_{11} is the damping loss factor in the 0° orientation, η_{22} is the damping loss factor in transverse direction, η_{12} is the damping loss factor of the in-plane shear, η_{23} is the shear damping loss factor in transverse direction, etc.

In case transverse isotropy can be assumed, Equation F.5 is valid [25].

$$\eta_{13} = \eta_{12} \tag{F.5}$$

This model shows an accurate result of the damping loss factor in fiber direction, however it shows a less accurate estimation in the other directions due to the transverse isotropy assumption.

G

ABD-matrices of a tubular cross-section

In order to determine the stiffness properties of a tubular composite cross-section, the ABD-matrix of the entire cross-section has to be defined. In Equation G.1 the A, B and D matrices of a tubular beam cross-section can be seen.

$$[\mathbf{A^0}] = \begin{bmatrix} A^0_{11} & A^0_{15} & A^0_{16} \\ A^0_{51} & A^0_{55} & A^0_{56} \\ A^0_{61} & A^0_{65} & A^0_{66} \end{bmatrix} \quad [\mathbf{B^0}] = \begin{bmatrix} B^0_{11} & B^0_{12} & B^0_{16} \\ B^0_{51} & B^0_{52} & B^0_{56} \\ B^0_{61} & B^0_{62} & B^0_{66} \end{bmatrix} \quad [\mathbf{D^0}] = \begin{bmatrix} D^0_{11} & D^0_{12} & D^0_{16} \\ D^0_{21} & D^0_{22} & D^0_{26} \\ D^0_{61} & D^0_{62} & D^0_{66} \end{bmatrix} \tag{G.1}$$

The extension-shear, coupling and bending-torsion terms of the cross-sectional ABD-matrix can be defined by the following equations. Note that these cross-sectional terms are indicated by the superscript 0 .

Extensional and shear stiffness terms

$$A^0_{11} = \oint A_{11} ds \tag{G.2}$$

$$A^0_{15} = \oint (A_{16} z_{,s}) ds \tag{G.3}$$

$$A^0_{16} = \oint (A_{16} y_{,s}) ds \tag{G.4}$$

$$A^0_{55} = \oint (A_{66} z^2_{,s}) ds + \oint (A_{55} y^2_{,s}) ds \tag{G.5}$$

$$A^0_{56} = \oint (A_{66} z_{,s} y^0_{,s}) ds + \oint (A_{55} z_{,s} y^0_{,s}) ds \tag{G.6}$$

$$A^0_{66} = \oint (A_{66} y^2_{,s}) ds + \oint (A_{55} z^2_{,s}) ds \tag{G.7}$$

Flexural and torsional stiffness terms

$$D^0_{11} = \oint (A_{11} z^2 + 2 z y_{,s} B_{11} + y^2_{,s} D_{11}) ds \tag{G.8}$$

$$D^0_{12} = \oint (A_{11} z y + (y y_{,s} - z z_{,s}) B_{11} - z_{,s} y_{,s} D_{11}) ds \tag{G.9}$$

$$D^0_{16} = \oint (-A_h z A_{16} - (A_h y_{,s} + 2z) B_{16} - 2 y_{,s} D_{16}) ds \tag{G.10}$$

$$D^0_{22} = \oint (A_{11} y^2 - 2 y z_{,s} B_{11} + z^2_{,s} D_{11}) ds \tag{G.11}$$

$$D^0_{26} = \oint (-A_h y A_{16} - (A_h z_{,s} + 2y) B_{16} - 2 z_{,s} D_{16}) ds \tag{G.12}$$

$$D^0_{66} = \oint (A^2_h + A_{66} + 4 A_h B_{66} + 4 D_{66}) ds \tag{G.13}$$

Coupling terms

$$B^0_{11} = \oint (A_{11}z + B_{11}y_{,s})ds \tag{G.14}$$

$$B^0_{12} = \oint (A_{11}y + B_{11}z_{,s})ds \tag{G.15}$$

$$B^0_{16} = \oint (-A_{16}A_h - 2B_{16})ds \tag{G.16}$$

$$B^0_{51} = \oint (A_{16}z + B_{16}y_{,s})z_{,s}ds \tag{G.17}$$

$$B^0_{52} = \oint (A_{16}y + B_{16}z_{,s})z_{,s}ds \tag{G.18}$$

$$B^0_{56} = \oint (-A_{66}A_h - 2B_{66})z_{,s}ds \tag{G.19}$$

$$B^0_{61} = \oint (A_{16}z + B_{16}y_{,s})y_{,s}ds \tag{G.20}$$

$$B^0_{62} = \oint (A_{16}y + B_{16}z_{,s})y_{,s}ds \tag{G.21}$$

$$B^0_{66} = \oint (-A_{66}A_h - 2B_{66})y_{,s}ds \tag{G.22}$$

Here the stiffness terms without a superscript correspond to the terms of the laminate's ABD matrix. y and z are the coordinates of the skin's midline, s is the curvilinear length and $y_{,s}$ and $z_{,s}$ are the derivatives of the coordinates of the skin's midline. Finally, $A_h = A_0/\lambda h$ and here h is the skin thickness and λ and A_0 are geometric section parameters, which are defined by Equation G.23 and Equation G.24

$$A_0 = \oint r_\zeta ds \tag{G.23}$$

$$\lambda = \oint \frac{1}{h} ds \tag{G.24}$$

Here r_ζ is the projection of the radius r^0 on the ζ-axis of the curvilinear coordinate system. This coordinate system can be seen in Figure 5.3.

In case of the composite tower, the cross-section will be circular and the skin thickness h constant. This type of cross-section can be seen in Figure G.1.

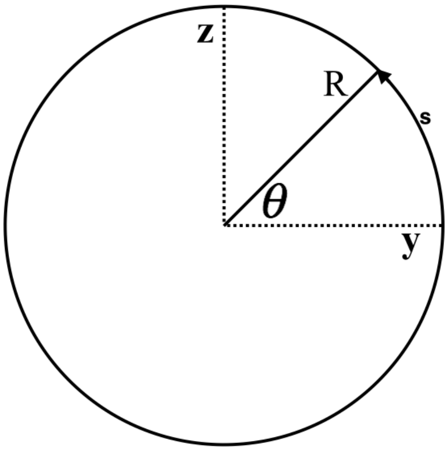

Figure G.1: A simple representation of the tower's circular cross-section.

The z- and y-coordinates of the skin's midline can be represented by Equation G.25 and Equation G.26 respectively.

$$z = R\sin(\theta) \tag{G.25}$$

$$y = R\cos(\theta) \tag{G.26}$$

Here R is the cross-section's radius and θ is the polar coordinate. However in order to determine the required derivatives, the coordinates z and y should be functions of the curvilinear length s. The definition of s can be seen in Equation G.27.

$$s = \frac{\theta}{2\pi}C = \theta R \tag{G.27}$$

Here C is the circumference of the circular cross-section. Note that both the curvilinear length s and the polar coordinate θ are zero at $Z = 0$ and $Y = R$.

By substituting Equation G.27 into Equation G.25 and Equation G.26, the following equations are derived.

$$z = R\sin\left(\frac{s}{R}\right) \tag{G.28}$$

$$y = R\cos\left(\frac{s}{R}\right) \tag{G.29}$$

Subsequently by differentiating Equation G.28 and Equation G.29 with respect to the circumferential coordinate s, the required derivatives can be found.

$$z_{,s} = \cos\left(\frac{s}{R}\right) \tag{G.30}$$

$$y_{,s} = -\sin\left(\frac{s}{R}\right) \tag{G.31}$$

Finally by applying a symmetrical and balanced laminate and the aforementioned coordinates and derivatives, the ABD matrix seen in Equation G.32 can be derived.

$$\mathbf{ABD^0} = \begin{bmatrix} A^0_{11} & 0 & 0 & 0 & 0 & 0 \\ 0 & A^0_{55} & 0 & 0 & 0 & 0 \\ 0 & 0 & A^0_{66} & 0 & 0 & 0 \\ 0 & 0 & 0 & D^0_{11} & 0 & 0 \\ 0 & 0 & 0 & 0 & D^0_{22} & 0 \\ 0 & 0 & 0 & 0 & 0 & D^0_{66} \end{bmatrix} \tag{G.32}$$

The corresponding stiffness terms can be seen in the equations below.

$$A^0_{11} = 2\pi R A_{11} \tag{G.33}$$

$$A^0_{55} = A^0_{66} = \pi R A_{66} + \pi R A_{55} \tag{G.34}$$

$$D^0_{11} = D^0_{22} = \pi R^3 A_{11} + \pi R^3 D_{11} \tag{G.35}$$

$$D^0_{66} = 2\pi R(A_h^2 A_{66} + 4D_{66}) \tag{G.36}$$

For a circular cross-section with a constant thickness the geometric parameters A_0 and λ become:

$$A_0 = 2\pi R^2 \tag{G.37}$$

$$\lambda = \frac{2\pi R}{h} \tag{G.38}$$

And therefore,

$$A_h = R \tag{G.39}$$

H

Validation of the FEM model

In order to validate FEM part of the damping model, a simple wire model has been modelled in Abaqus. As a cross-section a simple circular tube has been assumed with a radius of $5m$ and a wall thickness of $50mm$. The properties of Steel have been chosen as the tower's material properties.

The displacements of the tower can be calculated by using Equation H.1.

$$\mathbf{U} = [\mathbf{K}]^{-\mathbf{1}}\mathbf{F} \tag{H.1}$$

Where **U** is the displacement vector, $[K]$ is the cross-sectional stiffness matrix and **F** is the force vector.

First the axial displacement u will be validated. In order to validate this displacement the results of the FEM part of the damping model will be compared to the results calculated by Abaqus and by an analytical solution. The analytical solution can be seen in Equation H.2

$$u = \frac{FL}{EA} \tag{H.2}$$

Here F is the load, L is the length of the tower, E is the Young's modulus of the isotropic material and A is the cross-sectional area.

The results of the analytical and the two numerical methods can be seen in Table H.1.

Table H.1: Displacements due an axial load of 100 kN at the top of the tower.

Displacement	v [-]	Type of loading	Analytical	Numerical Abaqus	Numerical Model
$u\ [m]$	0	Axial	$3.047 * 10^{-5}$	$3.047 * 10^{-5}$	$3.047 * 10^{-5}$
$u\ [m]$	0.3	Axial	$3.047 * 10^{-5}$	$3.047 * 10^{-5}$	$2.773 * 10^{-5}$

It can be concluded that for $v = 0$ all the values are approximately the same. However, for $v \neg 0$ the FEM part of the damping model will differ from the analytical solution and Abaqus. Apparently, the wire model of Abaqus and the analytical solution do not take the effect of the poisson's ratio into account.

Subsequently the same can be done for the out-of-plane and torsional displacements. The analytical solutions of these displacements can be seen in Equation H.3, Equation H.4 and Equation H.5.

$$v = \frac{FL^3}{3EI} \tag{H.3}$$

$$\beta_z = \frac{FL^2}{2EI} \tag{H.4}$$

$$\theta = \frac{TL}{GJ} \tag{H.5}$$

Where, I is the second moment of area, G is the material's shear modulus and J is the polar moment of inertia.
The results of the out-of-plane (top) displacements can be seen in Table H.2

Table H.2: Displacements due an out-of-plane (bending) load of 100 kN at the top of the tower.

Displacement	υ [-]	Type of loading	Analytical	Numerical Abaqus	Numerical Model
$v\ [m]$	0	Bending	0.0082	0.0083	0.0083
$v\ [m]$	0.3	Bending	0.0082	0.0084	0.0075
$\beta_z\ [rad]$	0	Bending	$1.23 * 10^{-4}$	$1.23 * 10^{-4}$	$1.23 * 10^{-4}$
$\beta_z\ [rad]$	0.3	Bending	$1.23 * 10^{-4}$	$1.23 * 10^{-4}$	$1.12 * 10^{-4}$

Again the analytical solutions and the wire model of Abaqus do not take the effect of the poisson's ratio into account.

Finally, the results of the torsional displacement can be seen in Table H.3.

Table H.3: Displacements due a torsional load of 100 kN at the top of the tower.

Displacement	υ [-]	Type of loading	Analytical	Numerical Abaqus	Numerical Model
$\theta\ [rad]$	0	Torsion	$2.46 * 10^{-4}$	$2.46 * 10^{-4}$	$2.46 * 10^{-4}$
$\theta\ [rad]$	0.3	Torsion	$3.20 * 10^{-5}$	$3.20 * 10^{-5}$	$3.20 * 10^{-5}$

In case of torsion, all solutions show the same results.

It can be concluded that the FEM part of the damping model estimates the tower's displacements quite well.

I

Influence tower architecture

The variables concerning the tower's architecture, like the tower's radii, the tower's wall thicknesses and the length of the tower, have in general no influence on the tower's axial, shear or torsional damping. During these modes, the modal damping is mainly determined by the material properties and the laminate's architecture. On the other hand, they have a significant influence on the modal damping of the tower's bending modes. In order to determine the effects of these variables, a simple $104m$ tall thin-walled cylindrical structure has been assumed with a radius of $5m$, a wall thickness of $100mm$ and an element length of $1m$.

First of all, the effect of the radius on the tower's modal damping has been validated. The results of this validation can be seen in Figure I.1

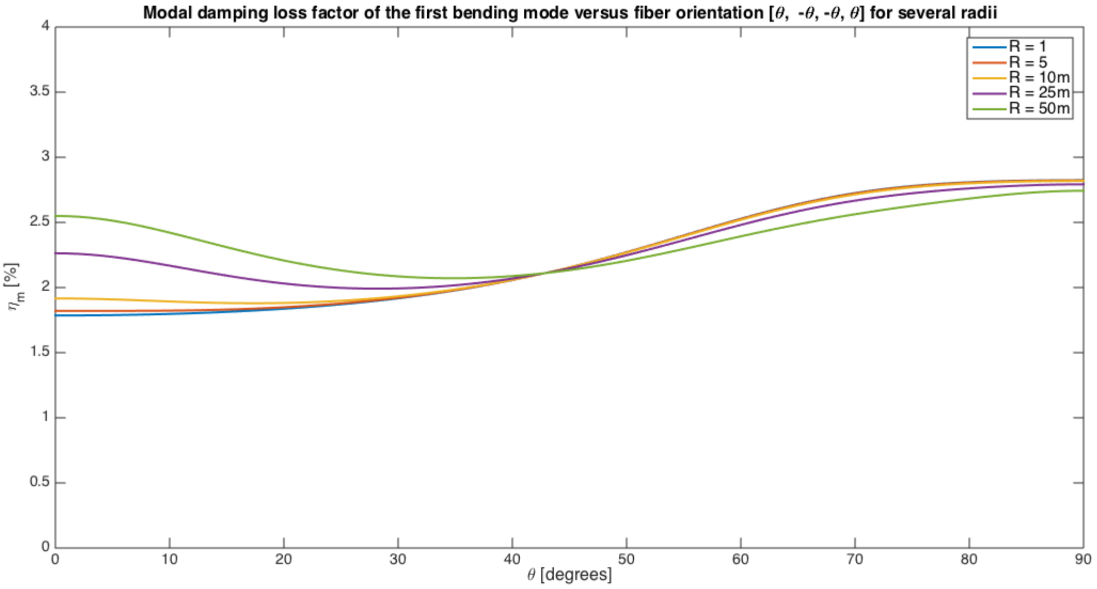

Figure I.1: The influence of the fiber orientation and tower's radius on the modal damping loss factor of the first bending mode. Note that the tower's element length is $1m$ and the tower's wall thickness is $100mm$

It can be seen that at $R = 1m$ the axial damping of the tower prevails, while from $R = 25$ the shear damping starts to be dominant. A similar plot can be made for the effect of the element length, which can be seen in Figure I.2.

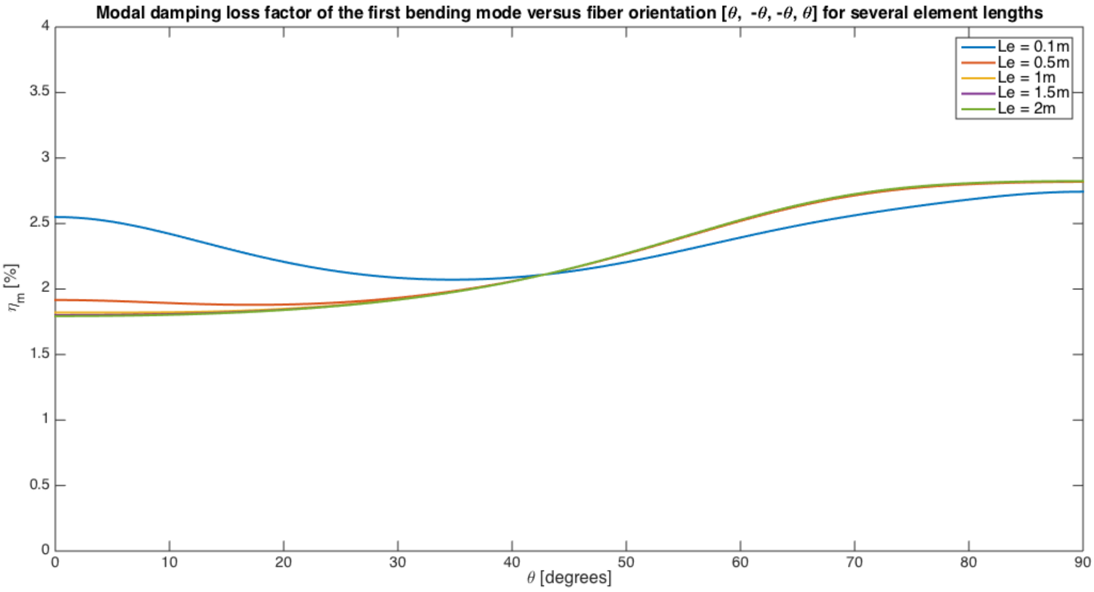

Figure I.2: The influence of the fiber orientation and tower's length on the modal damping loss factor of the first bending mode. Note that the tower's radius is $5m$ and the tower's wall thickness is $100mm$

Obviously, a shorter tower with the same wall thickness and the same radius, results in a larger amount of shear strain energy and therefore in a much larger influence of the material's shear damping. The last parameter that will be investigated is the tower's wall thickness. In Figure I.3 the influence of the wall thickness on the modal damping loss factor of the first bending mode can be seen.

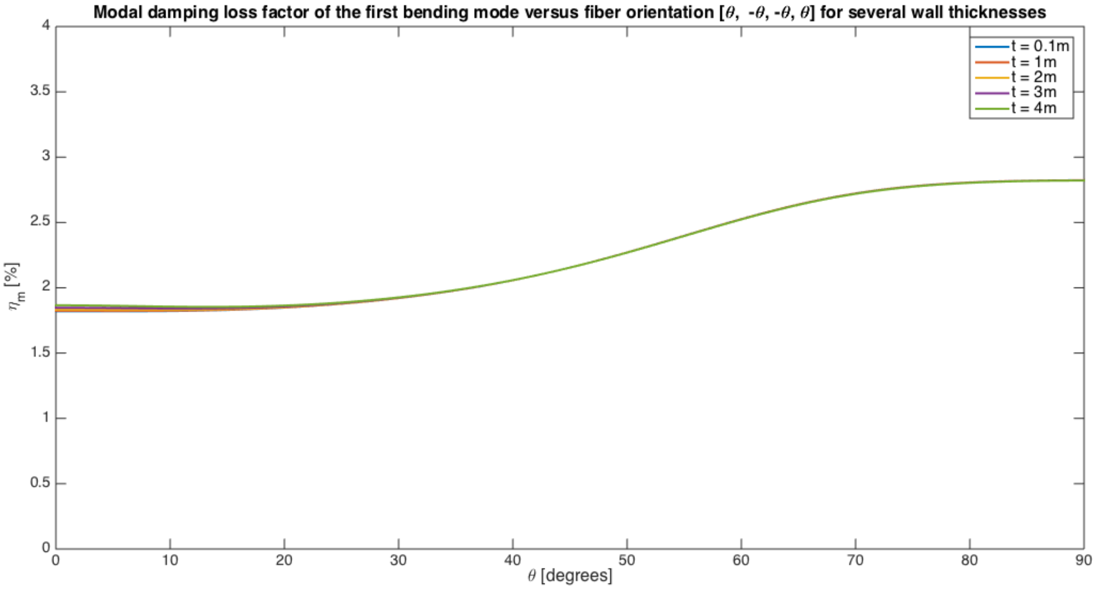

Figure I.3: The influence of the fiber orientation and tower's wall thickness on the modal damping loss factor of the first bending mode. Note that the tower's radius is $5m$ and the tower's element length is $1m$

It can be seen that a larger wall thickness will result in a larger influence of the shear damping in the fiber orientation range $0° - 30°$. Nevertheless its influence on the modal damping is compared to the radius and the element length very small and can be neglected. For wall thicknesses smaller than $1m$ the influence can be considered to be non-existent, which confirms the thin-walled assumption.

J

The influence of the core on the tower's damping behavior

There are three variables that influence the tower's modal damping loss factor. These variables are the core stiffness, the core's damping loss factors (η_{core} and the core thickness. In Figure J.1 the influence of the core stiffness and the fiber orientation on the tower's modal damping loss factor can be seen.

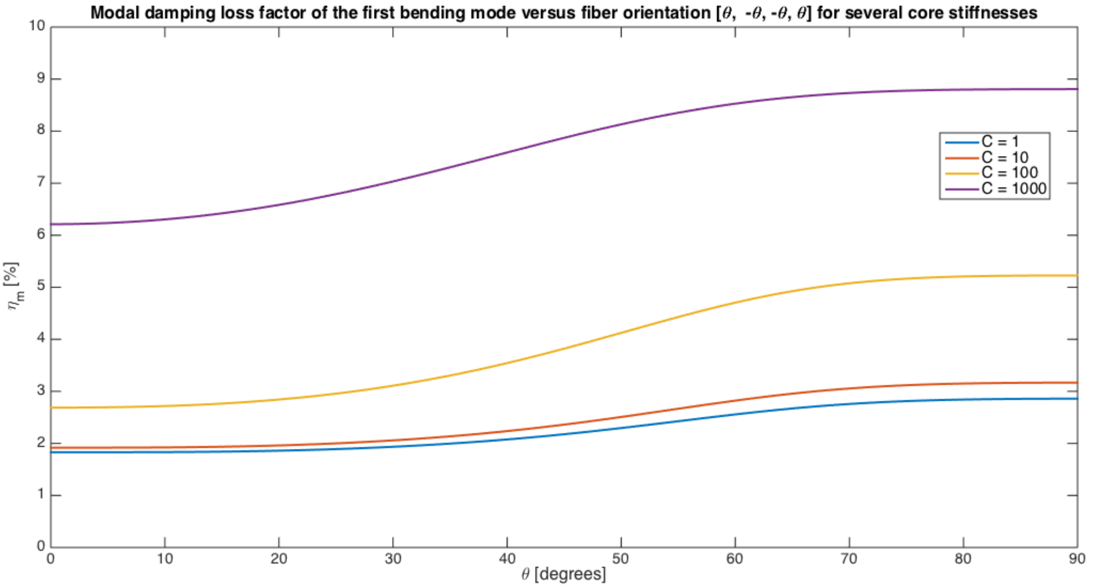

Figure J.1: The influence of the fiber orientation and the core stiffness on the modal damping loss factor of the first bending mode. The symbol C represents the multiplification factor, which is multiplied by both the core's tensile//compressive modulus and the core's shear modulus. Both moduli are equal to the moduli of the Airex T92.80 foam material, which can be seen in Appendix C. Note that the tower's radius is $5m$, the tower's element length is $1m$ and the total thickness of the face sheets is $100mm$. The core has a thickness of $100mm$ as well and a loss factor of 0.1 for both axial and shear damping.

As can be seen, the influence of the core on the tower's modal damping loss factor can be increased by increasing its stiffness with respect to the laminate's stiffness. By changing the core's damping loss factor and by keeping the stiffness equal to the stiffness of the Airex T92.80 foam a similar effect can be noticed, which is seen in Figure J.2.

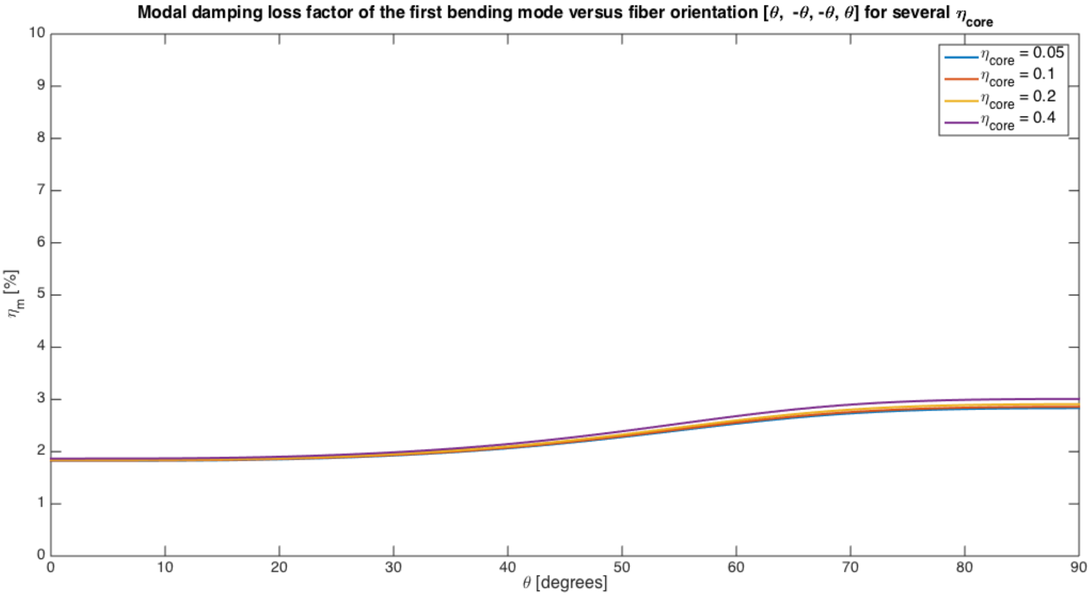

Figure J.2: The influence of the fiber orientation and the core's loss factor on the modal damping loss factor of the first bending mode. Note that the tower's radius is $5m$, the tower's element length is $1m$ and the total thickness of the face sheets is $100mm$. The core has a thickness of $100mm$ as well and the moduli are same as for the Airex T92.80 foam.

Note that a low modulus foam like the Airex T92.80 does not have a significant effect on the tower's modal damping loss factor, even if the core's loss factor is increased drastically. The biggest impact is seen at a fiber orientation of 90°, since at this orientation the difference between the stiffness of the composite material and the stiffness of the core material is at its minimum. A similar behavior is seen when the core thickness is altered. This can be seen in Figure J.3.

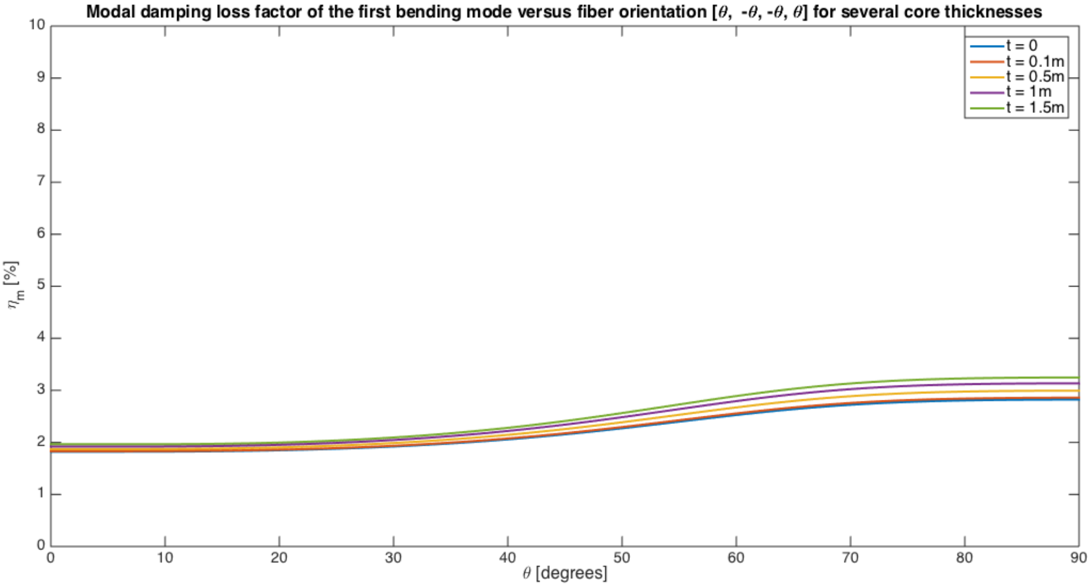

Figure J.3: The influence of the fiber orientation and the core thickness on the modal damping loss factor of the first bending mode. Note that the tower's radius is $5m$, the tower's element length is $1m$ and the total thickness of the face sheets is $100mm$. The core has a damping loss factor of 0.1 and the moduli are same as for the Airex T92.80 foam.

It can be concluded that the core material will only have a significant influence on the tower's modal damping loss factor if the core's stiffness has the same order of magnitude as the stiffness of the face sheets. Note that the current model ignores local effects like local buckling and wrinkling, it is therefore possible that in reality the contribution of the core material on the tower's modal damping loss factor is much higher.

Bibliography

[1] Blythe offshore wind farm. Internet. URL `http://offshorewind.works/wp-content/uploads/2015/05/Blyth-offshore-wind-farm.jpg`.

[2] R.D. Adams and D.G.C. Bacon. Effect of fibre orientation and laminate geometry on the dynamic properties of cfrp. *J. Composite Materials*, 7, 1973.

[3] L.M. Alexander. North sea. Brittanica.com, 2007.

[4] F. Alijani and M. Amabili. Theory and experiments for nonlinear vibrations of imperfect rectangular plates with free edges. *Journal of Sound and Vibration*, 332:3564–3588, 2013.

[5] G. Apolinario, P. Ienny, S. Corn, R. Léger, A. Bergeret, and J. Haudin. Effects of water ageing on the mechanical properties of flax and glass fibre composites : Degradation and reversibility. *Natural Fibres: Advances in Science and Technology Towards Industrial Applications*, 12, 2016.

[6] L. Arany, S. Bhattacharya, J.H.G. Macdonald, and S.J. Hogan. Closed form solution of Eigen frequency of monopile supported offshore wind turbines in deeper waters incorporating stiffness of substructure and SSI. *Soil Dynamics and Earthquake Engineering*, 83:18–32, 2016. ISSN 02677261. doi: 10.1016/j.soildyn.2015.12.011. URL `http://dx.doi.org/10.1016/j.soildyn.2015.12.011`.

[7] M. Assarar, A. El Mahi, and J. Berthelot. Damping Analysis of Sandwich Composite Materials. *Journal of Composite Materials*, 43(13):1461–1485, 2009.

[8] Christian et al. Bak. Description of the dtu 10 mw reference wind turbine. Technical report, DTU, 2013.

[9] J. Banhart, J. Baumeister, and M. Weber. Damping properties of aluminium foams. *Elsevier Materials Science and Engineering*, pages 221–228, 1996.

[10] J. Baur and A. Kulik. Optimal sample shape for internal friction measurements using a dual cantilevered beam. *Journal of Applied Physics*, 58:1489–1492, 1985.

[11] N. Bazeo, G.D. Hatzigeorgiou, I.D. Hondros, H. Karamaneas, D.L. Karabalis, and D.E. Beskos. Static, seismic and stability analysis of a prototype wind turbine steel tower. *Engineering Structures*, 24(1015-1025), 2002.

[12] B. A. Bednarcyk, J. Aboudi, and S.M. Arnold. Enhanced composite damping through engineered interfaces. *International Journal of Solids and Structures*, 92-93:91–104, 2016.

[13] B.S. Ben, B.A. Ben, K. Adarsh, K.A. Vikram, and C. Ratnam. Damping measurement in composite materials using combined finite element and frequency response method. *International Journal of Engineering Science Invention*, 2013.

[14] J. Berthelot and Y. Sefrani. Longitudinal and transverse damping of unidirectional fibre composites. *Composite Structures*, 79:423–431, 2007.

[15] J. Berthelot, M. Assarar, Y. Sefrani, and A. Mahi. Damping analysis of composite materials and structures. *Composite Structures*, 85(3):189–204, 2008.

[16] J.E. Bishop and V.K. Kinra. Elastothermodynamic damping in laminated composites. *J. Solids Structures*, 34, 1997.

[17] M.R.W. Brake. *The Mechanics of Jointed Structures: Recent Research and Open Challenges for Developing Predictive Models for Structural Dynamics.* Springer, 2017.

[18] L.C. Brinson and T.S. Gates. Effects of physical aging on long term creep of polymers and polymer matrix composites. *Journal of Solids Structures*, 32, 1995.

[19] P. Butaud, E. Foltête, and M. Ouisse. Sandwich structures with tunable damping properties: On the use of Shape Memory Polymer as viscoelastic core. *Composite Structures*, 153:401–408, 2016. ISSN 02638223. doi: 10.1016/j.compstruct.2016.06.040. URL `http://dx.doi.org/10.1016/j.compstruct.2016.06.040`.

[20] C. Cai, H. Zheng, M.S. Hung, and K.C. Hung. Modeling of material damping properties in ansys. In *ANSYS 2002 Users Conference and Exhibition*, 2002.

[21] M. Carfagni, E. Lenzi, and M. Pierini. The loss factor as a measure of mechanical damping. *Proceedings of SPIE - The International Society for Optical Engineering.*, 1998.

[22] E. Chailleux and P. Davies. Modelling the non-linear viscoelastic and viscoplastic behaviour of aramid fibre yarns. *Mechanics of Time-Dependent Materials*, 7:291–303, 2003.

[23] R. Chan and M. Nakamura. Mechanical properties of plastic foams: The dependence of yield stress and modulus on the structural variables of closed-cell and open-cell foams. *Journal of Cellular Plastics*, 5(2):112–118, 1969.

[24] R Chandra, S P Singh, and K Gupta. Damping studies in fiber-reinforced composites: a review. *Elsevier Composite Structures*, 46:41–51, 1999.

[25] R. Chandra, S.P. Singh, and K. Gupta. Micromechanical damping models for fiber-reinforced composites: a comparative study. *Elsevier Composites Part A: applied science and manufacturing*, 2002.

[26] R. Chandra, S. P. Singh, and K. Gupta. A study of damping in fiber-reinforced composites. *Journal of Sound and Vibration*, 262(3):475–496, 2003. ISSN 0022460X. doi: 10.1016/S0022-460X(03)00107-X.

[27] 3A Composites. Airex c70 data sheet, 2010.

[28] 3A Composites. Airex t92 data sheet, 2017.

[29] W.D. Cook, G.P. Simon, P.J. Burchill, M. Lau, and T.J. Fitch. Curing kinetics and thermal properties of vinyl ester resins. *Journal of Applied Polymer Science*, 64, 1997.

[30] M. Damgaard, J.K.F. Andersen, L.B. Ibsen, and L.V. Andersen. Natural Frequency and Damping Estimation of an Offshore Wind Turbine Structure. *Proceedings of the Twenty-second (2012) International Offshore and Polar Engineering Conference*, 4:300–307, 2012.

[31] Chortis D.I. *Structural Analysis of Composite WInd Turbine Blades.* Springer, 2013.

[32] F. Duc, C.J.G. Plummer, and J.-A.E. Manson. Damping of thermoset and thermoplastic flax fibre composites. *Elsevier Composites: Part A*, 64:115–123, 2014.

[33] A. El Mahi, M. Assarar, Y. Sefrani, and J. Berthelot. Damping analysis of orthotropic composite materials and laminates. *Composites: Part B*, 39:1069–1076, 2008.

[34] H.P. Gavin. Strain energy in linear elastic solids, 2015.

[35] R.F. Gibson. Damping characteristics of compoiste materials and structures. *Journal of Materials Engineering and Performance*, 1(1):11–20, 1992.

[36] R.F. Gibson. *Principle of composite material mechanics.* CRC Press, 3 edition, 2011.

[37] E.J. Graesser and C.R. Wong. The relationship of traditional damping measures for materials with high damping capacity: A review. In K. Kinra and A. Wolfenden, editors, *M3D: Mechanics and Mechanisms of Material Damping*, pages 316–343. ASTM, 1992.

[38] H. Gu. Dynamic mechanical analysis of the seawater treated glass/polyester composites. *Materials and Design*, 30 (7):2774–2777, 2009. ISSN 02641275. doi: 10.1016/j.matdes.2008.09.029. URL `http://dx.doi.org/10.1016/j.matdes.2008.09.029`.

[39] E. et al. Gutierrez. A wind turbine tower design based on the use of fibre-reinforced composites. Technical report, ELSA-JRC, 2003.

[40] A. S. Hadi and J. N. Ashton. Measurement and theoretical modelling of the damping properties of a uni-directional glass/epoxy composite. *Composite Structures*, 34(4):381–385, 1996. ISSN 02638223. doi: 10.1016/0263-8223(96)00005-0.

[41] D. Hartman, M.E. Greenwood, and D.M. Miller. High strength glass fibers. Technical report, AGY, 1996.

[42] Z. Hashin. Analysis of properties of fiber composites with anisotropic constituents. *Journal of Applied Mechanics*, 46, 1979.

[43] Z.X. He, S.W. Song, F. Li, X.T. Luan, and Q. Sun. Vibration fatigue life prediction of turbine disk based on bp neural networks. *Advances in Heterogeneous Material Mehcanics*, 2008.

[44] R.C. Hibbeler. *Mechanics of Materials*. Pearson, 7 edition, 2008.

[45] J.J. Hoyos, A.A. Chilarducci, H.R. Salva, C.A. Chaves, and J.M. Velez. Internal friction in martensitic carbon steels. *Elsevier Materials Science and Engineering A*, 521-522:347–350, 2009.

[46] S. J. Hwang and R. F. Gibson. Prediction of fiber-matrix interphase effects on damping of composites using a micromechanical strain energy/finite element approach. *Composites Engineering*, 3(10):975–984, 1993. ISSN 09619526. doi: 10.1016/0961-9526(93)90005-5.

[47] S.J. Hwang and R.F. Gibson. The effects of three-dimensional states of stress on damping of laminated composites. *Composites Science and Technology*, 41:379–393, 1991.

[48] S.J. Hwang and R.F. Gibson. The use of strain energy-based finite element techniques in the analysis of various aspects of damping of composite materials and structures. *Journal of Composite Materials*, 26, 1992.

[49] D.J. Inman. *Engineering Vibration*. Prentice Hall, 2001.

[50] Perkin Elmer Instruments. *Pyris Diamond DMA*. PerkinElmer, 2002.

[51] K. Kanny, H. Mahfuz, L.A. Carlsson, T. Thomas, and S. Jeelani. Dynamic mechanical analyses and flexural fatigue of pvc foams. *Elsevier Composite Structures*, 58:175–183, 2002.

[52] C. Kassapoglou. *Design and Analysis of Composite Structures with applications to aerospace engineering*. John Wiley & Sons, 2010.

[53] J. M. Kenny and M. Marchetti. Elasto-plastic behavior of thermoplastic composite laminates under cyclic loading. *Composite Structures*, 32(1-4):375–382, 1995. ISSN 02638223. doi: 10.1016/0263-8223(95)00052-6.

[54] B.G. Kumar, R.P. Singh, and T. Nakamura. Degradation of Carbon Fiber-reinforced Epoxy Composites by Ultraviolet Radiation and Condensation+. *Journal of Composite Materials*, 36(24):2713–2733, 2002. ISSN 0021-9983. doi: 10.1106/002199802028682.

[55] F. Lahuerta and R.P.L. Nijssen. Energy dissipation in thermoset composites in mode i fatigue. *Mechanics of Avanced Materials and Structures*, 2016.

[56] P. Lahuerta, R.P.L. Nijssen, F.P. van der Meer, and L.J. Sluys. Experimental-computational study towards heat generation in thick laminates under fatigue loading. *Elsevier International Journal of Fatigue*, 80, 2015.

[57] R. Lakes. Thermoelastic damping in materials with a complex coefficient of thermal expansion Roderic Lakes. *Journal of Mechanical Behavior*, 1(8):201–216, 1997.

[58] R.S. Lakes. High damping composite materials: Effect of structural hierarchy. *Journal of Composite Materials*, 36 (3), 2002.

[59] R.F. Landel and L.E. Nielsen. *Mechanical Properties of Polymers and Composites*. Marcel Dekker, Inc., 2 edition, 1994.

[60] R. Landers, R. Hubel, and R. Borgogelli. The importance of cell structure for viscoelastic foams. *PU Mag*, 1:40–47, 2008.

[61] C. Lawrence and A.A. Huckelbridge. Characterization of damped structural connections for multi-component systems. Technical report, NASA, 1988.

[62] Z. Li and M.J. Crocker. Effects of thickness and delamination on the damping in honeycomb-foam sandwich beams. *Journal of Sound and Vibration*, 294(3):473–485, 2006. ISSN 10958568. doi: 10.1016/j.jsv.2005.11.024.

[63] J.W. Liang and B.F. Feeny. Identifying coulomb and viscous friction from free-vibration decrements. *Nonlinear Dynamics*, 16:337–347, 1998.

[64] S. Lim, C. Kong, and H. Park. A study on optimal design of filament winding composite tower for 2mw class horizontal axis wind turbine systems. *International Journal of Composite Materials*, 3(1):15–23, 2013.

[65] D. Lombardi. Dynamics of offshore wind turbines. Master's thesis, University of Bristol, 2010.

[66] P. Macioce. Viscoelastic damping 101. *Sound and Vibration*, 1, 2003.

[67] A. Maher, F. Ramadan, and M. Ferra. Modeling of vibration damping in composite structures. *Composite Structures*, 46, 1999.

[68] S. Marouani, L. Curtil, and P. Hamelin. Ageing of carbon/epoxy and carbon/vinylester composites used in the reinforcement and/or the repair of civil engineering structures. *Composites Part B: Engineering*, 43(4):2020–2030, 2012. ISSN 13598368. doi: 10.1016/j.compositesb.2012.01.001.

[69] K.P. Menard. *Dynamic Mechanical Analysis: A Practical Introduction*. CRC Press, 2008.

[70] A Mlyniec, J. Korta, R. Kudelski, and T. Uhl. The influence of the laminate thickness, stacking sequence and thermal aging on the static and dynamic behavior of carbon/epoxy composites. *Composite Structures*, 118, 2014.

[71] D.E. Mouzakis, H. Zoga, and C. Galiotis. Accelerated environmental ageing study of polyester/glass fiber reinforced composites (gfrpcs). *Elsevier Composites: Part B*, 39:467–475, 2008.

[72] N. Ni, Y. Wen, D. He, X. Yi, T. Zhang, and Y. Xu. High damped and high stiffness cfrp composites with aramid non-woven fabric interlayers. *Composites Science and Technology*, 117, 2015.

[73] R. G. Ni and R. D. Adams. A rational method for obtaining the dynamic mechanical properties of laminae for predicting the stiffness and damping of laminated plates and beams. *Composites*, 15(3):193–199, 1984.

[74] G. Nikitas, Nathan J. Vimalan, and S. Bhattacharya. An innovative cyclic loading device to study long term performance of offshore wind turbines. *Soil Dynamics and Earthquake Engineering*, 82:154–160, 2016. ISSN 02677261. doi: 10.1016/j.soildyn.2015.12.008. URL `http://dx.doi.org/10.1016/j.soildyn.2015.12.008`.

[75] Van Oord. Offshore wind dutch ingenuity. Presentation.

[76] TKI Wind op Zee. Cost reduction options for offshore wind in the netherlands fid 2010-2020. Technical report, TKI Wind op Zee, 2015.

[77] M.V. Pathan, V.L. Tagarielli, and S. Patsias. Effect of fibre shape and interphase on the anisotropic viscoelastic response of fibre composites. *Composite Structures*, 2016.

[78] Polynt. Technical data sheet distitron ve370sc, 2002.

[79] D.J. Polyzois, I.G. Raftoyiannis, and N. Ungkurpinan. Static and dynamic characteristics of multi-cell jointed gfrp wind turbine towers. *Composite Structures*, 90:34–42, 2009.

[80] Brands Structural Products. Product review universal epoxy resin ce-sense 101, 2014.

[81] J.N. Reddy. *Mechanics of Laminated Composite Plates and Shells: Theory and Analysis*. CRC Press, 2004.

[82] A. Rezaei, D. Garoz, J. Faes, A. Gilabert, W. Desmet, and W. Van Paepegem. Micro-scale finite element study of the damping in unidirectional fiber reinforced composites. In *ECCM17 - 17th European Conference on Composite Materials*, 2016.

[83] Rijksoverheid. Windenergie op zee. webpage. URL `https://www.rijksoverheid.nl/onderwerpen/duurzame-energie/inhoud/windenergie-op-zee`.

[84] M. Roest. Design of a composite guitar. Master's thesis, TU Delft, 2016.

[85] D.A. Saravanos and C.C. Chamis. Unified micromehcanics of damping for unidirectional fiber reinforced composites. *Journal of Composites, Technology and Research*, 12(1):31–40, 1990.

[86] D.A. Saravanos, D. Varelis, T.S. Plagianakos, and N. Chrysochoidis. A shear beam finite element for the damping analysis of tubular laminated composite beams. *Journal of Sound and Vibration*, 291:802–823, 2006.

[87] J. Sargianis and J. Suhr. Core material effect on wave number and vibrational damping characteristics in carbon fiber sandwich composites. *Composites Science and Technology*, 72(13):1493–1499, 2012. ISSN 02663538. doi: 10.1016/j.compscitech.2012.06.024. URL `http://dx.doi.org/10.1016/j.compscitech.2012.06.024`.

[88] A.B. Schultz and S.W. Tsai. Dynamic moduli and damping ratios in fiber-reinforced composites. *Journal of Composite Materials*, 2(3):368–379, 1968.

[89] O.R. Shah and M. Tarfaoui. Effect of damage progression on the heat generation and final failure of a polyester-glass fiber composite under tension-tension cyclic loading. *Elsevier Composites: Part B*, 62, 2014.

[90] A.W. Signor and J.W. Chin. Effects of Ultraviolet Radiation Exposure on Vinyl Ester Matrix Resins : Chemical and Mechanical Characterization. *Polymer Degradation and Stability*, 79, 2003.

[91] C. Son, K. Kim, K. Lee, J. Lee, and J. Won. Study on natural frequency of offshore wind turbine tower.

[92] J.L. Sullivans. Creep and physical aging of composites. *Composites Science and Technology*, 39, 1990.

[93] G. Swaminathan and K. Shivakumar. A re-examination of dma testing of polymer matrix composites. *Journal of Reinforced Plastics and Composites*, 28(979-994), 2008.

[94] G. Swaminathan, K.N. Shivakumar, and L.C. Russell. Anomalies, influencing factors, and guidelines for dma testing of fiber reinforced composites. *Polymer Composites*, 30(7):962–969, 2009.

[95] A. Treviso, B. Van Genechten, D. Mundo, and M. Tournour. Damping in composite materials: Properties and models. *Composites Part B: Engineering*, 78:144–152, 2015. ISSN 13598368. doi: 10.1016/j.compositesb.2015.03.081. URL `http://dx.doi.org/10.1016/j.compositesb.2015.03.081`.

[96] E.E. Ungar. Loss factors of viscoelastically damped beam structures. *The Journal of the Acoustial Society of America*, 34(8), 1961.

[97] E.E. Ungar and M. Kerwin. Loss factors of viscoelastic systems in terms of energy concepts. *The Journal of the Acoustial Society of America*, 34(7), 1962.

[98] W.G. Versteijlen. Estimation of the vibration decrement of an offshore wind turbine support structure caused by its interaction with soil. Master's thesis, Delft University of Technology, 2011.

[99] R. Vescovini and C. Bisagni. A procedure for the evaluation of damping effects in composite laminated structures. *Progress in Aerospace Sciences*, 78:19–29, 2015.

[100] J. Vincent. *Structural Biomaterials*. Princeton University Press, 2012.

[101] M Witos and M. Stefaniuk. Compressor blade fatigue diagnostics and modelling with the use of modal analysis. *Fatigue of Aircraft Structures*, 1:112–133, 2011.

[102] WMC. Internal documentation.

[103] WMC. Internal documentation. unpublished, 2016.

[104] W. Xu. Effect of bolted joint preload on structural damping, January 2013.

[105] J. Yang, L. Ma, R. Schmidt, G. Qi, K.U. Schröder, J. Xiong, and L. Wu. Hybrid lightweight composite pyramidal truss sandwich panels with high damping and stiffness efficiency. *Composite Structures*, 148:85–96, 2016. ISSN 02638223. doi: 10.1016/j.compstruct.2016.03.056.

[106] R.J. Young and P.A. Lovell. *Introduction to Polymers*. CRC Press, 2011.

[107] B. A. Zai, M. K. Park, H. S. Choi, H. Mehboob, and R. Ali. Effect of moisture absorption on damping and dynamic stiffness of carbon fiber/epoxy composites. *Journal of Mechanical Science and Technology*, 23(11):2998–3004, 2010. ISSN 1738494X. doi: 10.1007/s12206-009-0908-0.

[108] C. Zener. Internal friction in solids ii. general theory of thermoelastic internal friction. *Phys. Rev.*, 53, 1938.

[109] Z Zhang and G Hartwig. Relation of damping and fatigue damage of unidirectional fibre composites. *Elsevier International Journal of Fatigue*, 24:713–718, 2002.

[110] Y.H. Zhao and G.J. Weng. Effective elastic moduli of ribbon-reinforced composites. *Journal of Applied Mechanics*, 112, 1990.

[111] C. Zweben, W.S. Smith, and M.W. Wardle. Test methods for fiber tensile strength, composite flexural modulus, and properties of fabric-reinforced laminates. In *Composite Materials: Testing and Design (Fifth Conference)*. ASTM International, 1979.